REPORT DOCUMENTATION PAGE

Form Approved
OMB No. 0704-0188

1. AGENCY USE ONLY *(Leave blank)*	2. REPORT DATE 14 May 96	3. REPORT TYPE AND DATES COVERED

4. TITLE AND SUBTITLE
Inferring Draining and Pooling Along Colorado Mountain Valleys Using Goes-8 Imagery

5. FUNDING NUMBERS

6. AUTHOR(S)
John Victor Werner

7. PERFORMING ORGANIZATION NAME(S) AND ADDRESS(ES)
AFIT Student Attending:

Colorado State University

8. PERFORMING ORGANIZATION REPORT NUMBER
96-055

9. SPONSORING/MONITORING AGENCY NAME(S) AND ADDRESS(ES)
DEPARTMENT OF THE AIR FORCE
AFIT/CI
2950 P STREET, BLDG 125
WRIGHT-PATTERSON AFB OH 45433-7765

10. SPONSORING/MONITORING AGENCY REPORT NUMBER

11. SUPPLEMENTARY NOTES

12a. DISTRIBUTION/AVAILABILITY STATEMENT
Approved for Public Release IAW AFR 190-1
Distribution Unlimited
BRIAN D. GAUTHIER, MSgt, USAF
Chief Administration

12b. DISTRIBUTION CODE

13. ABSTRACT *(Maximum 200 words)*

19960809 117

14. SUBJECT TERMS

15. NUMBER OF PAGES
98+

16. PRICE CODE

17. SECURITY CLASSIFICATION OF REPORT	18. SECURITY CLASSIFICATION OF THIS PAGE	19. SECURITY CLASSIFICATION OF ABSTRACT	20. LIMITATION OF ABSTRACT

DTIC QUALITY INSPECTED 1

GENERAL INSTRUCTIONS FOR COMPLETING SF 298

The Report Documentation Page (RDP) is used in announcing and cataloging reports. It is important that this information be consistent with the rest of the report, particularly the cover and title page. Instructions for filling in each block of the form follow. It is important to *stay within the lines* to meet *optical scanning requirements*.

Block 1. Agency Use Only *(Leave blank)*.

Block 2. Report Date. Full publication date including day, month, and year, if available (e.g. 1 Jan 88). Must cite at least the year.

Block 3. Type of Report and Dates Covered. State whether report is interim, final, etc. If applicable, enter inclusive report dates (e.g. 10 Jun 87 - 30 Jun 88).

Block 4. Title and Subtitle. A title is taken from the part of the report that provides the most meaningful and complete information. When a report is prepared in more than one volume, repeat the primary title, add volume number, and include subtitle for the specific volume. On classified documents enter the title classification in parentheses.

Block 5. Funding Numbers. To include contract and grant numbers; may include program element number(s), project number(s), task number(s), and work unit number(s). Use the following labels:

C	-	Contract	PR	-	Project
G	-	Grant	TA	-	Task
PE	-	Program Element	WU	-	Work Unit Accession No.

Block 6. Author(s). Name(s) of person(s) responsible for writing the report, performing the research, or credited with the content of the report. If editor or compiler, this should follow the name(s).

Block 7. Performing Organization Name(s) and Address(es). Self-explanatory.

Block 8. Performing Organization Report Number. Enter the unique alphanumeric report number(s) assigned by the organization performing the report.

Block 9. Sponsoring/Monitoring Agency Name(s) and Address(es). Self-explanatory.

Block 10. Sponsoring/Monitoring Agency Report Number. *(If known)*

Block 11. Supplementary Notes. Enter information not included elsewhere such as: Prepared in cooperation with...; Trans. of...; To be published in.... When a report is revised, include a statement whether the new report supersedes or supplements the older report.

Block 12a. Distribution/Availability Statement. Denotes public availability or limitations. Cite any availability to the public. Enter additional limitations or special markings in all capitals (e.g. NOFORN, REL, ITAR).

DOD	-	See DoDD 5230.24, "Distribution Statements on Technical Documents."
DOE	-	See authorities.
NASA	-	See Handbook NHB 2200.2.
NTIS	-	Leave blank.

Block 12b. Distribution Code.

DOD	-	Leave blank.
DOE	-	Enter DOE distribution categories from the Standard Distribution for Unclassified Scientific and Technical Reports.
NASA	-	Leave blank.
NTIS	-	Leave blank.

Block 13. Abstract. Include a brief *(Maximum 200 words)* factual summary of the most significant information contained in the report.

Block 14. Subject Terms. Keywords or phrases identifying major subjects in the report.

Block 15. Number of Pages. Enter the total number of pages.

Block 16. Price Code. Enter appropriate price code *(NTIS only)*.

Blocks 17. - 19. Security Classifications. Self-explanatory. Enter U.S. Security Classification in accordance with U.S. Security Regulations (i.e., UNCLASSIFIED). If form contains classified information, stamp classification on the top and bottom of the page.

Block 20. Limitation of Abstract. This block must be completed to assign a limitation to the abstract. Enter either UL (unlimited) or SAR (same as report). An entry in this block is necessary if the abstract is to be limited. If blank, the abstract is assumed to be unlimited.

THESIS

INFERRING DRAINING AND POOLING
ALONG COLORADO MOUNTAIN VALLEYS
USING GOES-8 IMAGERY

Submitted by

John Victor Werner

Atmospheric Science Department

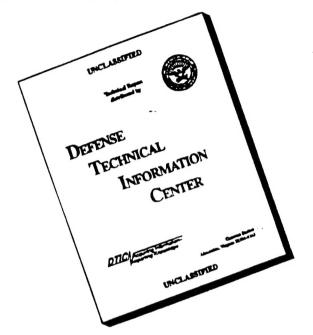In partial fulfillment of the requirements

for the Degree of Master of Science

Colorado State University

Fort Collins, Colorado

Summer 1996

DISCLAIMER NOTICE

THIS DOCUMENT IS BEST QUALITY AVAILABLE. THE COPY FURNISHED TO DTIC CONTAINED A SIGNIFICANT NUMBER OF PAGES WHICH DO NOT REPRODUCE LEGIBLY.

COLORADO STATE UNIVERSITY

May 14, 1996

We hereby recommend that the thesis prepared under our supervision by

John Victor Werner entitled "Inferring Draining And Pooling Along Colorado Mountain

Valleys Using Goes-8 Imagery" be accepted as fulfilling in part requirements for the

Degree of Master of Science.

Committee on Graduate Work

_____

_____

_____
Adviser

_____
Department Head

ABSTRACT OF THESIS

INFERRING DRAINING AND POOLING ALONG COLORADO MOUNTAIN VALLEYS USING GOES-8 IMAGERY

The focus of this research was to assess the feasibility of employing GOES-8 channel 04 satellite imagery to infer regions of pooling and draining along inner-mountain valley floors.

Utilizing a computer model, an analysis using the radiative transfer equation was performed. This analysis demonstrated that during the night, under stable conditions, clear skies, and weak large scale forcings the GOES-8 channel 04 sensor could be employed to discern these along valley temperatures. The analysis demonstrated that over a suitably defined atmosphere over Paonia, Colorado approximately 92% of the radiance sensed by the satellite originated from the earth's surface. Although 8% of the radiance originated from the atmosphere, the strongest emissions originated from within the inversion near the earth's surface. This simulation produced a satellite brightness temperature which correlated exactly with the 283 K surface temperature inputted into the model.

Three days offering favorable meteorological conditions between 0315 UTC and 0745 UTC were selected to evaluate the GOES-8 satellite sensors ability to discern regions of pooling and draining along six relatively wide Colorado inner-mountain valley segments.

A computer program was developed which retrieved the brightness temperatures of each satellite pixel, converted these temperatures to potential temperatures and then mapped the pixels with their respective potential temperature onto 30 second topography data of the selected valley floor.

An analysis of the potential temperature gradients and trends inferred from the satellite suggested regions of draining and pooling in the six Colorado valley segments examined. Although the actual magnitude of the gradients cannot be resolved using the methodology developed, the discerned regions of draining and pooling are consistent with the available documented evidence.

John Victor Werner
Atmospheric Science Department
Colorado State University
Fort Collins, CO 80523
Summer 1996

Acknowledgments

Table of Contents

Chapter 1

Introduction

1.1 Background

Nocturnal valley flows have been an active area of research for many years. Such research remains important today as commercial and industrial developments impinge on previously uninhabited or sparsely populated mountain-valley systems in the inner-mountain western United States. A knowledge of these flows is essential to assessing the pollutant transport and dispersion properties of a given valley location.

Research on mountain-valley circulations is well documented. Early research by Wagner (1938) suggests that unequal cooling and heating differences between higher mountain areas and the adjacent plains generated the down-valley nighttime wind and the up-valley daytime winds.

Petkovsek (1978) used parameters such as the linear openness of basins to develop methods for determining the depth of cold air pools; however, Petkovsek (1980) notes that his technique doesn't apply to narrow, deep, and complex terrain basins which are common in the Colorado inner-mountain region. Whiteman (1982) provides a review of the historical literature along with tethersonde soundings confirming that under favorable synoptic conditions each valley is capable of producing its own temperature and wind regime. Steinacker (1984) uses energy budget reasoning based on area-height distributions in valleys to explain the large diurnal variation in barometric mean temperature between the valley and plains. Vergeiner and Dreiseitl (1987) provide an

overview of the current understanding of valley and slope winds. Their overview states that the horizontal temperature contrast between the mountains and plains builds up a pressure gradient hydrostatically which in-turn generates the up and down-valley winds. McNider and Peilke (1984), Egger (1987), Vergeiner (1987), and Tamada and Bunker (1989) have attempted to model drainage winds.

Although most investigators recognize the local topography, in one form or another, is responsible for the occurrence and intensity of nocturnal drainage flows, the actual control mechanism is still a subject of active research. McKee and O'Neal (1989) point out the difficulty in reaching a clear understanding of the manner in which the topography controls the nocturnal down-valley wind is perhaps due to not one but to a variety of mechanisms operating in different terrain structures. The valleys of Colorado and other western States have been formed in a variety of terrains including mountains and plateaus. Many of these valleys do not have a mountain-plain contrast for hundreds of kilometers; yet, many of them do produce nocturnal drainage winds which form following the net radiation reversal near sunset. Such valleys again pose the question of just how topography controls or initiates along valley drainage winds. Based on energy budget reasoning such as Steinacker (1984) and valley geometry, McKee and O'Neal (1989) extended energy budget reasoning to inner-mountain valleys without a mountain-plain contrast by developing a method of classifying draining and pooling valleys caused by topographic features along valleys within complex terrain.

Numerous field experiments have been conducted to determine how and why particular valleys drain or pool colder air. Perhaps the largest field study conducted in this

area is the 1984 ASCOT field study, Clements and Archuleta (1989). The ASCOT program was essentially designed to assess pollutant transport and diffusion associated with valley flows and the impact of energy production on air quality in areas of complex terrain. The initial study focused on the nocturnal drainage winds which frequently occur in complex terrain. The motivation for this study was that each valley system has the potential of either trapping or transporting pollutants with minimum dilution. Under the 1984 ASCOT program extensive field studies investigating the deep V-shaped Brush Creek valley in the Roan Plateau north of Grand Junction were conducted. The research conducted along the Brush Creek valley demonstrated that the valley, under favorable meteorological conditions, is characterized by strong drainage flows (Gudiksen, 1989). Measurements from this study showed that down-valley temperature gradients developed which ranged from 0.5 to 0.9 K km^{-1}. The down valley surface winds ranged from 1 to 4 m s^{-1}; while jet core winds forming at the top of the surface based temperature inversion, approximately 100 meters above the ground, attained speeds of 4 to 8 m s^{-1}, (McKee and O'Neal, 1989 and Whiteman et al., 1989).

Although our understanding of valley system circulations has been greatly enhanced over the last couple of decades by such research, there exists scant information available to the public and scientific community as to which valleys drain or pool. Why not? Perhaps because of the scarcity of weather observation data available in these fairly remote valleys, as well as the extensive amount of manpower and money required to conduct field studies such as those performed at Brush Creek under the ASCOT program. Certainly, residents who dwell in some of these fairly remote valleys could provide us with

information regarding their particular area as to whether or not their section of the valley drains or pool. Yet such information is certainly not consolidated into one package, for instance, for the state of Colorado. If such information were available, a knowledge of which Colorado valleys drain and which ones pool, could greatly assist federal, state, and local planners as to where and where not to locate key industry. In addition this information could assist them in determining and imposing key environmental regulations needed to maintain air quality standards at a given location. The military could also benefit from such information. Military operations are often conducted in remote locations around the globe; locations where very little information is available regarding local valley flows. A methodology which allows one to distinguish between draining and pooling valley regions would certainly benefit military planners, e.g., in a situation where chemical weapons are a concern one certainly wouldn't want to set up operations in a pooling valley.

1.2 Purpose

The purpose of this research is to examine the hypothesis that GOES-8 satellite imagery can be used to determine whether valley segments drain or pool. Six Colorado valleys using GOES-8 infrared (IR) satellite imagery are examined and evaluated to infer whether they are either pooling or draining valleys. To confirm whether or not the satellite inferred valley flows actually exist, valleys on which documented evidence already exists should be examined. Unfortunately, such information is scarce to non-existent. The one well researched and documented valley in Colorado, Brush Creek, is far to narrow for GOES-8 IR satellite imagery to discern temperature gradients -- this limitation will be

discussed in more detail in chapter 3. However, although there is very little documented evidence verifying whether or not the valleys examined are characteristic of pooling or draining, there is some which suggests that sections of the valley regions examined are areas of pooling or draining. This evidence will be presented in chapter 6.

1.3 Overview

Having defined the purpose of this research, the first step is to develop an understanding of how valley flows without a mountain-plain contrast or synoptic forcing develop. Chapter 2 provides this background, relying heavily on the research conducted by McKee and O'Neal (1989) to demonstrate how valley shape dictates whether or not an along valley temperature gradient will develop leading to a down valley pressure gradient force and subsequent drainage flow. Such flows dominate only under certain meteorological conditions as is made evident in chapter 2.

In chapter 3, the meteorological conditions required for the local thermodynamic effects within the valley system to dominate and to allow for the remote sensing of the valley floor are described. After describing these conditions, several days from Jul 95 to Sep 95 are selected for evaluation and the meteorological conditions existing on these days presented.

Chapter 4, provides background into the operation of GOES-8 and some basic concepts regarding satellite operations. The sensitivity of the GOES-8 channel 04 sensor to fluctuations in surface temperature, mixing ratios, as well as different satellite viewing angles of a prescribed atmosphere during near optimum meteorological conditions over Paonia, Colorado are examined. A radiative transfer program employing the Radiative

Transfer equation was used to examine these sensitivities as well as to determine the correlation between the actual surface temperature and the surface temperature sensed by the satellite.

Chapter 5 provides a general discussion of steps employed to create and display the imagery in a form suitable for analyses. Chapter 5 also describes an initial test case over a segment of the North Fork of the Gunnison Valley near Paonia. The test case demonstrated the need to display the temperatures on a horizontal surface to determine whether or not draining occurred. Hence, the temperature of each pixel was adjusted to the value it would have at mean sea level. The procedure and reasons for doing this are further described in chapter 5.

Moving into the analysis phase of this research, chapter 6 provides a discussion on how the analysis was conducted and examines a number of Colorado valley regions to determine whether or not they are indicative of draining or pooling. The following valley regions were evaluated (See figure 1):

Gunnison River Valley:

       Paonia to Delta
       Delta to Grand Junction

Uncompahgre River Valley:

       Montrose to Delta

Colorado River Valley:

       Parachute to Grand Junction

Arkansas River Valley:

       Leadville to Salida

Yampa River Valley:

Steamboat Area
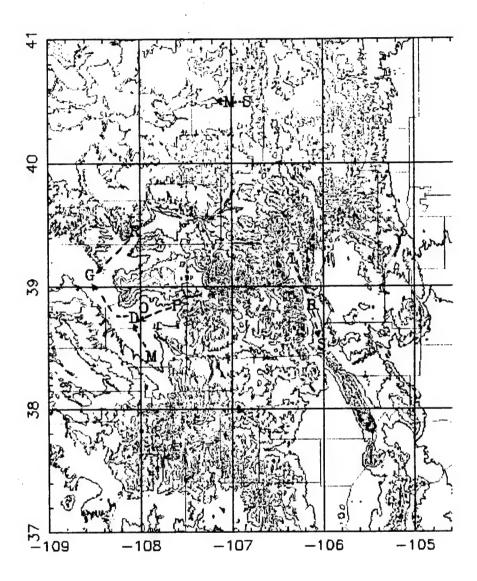
Figure 1.1 Topographical map of Western Colorado with the locations of the six valley sections evaluated in this project indicated by dashed lines and arrow heads. The elevation contours range from 1500 to 4000 meters in 500 m increments. The northernmost S depicts the approximate location of Steamboat while the southernmost S indicates the location of Salida. The northernmost M represents the town of Milner while the southern M marks the location of Montrose. The letters L, B, P, D, R, and G represent the approximate locations of Leadville, Buena Vista, Paonia, Delta, Parachute, and the Grand Junction (GJT) Weather Service Office (WSO), respectively.

Chapter 2

Nocturnal Valley Behavior

2.1 Concept

An understanding of how pressure gradients may form along valley floors is essential to inferring whether draining or pooling regimes occur. When large scale, synoptic, forcing is minimal and the sky is clear of clouds, it has long been understood that nocturnal valley flows are driven by horizontal pressure gradients caused primarily by differential atmospheric cooling within the valley. As pointed out by McKee and O'Neal (1989) each valley has the potential to form along-valley temperature gradients which may generate winds; however, this potential may be thwarted due to topographical features such as constrictions, bends and merging valleys. McKee and O'Neal (1989) provide an analysis of how the geometry of the valley in relation to the local energy budget can provide a mechanism by which intravalley cooling rates lead to an along-valley pressure gradient.

Their analysis, described in this section, focuses on the time period near sunset when the temperature structure within the valley is relatively uniform as the diurnal wind system is reversing direction. It is assumed that the cross-valley air exchange acts efficiently so a valley cross section can be considered uniform in the horizontal, although not in the vertical.

2.2 Analysis

Only after a nocturnal wind develops will the role of advection become important; thus, during the initial stages advection along and from the top of the valley are not considered. Neglecting the advective terms, from the first law of thermodynamics the rate of temperature change for a volume of air in a valley cross section is given by:

$$\frac{dQ}{dt} \approx \rho C_P A x \frac{\partial T}{\partial t} - A x \frac{\partial P}{\partial t} .$$

(2.1)

Thus, the change in heat (**Q**) and time (**t**) are related to valley average cross section properties of density (ρ), temperature (**T**) and pressure (**P**). A valley cross section is depicted in figure 2.1 which includes a width at the top (**W**), cross-sectional area (**A**), cross surface length (**S**), and an arbitrary along valley length (**x**).
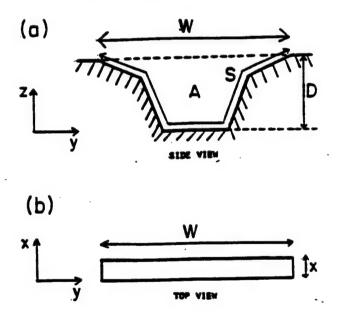

Figure 2-1 Idealized valley cross section where (a) is the side view and (b) is the top view. W = valley width from ridgetop to ridgetop. A = cross-sectional area of valley. S = distance along cross-section surface from ridgetop to ridgetop. X = along-valley length. (McKee and O'Neal 1989)

In equation 2.1, the pressure at the surface will change as the air is diabatically cooled. An expression for the surface pressure, assuming a pressure P_0 at the top of the valley with a depth z measured downward from the top of the valley is given hydrostatically as

$$P(z) = P_0 e^{\int gdz/RT}.$$
(2.2)

Furthermore, a derivative of equation 2.2 with time using a valley averaged temperature leads to a revised version of equation 2.1,

$$\frac{dQ}{dt} \approx \rho Ax \left(C_P + \frac{gz}{T} \right) \frac{\partial T}{\partial t}.$$
(2.3)

Since gz/T is so small in magnitude to that of C_P, for example gz/T is about 1% to 2% of C_P for valleys with depths of 300 m to 600 m, it is neglected. The diabatic heat flux, dQ/dt, includes the sensible heat flux and radiative flux divergence. Restricting cooling to the volume of air within the valley and dealing only with valleys in which clear skies prevail, the local change in temperature then becomes

$$\frac{\partial T}{\partial t} \approx \frac{1}{\rho C_P} \left[H\left(\frac{S}{A}\right) - \frac{Rad.Div.}{Ax} \right].$$
(2.4)

The sensible heat flux, H, is a valley average along the valley surface and the radiative divergence is a valley volume total. S, A, and x are defined in figure 2.1 as the distance along the cross-section surface from ridgetop to ridgetop, the cross-sectional area of the valley, and the along valley length, respectively.

The definition of the radiative divergence is given by:

$$Rad.Div. = R_S Sx - R_T Wx. \tag{2.5}$$

where R_S is net radiation at the surface and R_T is net radiation at the top of the valley. The surface energy budget for the valley cross section is given by

$$R_S Sx = HSx + (LE)Sx - GSx. \tag{2.6}$$

where LE is the latent heat flux and G is the ground heat flux. The sign convention used is that H, LE, and G are all positive for heat moving upward. Substituting (2.6) into (2.5), results in:

$$Rad.Div. = HSx + LESx - GSx - R_T Wx. \tag{2.7}$$

Substituting for $Rad.Div.$ in equation 2.4 the local rate of temperature change becomes

$$\frac{\partial T}{\partial t} \approx \frac{1}{\rho C_P}\left[R_T\left(\frac{W}{A}\right) - LE\left(\frac{S}{A}\right) + G\left(\frac{S}{A}\right)\right]. \tag{2.8}$$

From equation 2.8 the local rate of temperature change is a product of two terms. The term $(1/\rho C_P)$ is the reciprocal of the volume heat capacity for valley air in the cross section, while the term within the brackets is the rate at which the energy is being removed from the volume. The sensible heat and radiative divergence terms within the brackets contain the explicit mechanisms for energy to be removed from the volume of air; whereas the ratios they are multiplied by represent the effects of topography. McKee and O'Neal (1989) point out that for valleys with slopes less than 25^0, W/S > 0.9. Thus W $\cong$ S which allows 2.8 to be simplified to

$$\frac{\partial T}{\partial t} \approx \frac{1}{\rho C_P}[R_T - LE + G]\left(\frac{W}{A}\right). \qquad (2.9)$$

Therefore, in equation 2.9 the basic energy terms are now separated from the term representing the topographical influence of the valley. The net radiation at the top of the valley is the driving mechanism for the cooling; however, the magnitude of the cooling is governed by the difference between the net radiation at the surface which is taken up by latent heat and ground flux. The second factor controlling the cooling rate is **W/A**, the valley geometric factor.
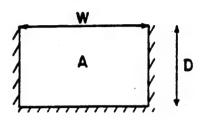
Thus, if the time rate of change of temperature varies along the valley, an along valley temperature gradient will result. A temperature gradient along the valley implies a pressure gradient which, in turn, implies the generation of an along-valley wind. The gradient of the cooling rate from equation 2.9 is defined as follows:

$$\frac{\partial}{\partial x}\frac{\partial T}{\partial t} \approx \frac{1}{\rho C_P}[R_T - LE + G]\frac{\partial}{\partial x}\left(\frac{W}{A}\right)$$

$$+ \frac{1}{\rho C_P}\left(\frac{W}{A}\right)\frac{\partial}{\partial x}[R_T - LE + G]. \qquad (2.10)$$

To simplify discussion, the case for a constant along-valley energy budget is considered. In this scenario, the valley cooling rate and thus horizontal temperature gradients are directly proportional to the gradient of **W/A**. Therefore, **W/A** alone is the driving mechanism for the generation of along valley winds. The question then arises as to what can be expected of **W/A** and its variation with along valley distance? Two idealized examples are depicted in figure 2.2. As suggested one would generally expect the shape

12

high in a valley to closely resemble an equilateral triangle. For a triangle **W/A = 2/D**, where **D** is the depth of the valley.
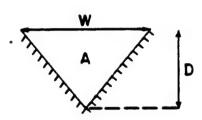

Figure 2-2 (a) Rectangular idealized valley cross section A= WD, (b) Triangular valley cross section A = 1/2WD. (McKee and O'Neal 1989)

Down lower in the valley the shape becomes more rectangular and **W/A = 1/D**. Hence, the variation of **W/A** from one shape to another specifies the volume of air contained for a given width. Thus for a given depth the cooling rate would be a factor of 2 greater than that of a rectangular valley. Also, the value of **1/D** applies to flat terrain as well as to rectangular valleys so valley cooling rates which are multiples of **1/D** are indicative of the relative cooling rate due to the valley geometry. Assuming the cooling within a valley proceeds for some arbitrary time, **t**, no along-valley gradient of energy budget exists, the valley forms a deep isothermal layer from the top of the valley downward to some

distance, **z**, and that a constant pressure, **P₀**, exists at the top of the valley, an estimate of the pressure gradient resulting from the cooling can be calculated.

Integrating equation (2.10) for a time, $\mathbf{t'}$, gives

$$\frac{\partial T}{\partial x} \approx \frac{1}{\rho C_P}[R_T - LE + GE]t'\frac{\partial}{\partial x}\left(\frac{W}{A}\right). \tag{2.11}$$

The pressure at level **z** below the top of the valley is given by Eq (2.3) integrated to depth $\mathbf{z'}$ as :

$$P(z) = P_0 e^{gz'/RT}. \tag{2.12}$$

Thus the pressure gradient becomes

$$\frac{\partial P(x,z)}{\partial x} \approx -P_0 e^{gz'/RT}\left(\frac{gz'}{RT^2}\right)\frac{1}{\rho C_P}$$

$$X \quad (R_T - LE + G)t'\frac{\partial}{\partial x}\left(\frac{W}{A}\right). \tag{2.13}$$

During the night $[\mathbf{R_T} - \mathbf{LE} + \mathbf{G}]$ is usually negative, hence $\partial \mathbf{P}/\partial \mathbf{x}$ is the same sign as $\partial/\partial \mathbf{x}(\mathbf{W}/\mathbf{A})$. The sign of $\partial/\partial \mathbf{x}(\mathbf{W}/\mathbf{A})$ can be positive or negative so that the valley geometry can create an up or down-valley pressure gradient leading to an along valley wind. Studies and observations of wind and temperatures made by McKee and O'Neal(1989) in three Colorado valleys representing pooling and draining valleys are consistent with this concept. Furthermore, they discovered this concept can produce pressure gradients 60% larger than the mountain-plain mechanism.

14

In a draining valley, once the drainage flow becomes established, air will advect into and along the valley rendering the no advection assumption invalid. Advection should, in time, modify the change in temperature and result in an along valley temperature gradient consistent with the resulting wind. Hence, for a draining valley the wind speed should be of significant magnitude, and a horizontal temperature gradient along the valley floor should be apparent, which follows from equation 2.10.

For a pooling valley the horizontal along valley temperature gradients should be weak to non-existent and hence, lack any significant wind.

Chapter 3

Meteorological Conditions

3.1 Requirements

From the contents of chapter 2, it's evident that to evaluate the topographically-induced intravalley wind flows, favorable meteorological conditions must prevail over the region being investigated. Optimum meteorological conditions are those in which the airmass is stable, the sky is clear, temperature and pressure gradients associated with larger scale, synoptic, patterns are minimal, and the winds aloft at mountain top are relatively weak. If such favorable conditions exist, the local thermodynamic effects within a given valley will dominate and subsequently dictate the development of intravalley wind flows.

3.2 Selection

Analysis of an available data set, in which GOES 8 satellite imagery was collected and archived from July 95 through September 95, showed the scarcity of periods in which favorable meteorological conditions occurred. One period, 26 July 95, appeared to offer close to optimum conditions. The airmass was stable as an upper level ridge dominated the weather pattern over the region and the skies during the early morning hours of 26 July 95 appeared to be clear over the entire Colorado region. Figure 3.1 and 3.2 depict the surface analysis and 500 mb analysis valid for 26 July 95 at 1200 UTC, respectively. In figure 3.3, a GOES-8, channel 1 (visible or VIS) satellite imagery is provided valid 26 July 95 at 1415 UTC which depicts the clear skies prevailing over the

Colorado region. The upper air soundings for Grand Junction (GJT) and Denver (DNR) valid for 26 July 95 at 1200 UTC are provided in figures 3.4 and 3.5. The sounding shows the mountain top winds to be relatively weak and once above the low-level effects, the soundings suggest the airmass is relatively homogeneous across the state.
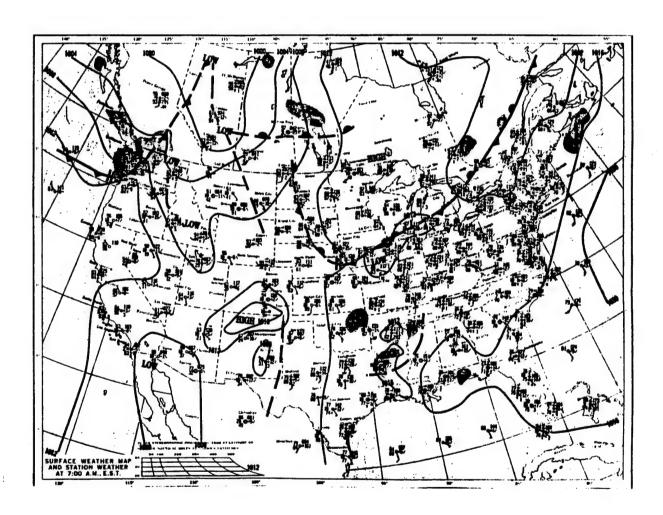

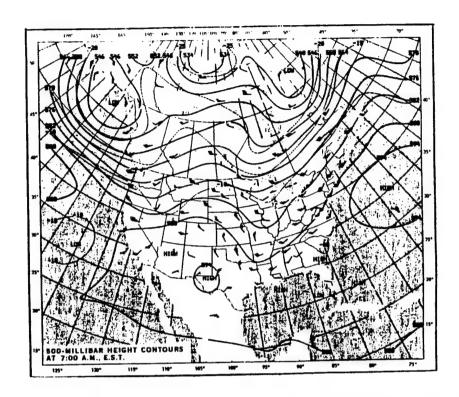Figure 3.1 Surface weather map for 26 July 1995 at 1200 UTC. (NOAA)

Figure 3.2 500 mb geopotential height analysis for 26 July 1995 at 1200 UTC. (NOAA)

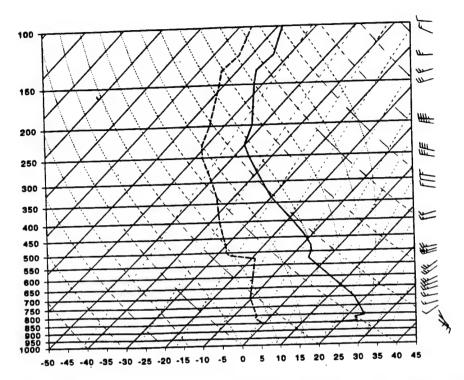Figure 3.3 GOES-8, channel 01 imagery - 26 July 1995 at 1415 UTC.

Figure 3.4   26 July 1995 Grand Junction, CO 1200 UTC sounding. The solid and dashed lines represent the temperature and dewpoint profiles, respectively.
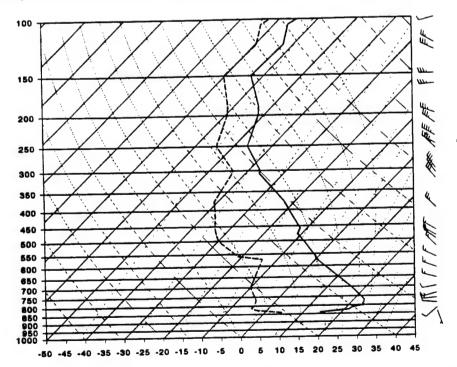

Figure 3.5   26 July 1995 Denver, CO 1200 UTC sounding. The solid and dashed lines represent the temperature and dewpoint profiles, respectively.

The meteorological conditions which prevailed on the morning of 26 July 95, were the most favorable found within the available data set. Being reluctant to focus the analysis on just one period, two other days were selected although the weather conditions for neither day were favorable for all the valleys evaluated.

The Yampa valley region from Steamboat to west of Milner was examined during the nocturnal morning hours of 6 Aug 95. Other valley regions were not evaluated as they were contaminated by scattered high cloudiness during this period. The surface and 500 mb analysis for 6 Aug 95 at 1200 UTC are depicted in figures 3.6 and 3.7. The upper level soundings for GJT and DNR are provided in figures 3.8 and 3.9.
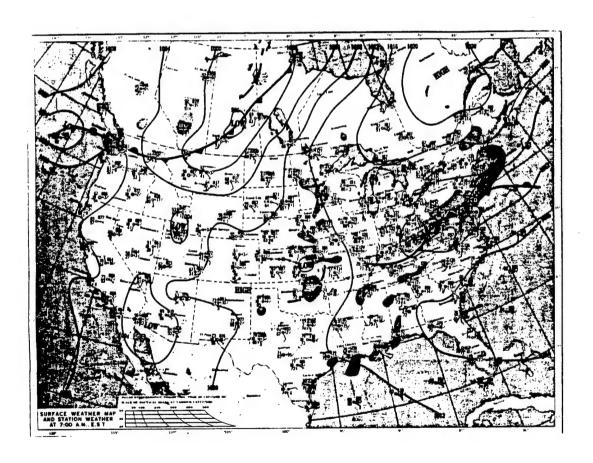

Figure 3.6 Surface weather map for 6 August 1995 at 1200 UTC. (NOAA)
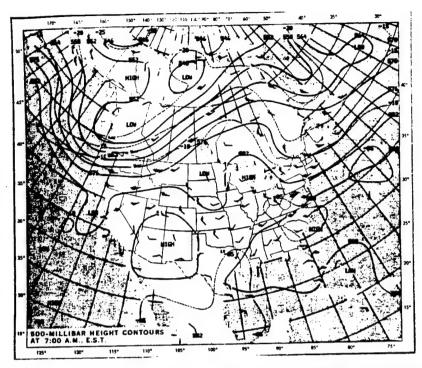
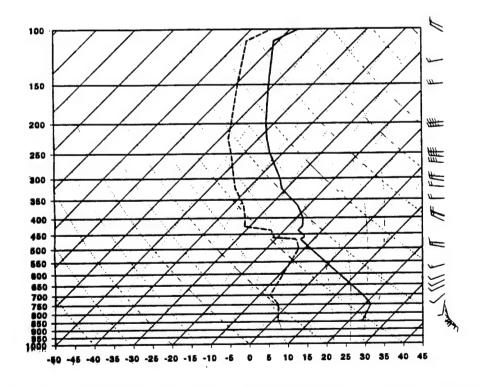Figure 3.7 500 mb geopotential height analysis for 6 August 1995 at 1200 UTC. (NOAA)

Figure 3.8   6 August 1995 Grand Junction, CO 1200 UTC sounding. The solid and dashed lines represent the temperature and dewpoint profiles, respectively.
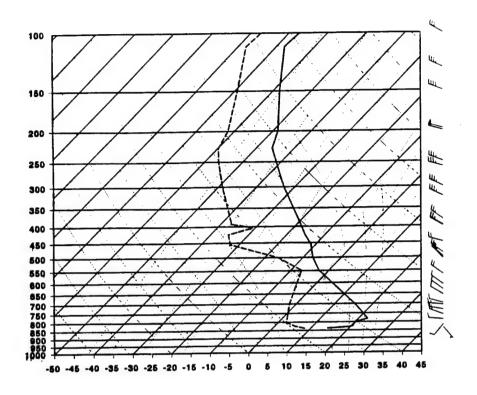
Figure 3.9 6 Aug 1995 Denver, CO 1200 UTC sounding. The solid and dashed lines represent the temperature and dewpoint profiles, respectively.

The early morning hours (UTC) of 31 Aug 95 were chosen as a period in which to evaluate the intravalley flows of all the selected valleys with the exception of the Yampa valley. Scattered high level cloudiness was observed over the Yampa valley region, and a weak cold front had invaded the region as depicted in figure 3.10. With the exception of the Parachute to GJT valley segment, which will be discussed in chapter 6, the other valleys appeared to remain free of clouds. The 500 mb analysis for 31 Aug 95 at 1200 UTC is shown in figure 3.11 and the upper soundings for GJT and DNR valid for the same time are shown in figures 3.12 and 3.13, respectively.
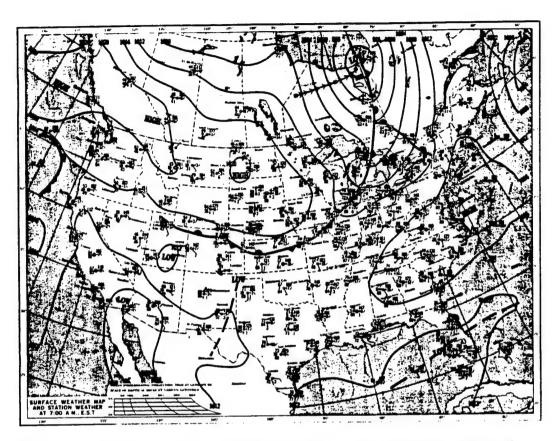
Figure 3.10 Surface weather map for 31 August 1995 at 1200 UTC. (NOAA)
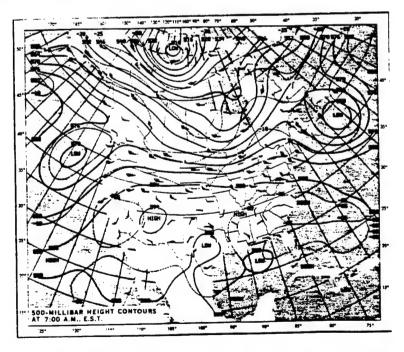
Figure 3.11 500 mb geopotential height analysis for 31 August 1995, 1200 UTC.(NOAA)
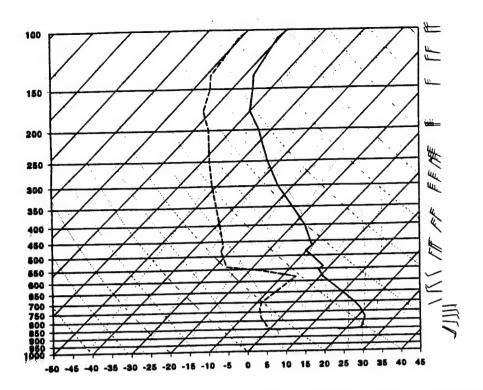
Figure 3.12   31 August 1995 Grand Junction, CO 1200 UTC sounding. The solid and dashed lines represent the temperature and dewpoint profiles, respectively.
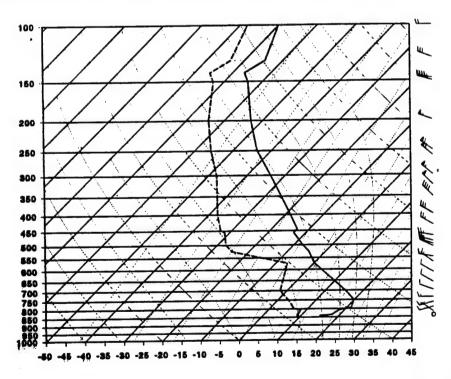
Figure 3.13 31 August 1995 Denver, CO 1200 UTC sounding. The solid and dashed lines represent the temperature and dewpoint profiles, respectively.

3.3 Summary

Chapter 2 provided insight as to how temperature gradients may develop along valley floors due to variations in the valley's shape, resulting in a variation of cooling rates along the valley. Under favorable meteorological conditions, a valley which possesses a V-shape along its upper reaches, gradually widening to a more rectangular shape down the valley can produce a temperature gradient which results in the formation of a down valley pressure gradient and a subsequent drainage flow. In chapter 3, three days were selected in which to employ GOES-8 satellite IR imagery to assess whether pooling or draining occurred along the selected valley segments discussed in chapter 1. The next step is to develop a more in-depth understanding of the tool which will be employed. Chapter 4 provides a basic background into the operation of GOES-8 and assesses the applicability of its use to this project by testing its sensitivity to a variety of parameters.

Chapter 4

GOES-8 Satellite Imagery

4.1 Background

In April of 1994, the first National Oceanic and Atmospheric Administration's (NOAA's) next generation of geostationary satellites, GOES-8, was launched. GOES-8 was moved and stabilized at its present location near 75 degrees west longitude by July 95. All major components of the GOES-8 system are new and greatly improved over those of the GOES-VAS system. To improve calibration, GOES-8 reference blackbodies are external to the instrument telescopes so that space and blackbody looks are used directly to convert responses to radiances. Calibration provides brightness temperatures with a 1.0 K accuracy and 0.3 K relative precision, and greatly reduced noise levels -- a factor of 2 to 3 times less than that of GOES-7. For channel 04, the detector instantaneous geometric field of view (IGFOV) or "footprint" and the derived sampled subpoint resolution (SSR) at nadir, looking directly beneath the satellite, are 4.0 km by 4.0 km and 2.3 km by 4.0 km, respectively. The noise level of the channel 04 sensor ranges from 0.20 K @ 300K increasing to 0.40 K @ 230 K (Menzel and Purdom, 1994). The SSR modifies IGFOV by accounting for instrument response and sampling. GOES-8 oversamples channel 04 IGFOV along a scan line by a factor of 1.75, Gabriel and Purdom (1990).

4.2 Basic Concepts

The infrared radiance detected by the satellite is emitted from both the earth's surface and the atmosphere. The radiance sensed from a surface is a product of its black body radiance, the emissivity of a given wavenumber (or wavelength), and the transmittance from the surface to the top of the atmosphere. Most surfaces have an emissivity close to unity. The emissivity is the ratio of emitted radiance to blackbody radiance. The total atmospheric radiance for any given wavenumber for any given layer is determined by layer black body radiance, layer emissivity, and atmospheric transmittance from each individual layer. Earth emitted radiance must pass through the atmosphere, which selectively absorbs and emits infrared radiance. The sum of the radiance or total radiance reaching the satellite sensor can be expressed by the Radiative Transfer equation. The amount of radiance reaching a satellite comes from two sources: the radiance received from the earth's surface plus the total atmospheric radiance for any given wave number given as the sum of the radiances from each individual layer such that:

$$B_\nu(T_{SAT}) = B_\nu(T_{SFC})\mathfrak{J}_{SFC} + \int_{\mathfrak{J}=1}^{\mathfrak{J}=\mathfrak{J}_{SFC}} B_\nu(T_{ATM})d\,\mathfrak{J}_{ATM} \qquad (4.1)$$

$B_\nu(T_{SAT})$ is the total black body radiance reaching the satellite sensor.

$B_\nu(T_{SFC})\mathfrak{J}_{SFC}$ is the black body radiance emitted by the earth reaching the satellite sensor, here after, referred to as surface emission.

$\int_{\mathfrak{J}=1}^{\mathfrak{J}=\mathfrak{J}_{SFC}} B_\nu(T_{ATM})d\,\mathfrak{J}_{ATM}$ represents the total atmospheric radiance sensed by the satellite.

T_{SAT}, T_{SFC}, and T_{ATM} represent the equivalent temperature from the radiance reaching the satellite, the temperature at the earth's surface, and the equivalent temperature of the atmosphere from which the radiance is being emitted, respectively.

$\mathcal{T}_{SFC}$ and $d\mathcal{T}_{ATM}$ represent the transmittance from the top of the atmosphere to the earth's surface and the change in transmittance from the top of the atmosphere to some arbitrary layer of the atmosphere, respectively.

The longwave IR atmospheric window is located in the wavenumber domain between 800 cm^{-1} to 1200 cm^{-1}. Aside from the low level water vapor band centered near 800 cm^{-1} and the ozone band near 1030 cm^{-1}, this region is not significantly attenuated by atmospheric gases. GOES-8 offers channel (CH) 04 and CH05 which sense radiation within this window. CH04 effectively senses radiation between wavenumbers 892 and 980 cm^{-1} and CH05 between 800 and 870 cm^{-1}. Since energy radiated by the earth's surface and clouds, at these wavenumbers, is not significantly attenuated, the brightness temperature, derived by inverting the Planck function, should be close to the actual surface or cloud top temperature - for opaque clouds. The brightness temperature derived from the satellite sampled radiance of the earth's surface when clear skies prevail is commonly referred to as the skin surface temperature. The remainder of this chapter is primarily devoted to evaluating the sensitivity of the satellite received radiance and determining whether the satellite sensor provides an accurate measure of the skin surface temperature for the application of evaluating nocturnal, along-valley temperature gradients.

4.3 Evaluation

When clear skies prevail over a region GOES-8 IR satellite imagery can be used to discern the skin surface temperatures of the area. The question remains as to how representative the skin surface temperature derived from the imagery is to the actual skin surface temperature.

Although it can't be assumed that the skin surface temperature of a particular location is the same as the ambient air temperature, it's reasonable to assume that the skin surface temperature gradients which develop are indicative of the ambient surface temperature gradient. To assess the accuracy of the skin surface temperature which is derived by satellite to the actual temperature of the earth's surface, an analysis, using MODTRAN3 - Air Force Geophysics Laboratory (1995), was performed over a valley, wherein lies the town of Paonia, in western Colorado (See figure 1.1). MODTRAN 3 is a radiative transfer propagation model and computer code for calculating atmospheric transmittance and background radiance from 0 to 50,000 cm^{-1} at a resolution of 2 cm^{-1}. The code is based on the LOWTRAN 7 (1988) model.

4.3.1 Meteorological Conditions

To ensure clear skies and weak winds, a stable weather regime in which a relatively strong upper level ridge and weak surface pressure gradients prevailed across the state had to be chosen. These conditions existed on 26 Jul 95 over Colorado (See figures 3.1 thru 3.3) and hence, was used for this evaluation.

The atmospheric vertical profile of GJT was translated to Paonia to evaluate the sensitivities of the GOES-8 sensor and the sensor's ability to discern the actual skin surface temperature. With the relatively homogeneous, meteorological conditions depicted in chapter 3, such translations are not unreasonable.

The atmospheric upper air profiles of DNR and GJT for 26 Jul 95 at 1200 UTC are provided in figures 3.4 and 3.5. A comparison of these two soundings show that once above the local terrain effects the atmosphere is relatively homogeneous. Due to the

homogeneity of the atmosphere over Colorado, the GJT sounding was used to represent the atmospheric profile over Paonia; however, modifications had to be made to the lower atmospheric portion of the sounding. A discussion of how and why modifications were made follows.

Grand Junction's elevation is approximately 1475 m above mean-sea level (ASL) while Paonia is located at approximately 1701 m ASL. Note, from figure 3.4, a strong temperature inversion, as would be expected considering the previously described weather regime, exists at GJT from the surface to 840 mb or 1609 m ASL. From 840 mb to 817 mb (1850 meters ASL) no inversion exists but from 817 mb to 807 mb another temperature inversion is evident (1957 meters ASL). For simplicity, the two low level inversions were merged when transposing the GJT sounding over Paonia.

The temperature retrieved from GOES-8 CH04 (892 cm^{-1} to 980 cm^{-1}), using a lookup table obtained from NOAA/NESDIS which converts the radiance of a pixel to brightness temperature, indicated the skin surface temperature at Paonia to be 10 C (The upper air sounding indicated that the GJT surface temperature was 17.6 C). Although it is assumed that the ambient surface temperature over Paonia may be several degrees warmer than the ground surface temperature, 10 C was used to approximate the ambient air temperature in the sensitivity analysis. As will be discussed, the resolution of the GOES-8 CH04 sensor is such that much of the radiance sensed in the pixel representing Paonia was from the slopes above the valley floor. Hence, the skin surface temperature retreived from satellite would be expected to be warmer than that actually existing at Paonia near the

valley bottom. A constant lapse rate was applied from the surface to 807mb (1957 m

ASL) where the temperature was 24 C: the same as that over GJT. The inversion is

assumed to end at 807 mb. Hence, the average lapse rate of the temperature inversion

over GJT was approximately 49 C km^{-1}; whereas the lapse rate of the inversion transposed

over Paonia was 55 C km^{-1}. The GJT sounding recorded two significant levels between

1701 m and 1957 m at 1850 m and 1829 m. Assuming a 55 C km^{-1} lapse rate over Paonia

and working downward from 1957 m using the hypsometric equation in terms of

geopotential height the following were derived:

Height	Temperature	Pressure
1850 m	18 C	817 mb
1829 m	17 C	819 mb
1701 m	10 C	832 mb

The mixing ratios at these levels were computed using the dewpoints from the GJT upper

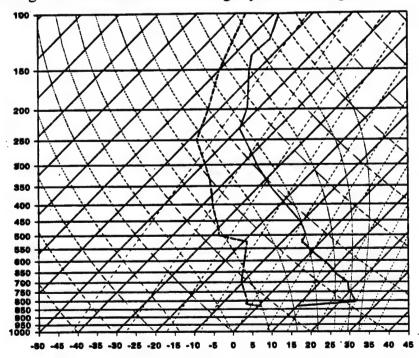air sounding. The derived Paonia sounding is presented in figure 4.1.

Figure 4.1 26 July 96 Paonia, CO 1200 UTC derived upper air sounding. The solid and
dashed lines represent the temperature and dewpoint profiles, respectively.

31

4.3.2 GOES-8 Resolution

GOES-8 offers two channels, channel 04 (CH04) and channel 05 (CH05) which measure radiance at wavelengths within the atmospheric window. The satellite resolution for both channels at nadir, when the satellite is directly overhead, is 2.3km by 4.0 km. The resolution over Paonia is approximately 3.2 km by 6.9 km. Hence, the satellite's resolution greatly restricts the number of valleys that can be effectively evaluated.
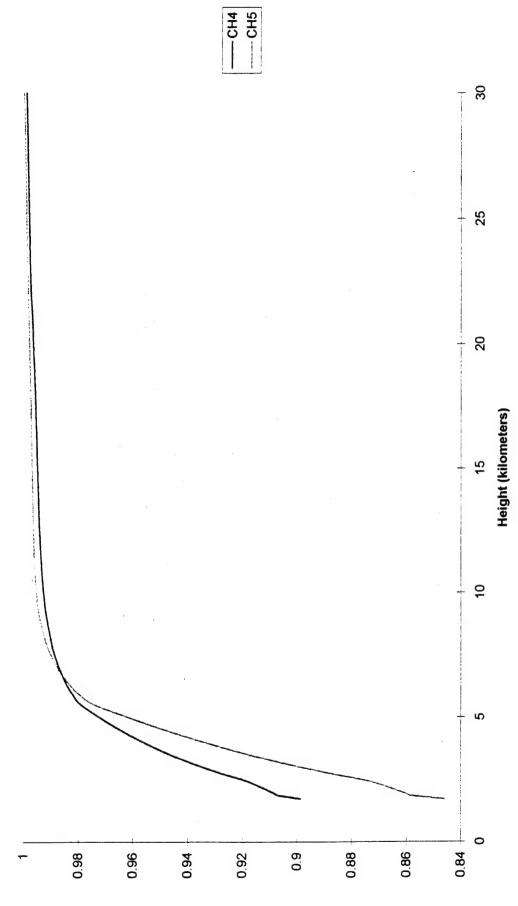
4.3.3 CH04 Versus CH05

Since the goal is to accurately derive the skin surface temperature, the transmittance of CH04 and CH05, over the defined Paonia atmosphere, was compared. Using MODTRAN3 the transmittance of each channel can be determined. The key parameters defining the Paonia atmosphere (mixing ratio, temperature, etc.) were input into MODTRAN3. The MODTRAN3 tape5, list of input parameters, is provided in table 4.1. Before MODTRAN3 can be utilized to compute the transmittance of each channel, another important parameter must be defined: the location of the satellite with respect to Paonia. To determine this, the location of the satellite with respect to the local zenith over Paonia must be defined. By convention the zenith angle is 0 degrees when looking directly upward from a horizontal plane on the earth's surface; however, this angle is 180 degrees when the viewing angle is reversed as is the case when a satellite is directly overhead viewing the earth's surface. Using spherical trigonometry the satellites location was determined to be approximately 56 degrees off the zenith angle; thus, the satellite is located at 124 degrees with respect to Paonia's zenith.

Table 4.1 MODTRAN3 input, tape 5, for 26 July 95 Paonia, CO 1200 UTC. In column 1, 2, 3, and 4 the heights (km), pressures (mb), temperatures (K), and mixing ratios, respectively, are given.

```
t    7    2    1    0    0    0    0    0    0    0    0    1    1    .000    .00
f   2f    0  355.000
    6    0    0    0    0    0    .000    .000    .000    .000    1.701
   30    0    ORProj PAO sndg
    1.701   .832E+03   .283E+03   .481E+01   .000E+00   .000E+00AAC666666666666
    1.829   .819E+03   .290E+03   .358E+01   .000E+00   .000E+00AAC666666666666
    1.850   .817E+03   .291E+03   .354E+01   .000E+00   .000E+00AAC666666666666
    1.957   .807E+03   .297E+03   .359E+01   .000E+00   .000E+00AAC666666666666
    2.428   .763E+03   .294E+03   .312E+01   .000E+00   .000E+00AAC666666666666
    2.743   .737E+03   .292E+03   .285E+01   .000E+00   .000E+00AAC666666666666
    3.184   .700E+03   .290E+03   .249E+01   .000E+00   .000E+00AAC666666666666
    3.658   .661E+03   .285E+03   .229E+01   .000E+00   .000E+00AAC666666666666
    4.267   .613E+03   .280E+03   .206E+01   .000E+00   .000E+00AAC666666666666
    4.877   .569E+03   .274E+03   .184E+01   .000E+00   .000E+00AAC666666666666
    5.552   .524E+03   .268E+03   .162E+01   .000E+00   .000E+00AAC666666666666
    5.920   .500E+03   .267E+03   .760E+00   .000E+00   .000E+00AAC666666666666
    6.271   .478E+03   .265E+03   .690E+00   .000E+00   .000E+00AAC666666666666
    6.927   .439E+03   .260E+03   .520E+00   .000E+00   .000E+00AAC666666666666
    7.630   .400E+03   .255E+03   .380E+00   .000E+00   .000E+00AAC666666666666
    7.925   .384E+03   .252E+03   .340E+00   .000E+00   .000E+00AAC666666666666
    8.924   .335E+03   .243E+03   .220E+00   .000E+00   .000E+00AAC666666666666
    9.700   .300E+03   .237E+03   .140E+00   .000E+00   .000E+00AAC666666666666
   10.930   .250E+03   .227E+03   .600E-01   .000E+00   .000E+00AAC666666666666
   12.390   .200E+03   .220E+03   .400E-01   .000E+00   .000E+00AAC666666666666
   14.200   .150E+03   .211E+03   .200E-01   .000E+00   .000E+00AAC666666666666
   16.670   .100E+03   .204E+03   .100E-01   .000E+00   .000E+00AAC666666666666
   20.950   .500E+02   .218E+03   .100E+00   .000E+00   .000E+00AAC666666666666
   22.655   .380E+02   .217E+03   .130E+00   .000E+00   .000E+00AAC666666666666
   30.000                                                          66666666666666
   35.000                                                          66666666666666
   40.000                                                          66666666666666
   50.000                                                          66666666666666
   70.000                                                          66666666666666
  100.000                                                          66666666666666
  100.000      1.701    124.000      .000      .000      .000      0
     100       2500         2         2
    0
```

The mean transmittance for CH04 was found to be approximately 89% and CH05 was 85%; therefore, CH04 was chosen to evaluate the skin surface temperature of the Paonia region. Figure 4.2 depicts the change in transmittance as a function of height for CH04 and CH05. From 6.271 km and below the transmittance for CH04 is greater than that of CH05. CH05 is more sensitive to absorption by the rotational water vapor band (200 cm^{-1} to 900 cm^{-1}) and although the atmosphere is relatively dry the impact of the water vapor is quite noticeable, especially below 5 km.

CH04 VS CH05 Total Transmittance as a Function of Height Over Paonia on 26 Jul 95 at 1200 UTC <124>

Height (kilometers)

Figure 4.2

CH4
CH5

4.3.4 CH04(892 cm^{-1} to 980 cm^{-1}) Sensitivity Analysis

4.3.4.1 Surface Temperature

A MODTRAN3 run of the "observed" Paonia atmosphere with surface temperature of 283K was made. MODTRAN3 calculations were also made with surface temperatures of 293K and 273K to determine how the surface emission and total radiance fluctuated with varying surface temperatures (see figures 4.3 and 4.4). For the 293K and 273K runs, a layer was inserted at 1751 meters (50 meters above ground level) which had a temperature and mixing ratio value of the "observed" Paonia surface. This was done to ensure that modifying the surface temperature had minimal impact on the rest of the atmospheric column in an effort to better isolate the effects of varying the surface temperature.

The effect of warming the surface temperature by 10 K on the surface emission is readily noticeable in the atmospheric window portion of the spectrum (800 to 1200 cm^{-1}). An increase in surface emission is also discernible from 1864 thru 2200 cm^{-1}. At 936 cm^{-1} (approximately the mean wavenumber within the CH04 band) the surface emission decreases by approximately 16% when the surface temperature is decreased from 283 K to 273 K. Whereas when the surface temperature is increased from 283 K to 293K the surface emission increases by an average of 1.39×10^{-6} R K^{-1} or approximately 15%. Hence, the higher the surface temperature the greater the surface emission. A ten degree change in temperature at this temperature range results in a 15% to 16% change in surface emission.

The total radiance over Paonia follows a similar pattern to that of the surface emission in the sense that the most noticeable changes occur in the atmospheric window. The total radiance between 600 to 800 cm^{-1} is interesting as it demonstrates the opacity and strong absorptive characteristics of the carbon dioxide in our atmosphere. Due to the opacity of carbon dioxide in this wavenumber band, the satellite is sensing the radiance in the upper atmosphere which is emitting at far cooler temperatures than that of the atmospheric window and rotational water vapor bands adjacent to it.
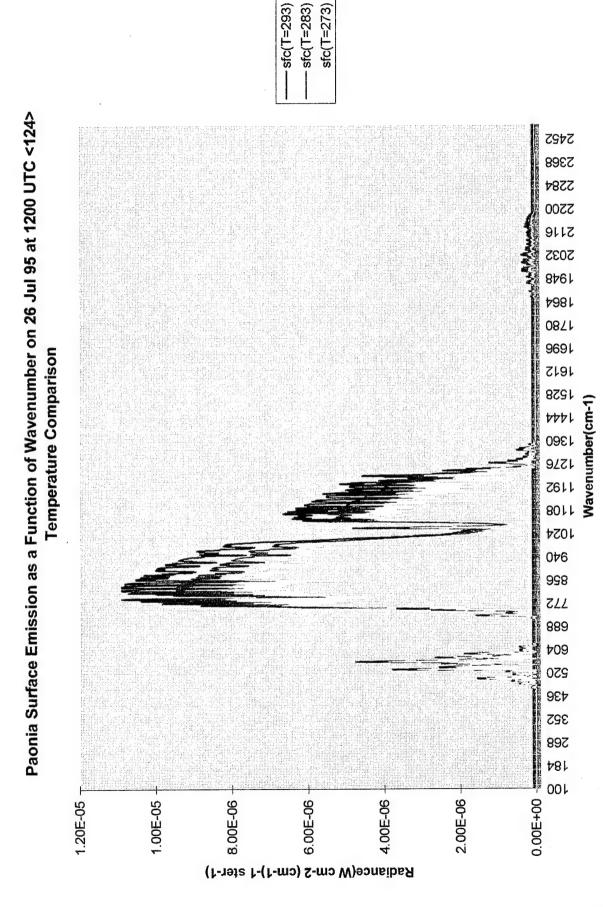
Upon reviewing figures 4.3 and 4.4 it is apparent that surface emission and total radiance within the atmospheric window are sensitive to temperature changes at the earth's surface.

4.3.4.2 H_2O

4.3.4.2.1 Increasing Mixing Ratios:

MODTRAN3 runs were made for the Paonia atmosphere with increased mixing ratios at all levels of the "observed" atmosphere of 25%, 50%, and 75%. Figures 4.5 thru 4.7 show the effect of these increases on surface emission, total radiance, and transmittance - respectively.

Increasing the mixing ratios caused a noticeable change in the surface emission between 892 cm^{-1} and 980 cm^{-1}. An increase in the mixing ratios at all levels of 25% caused a decrease in surface emission of approximately 3% at 936 cm^{-1}. Note in figure 4.5 that increasing the mixing ratio also caused a pronounced decrease in the surface emission of the wavenumber region 450 to 600 cm^{-1}, a region of the spectrum greatly influenced by the rotational water vapor band.
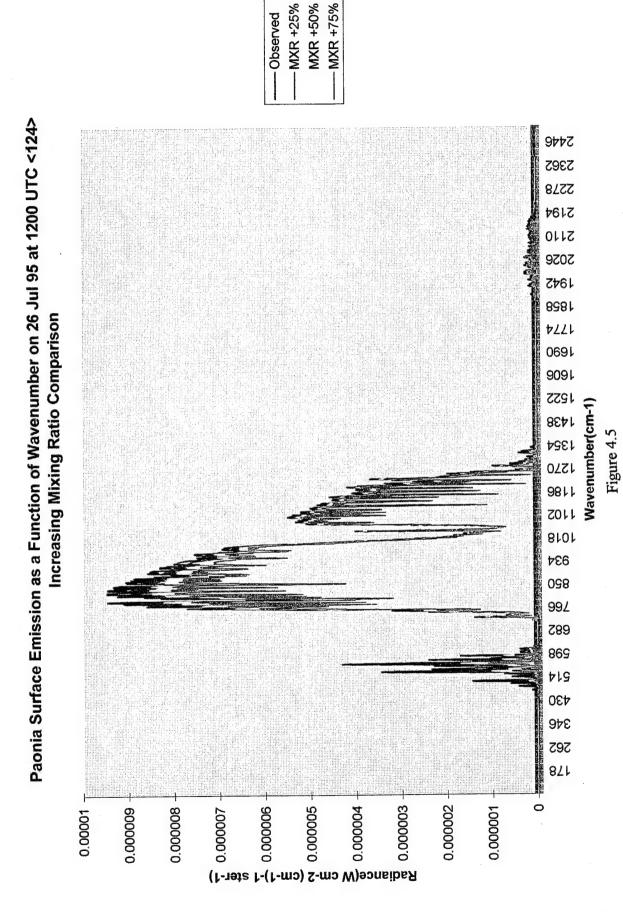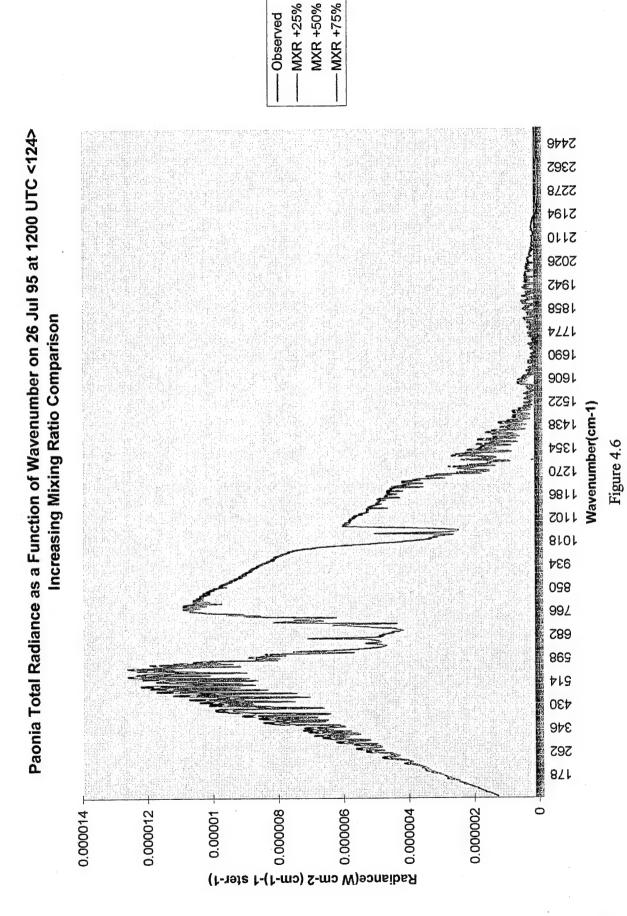
Paonia Surface Emission as a Function of Wavenumber on 26 Jul 95 at 1200 UTC <124> Temperature Comparison

Figure 4.3

Paonia Total Radiance as a Function of Wavenumber on 26 Jul 95 at 1200 UTC <124>
Temperature Comparison

Legend:
sfc(T=293)
sfc(T=283)
sfc(T=273)

Radiance(W cm-2 (cm-1)-1 ster-1)

Wavenumber(cm-1)

Figure 4.4

38

Paonia Surface Emission as a Function of Wavenumber on 26 Jul 95 at 1200 UTC <124>
Increasing Mixing Ratio Comparison

Figure 4.5

39

Paonia Total Radiance as a Function of Wavenumber on 26 Jul 95 at 1200 UTC <124>
Increasing Mixing Ratio Comparison

Figure 4.6

40

Paonia Total Transmittance as a Function of Wavenumber on 26 Jul 95 at 1200 UTC <124>
Increasing Mixing Ratio Comparison

Wavenumber(cm-1)

Figure 4.7

41

Increasing the mixing ratios at each level had little noticeable effect on the total radiance sensed by the satellite; thus illustrating the fact that the atmosphere's contribution to the total radiance is increasing with increasing water vapor while that of the surface emission is decreasing. Although slight, calculation of the MODTRAN3 numerical output showed that the total radiance was increased by 0.2%, 0.5% and 0.6% from the "observed" total radiance for an increase of 25%, 50%, and 75%, respectively. Due to the strong low level inversion, increasing the water vapor has apparently caused the bulk of the radiation emitted by the atmosphere and sensed theoretically by satellite to originate from sources whose temperatures are warmer than the earth's surface.

The effect of increasing the water vapor on transmittance is similar to the impact on surface emission. It's important to note that transmittance decreased by approximately 3% per 25% increase in the mixing ratio. Although the CH04 wavenumber band is less sensitive to attenuation from water vapor than other regions of the IR spectrum, a sensitivity does exist.

4.3.4.2.2 RH 10% and 100%:

The previous cases comparing various increases of mixing ratio were realistic in the sense that doing so maintained the integrity of the atmosphere. For example, an atmosphere under the same weather regime in a more moist environment could feasibly have the same vertical profiles as the increased mixing ratio simulations. However, it would be interesting to see how the surface emission, total radiance, and transmittance might fluctuate between 2 extreme conditions. This is precisely why figures 4.8 thru 4.10,
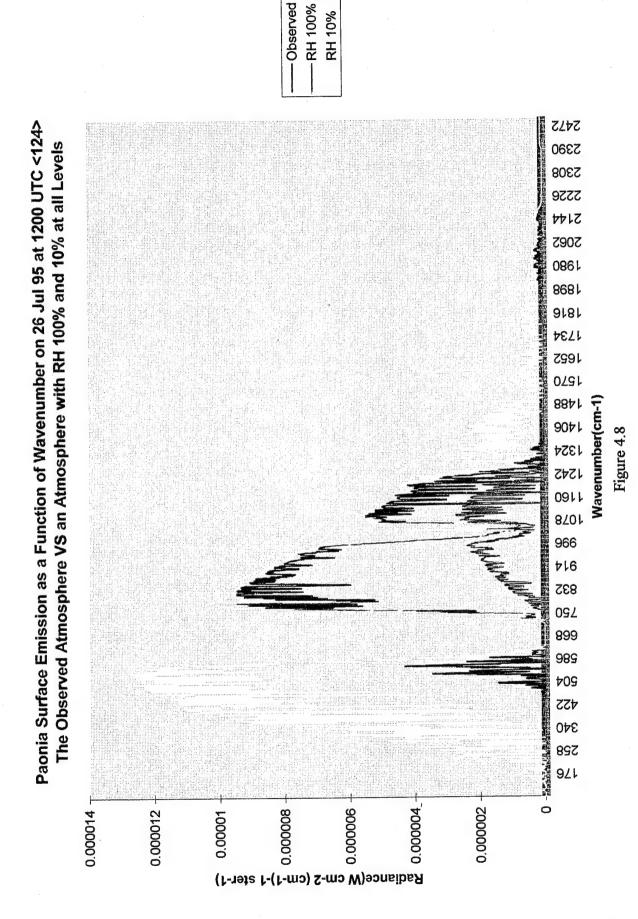
comparing the Paonia atmosphere with an atmosphere having 100% and 10% RH at all levels, were constructed.

A dramatic decrease in the surface emission and the transmittance occurs when the RH of the atmosphere is increased to 100%. The only significant surface emissions occur in the atmospheric window although these emissions are greatly reduce. Noticeable changes in the surface emission are evident when the RH of the atmosphere is reduced to 10%. Significant increases in surface emissions occur throughout the spectrum except in the atmospheric window, carbon dioxide absorption band, and the low energy region. The small increase in radiance in the atmospheric window implies that the "observed" atmosphere is relatively dry as indicated in figure 4.1.

The extremes (10% and 100% RH) have a similar effect on transmittance. Note how the transmittance in the CH04 band approaches 100% when the RH is 10%. Also note the regions of high transmittance over the entire right wing of the spectrum. Although the transmittance is high, very little radiation is emitted at these wavenumbers.
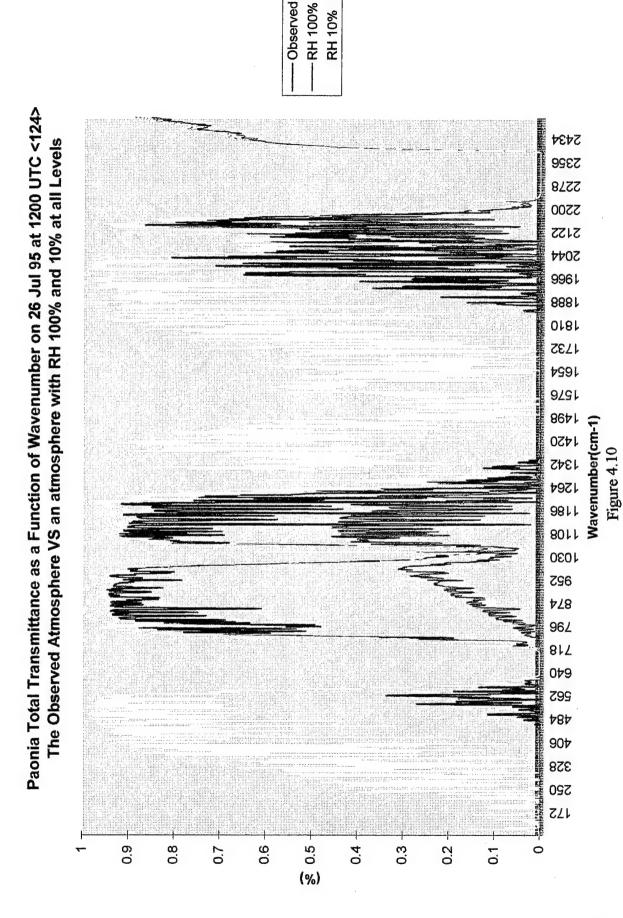
Total radiance changes very little between the two extremes except near the wings of the spectrum where total radiance increases with decreased RH. However, the total radiance for the case where RH = 100% is approximately 3.5% greater than that of the RH = 10% case. Again, this is due to the effects of the low level inversion as the bulk of the atmospheric emissions reaching the satellite are originating from water vapor molecules within the temperature inversion.

Paonia Surface Emission as a Function of Wavenumber on 26 Jul 95 at 1200 UTC <124> The Observed Atmosphere VS an Atmosphere with RH 100% and 10% at all Levels

Figure 4.8

44

Paonia Total Radiance as a Function of Wavenumber on 26 Jul 95 at 1200 <124>
The Observed Atmosphere VS an Atmosphere with 100% RH and 10% at all Levels

Figure 4.9

45

Paonia Total Transmittance as a Function of Wavenumber on 26 Jul 95 at 1200 UTC <124>
The Observed Atmosphere VS an atmosphere with RH 100% and 10% at all Levels

Figure 4.10

4.3.4.3 Angle

Figures 4.11 through 4.13 compare the sensitivity of surface emission, total radiance, and transmittance, respectively, by changing the viewing angle of the satellite - from 180 to 124 degrees.

When the satellite is directly overhead (180) versus at 124 degrees, the amount of surface emission reaching the sensor is only slightly greater. At 936 cm^{-1} the surface emission increases to 8.09 x 10^{-6} and increase of 2.8 x 10^{-6} or an increase of 3.6%.

Changing the zenith angle had little impact on total radiance -- the total radiance values retrieved were approximately the same throughout the atmospheric window portion of the spectrum. Although the surface emission decreased with the increased zenith angle, the radiation sensed from the atmosphere increased. When the satellite was directly overhead the transmittance was increased by 3.3%. Next a more quantitative evaluation of the relationship between the brightness temperature sensed by the satellite and the temperature at the earth's surface is performed.

4.4 Quantitative Evaluation

As previously discussed the amount of radiance reaching a satellite comes from two sources: the radiance emitted from the earth's surface plus the radiance emitted by the atmosphere as defined by the Radiative Transfer equation.

$$B_\nu(T_{SAT}) = B_\nu(T_{SFC})\mathfrak{I}_{SFC} + \int_{\mathfrak{I}=1}^{\mathfrak{I}=\mathfrak{I}_{SFC}} B_\nu(T_{ATM})d\,\mathfrak{I}_{ATM} \qquad (4.1)$$

Paonia Surface Emission as a Function of Wavenumber on 26 Jul 95 at 1200 UTC
Angle Comparison

Figure 4.11

48

Paonia Total Radiance as a Function of Wavenumber on 26 Jul 95 at 1200 UTC
Angle Comparison

Figure 4.12

49

Paonia Total Transmittance as a Function of Wavenumber on 26 Jul 95 at 1200 UTC
Angle Comparison

Figure 4.13

50

From the previous graphic analysis, it's clear that the total radiance and surface emission increased relatively linearly from 980 cm-1 to 892 cm-1; hence, a further simplification is made in this analysis by using the mean wavenumber of this narrow band.

Using the mean wavenumber (936 cm-1) of the CH04 band we can derive the following from the MODTRAN3 output:

$B_\gamma(T_{SAT})$ = the total radiance

$B_\gamma(T_{SFC})\mathcal{J}_{SFC}$ = the surface emission (The amount of radiation emitted by the earth's surface reaching the satellite sensor.)

$B_\gamma(T_{SFC})$ = the surface emission/total transmittance($\mathcal{J}_{SFC}$)

$$\int_{\mathcal{J}=1}^{\mathcal{J}=\mathcal{J}_{SFC}} d\,\mathcal{J}_{ATM} = 1 - \mathcal{J}_{SFC} \tag{4.2}$$

$$B_\gamma(T_{ATM}) = (B_\gamma(T_{SAT}) - B_\gamma(T_{SFC})\mathcal{J}_{SFC})/(1 - \mathcal{J}_{SFC}) \tag{4.3}$$

By inverting the Planck Function and solving for brightness temperature, temperatures were obtained for the different atmospheric moisture profiles derived over Paonia on 26 July 95 at 1200 UTC (See table 4.2). The input surface temperature into MODTRAN3 for the 26 July 95 calculations was 283 K. MR and RH denote the mixing ratio and the relative humidity, respectively.

Table 4.2 Brightness temperatures obtained for the different atmospheric moisture profiles.

	Observed	MR + 25%	MR + 50%	MR + 75%	RH =100%	RH = 10%
T_{SAT}	283.0	283.1	283.2	283.3	285.3	282.8
T_{SFC}	283.0	283.0	283.0	283.0	283.0	283.0
T_{ATM}	283.0	283.8	284.5	284.6	285.3	276.7
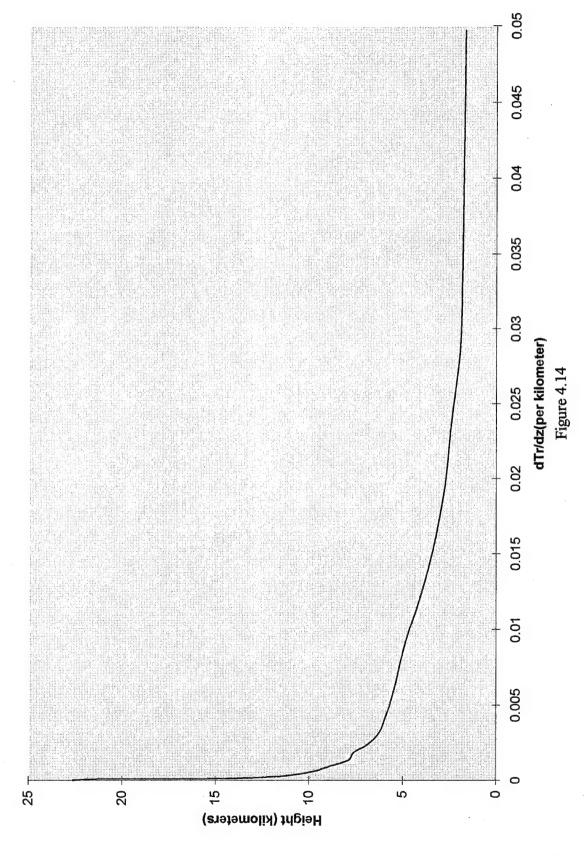
Temperatures were also obtained for the different surface temperatures evaluated at Paonia on 26 July 95 at 1200 UTC (See table 4.3).

Table 4.3 Brightness temperatures obtained for the different surface temperatures.

	T = 273	Observed	T=293
T_{SAT}	273.9	283.0	292.2
T_{SFC}	273.0	283.0	293.0
T_{ATM}	282.5	282.7	283.3

It's apparent that the bulk of the radiance emitted by the atmosphere, T_{ATM}, is originating from near the earth's surface. Figure 4.14 demonstrates why this is the case. Figure 4.14 depicts the change in transmittance with height for the atmosphere over Paonia.

dTr/dz with height over Paonia - 26 Jul 95 at 1200 UTC

Figure 4.14

53

4.5 Discussion

From the analysis up to this point, it's apparent that increased or high water vapor amounts below 500 mb can decrease the satellite's ability to sense the earth's skin surface temperature. However, it's also evident that under an airmass such as that existing over Colorado on 26 Jul 95 at 1200 UTC, atmospheric temperatures in the lower levels above the surface which are greater than the temperature at the surface, can actually decrease the difference between T_{SAT} and T_{SFC}. The quantitative analysis for the Paonia atmosphere demonstrated that with the satellite located at 124 degrees with respect to Paonia, the difference between T_{SAT} and T_{SFC} was within the 1 degree error of the sensor for the realistic atmospheric water vapor loadings evaluated for the 26 July 95/1200 UTC case. For the observed Paonia conditions approximately 92% of the radiation reaching the satellite originates from the earth's surface with 8% of the radiance originating from the atmosphere. However, the bulk of the radiance originating from the atmosphere occurred in the the lower levels near the earth's surface which resulted in a T_{ATM} which equaled T_{SAT}. Given the described meteorological conditions it's apparent from this analysis that the GOES-8 CH04 sensor can reasonably discern skin surface temperatures.

The brightness and surface temperatures for the observed surface temperature, 283 K, compared better than those for the adjusted surface temperatures, 273 K and 293 K. However, the surface temperature and the brightness temperature for the adjusted surface temperatures were within a degree Kelvin of each other. Changing the surface temperature to 273 K increased the temperature difference between the top of the inversion and the surface by 10 K or by 42%. Modifying the surface temperature to

293 K would have destroyed the inversion near the surface. Both surface temperature modifications create a low level atmospheric profile which is unlikely to occur along the valley floors which will be evaluated later. The temperature lapse rate over Paonia, 55 C km^{-1}, is already quite steep; hence, such increased steepening of the lapse rate near the surface seems unlikely, and considering the weather regimes evaluated destroying the low level inversion would be inappropriate. Even if the two surface temperatures represented the extremes in the satellite derived temperature to actual surface temperature due to variations in the atmospheric profile along the valley floor, GOES-8 should still detect surface temperature gradients. Field studies conducted in the Brush Creek Valley of Colorado found draining gradients ranging from 0.5K km^{-1} to 0.9K km^{-1}, McKee and O'Neal (1989) and Whiteman et al. (1989). The greatest limitation then to assessing the along valley temperature gradients is the resolution of the satellite. In essence, the temperature retrieved from the satellite for a given pixel is the average temperature of the area viewed by the satellite -- in the case of the CH04 sensor, 3.2 km by 6.9 km. Provided the valley under evaluation is wide enough to accommodate the large resolution of the sensor, extensive down-valley surface temperature gradients should be detectable.

Chapter 5

Data Gathering and Manipulation

The next step was to accurately map GOES-8 CH04 satellite imagery to relatively high resolution topographical data and create GIF images from which the nocturnal skin surface temperatures developing along the valley floors could be analyzed for draining or pooling gradients.

5.1 Data Collection

GOES-8 satellite imagery was retrieved via the Cooperative Institute for Research in the Atmosphere (CIRA) archives using the Subsect routine executed on IRIS (Whitcomb et al., 1996). IRIS is a CIRA workstation operating on a DOS/Windows NT platform. SubSect is a routine which can be used to extract a user-defined portion of the full disk GOES-8 image, referred to as a sub-sector, and generates the user-defined image. Subsect allows any number of sub-sectors to be defined and extracted using the same or a variety of resolutions and channels from GOES Variable (GVAR) formatted imagery files which can be located on up to three different paths. As well, log files are produced to inform the user as to the success and progress of SubSect. Sub-sectors of the Colorado region were retrieved and archived during the summer of 95.

5.2 Selection Process

Daily weather maps and observations were analyzed to determine weather periods in which clear skies and favorable meteorological conditions may have prevailed over the state of Colorado. VIS and IR satellite imagery corresponding to these potentially favorable periods were then displayed and analyzed on IRIS using the Interactive Display Language (IDL), version 4.0, Research Systems Inc. (1995), software and the GVAR View (GVIEW) function to determine whether or not the region was indeed clear, and thus suitable for evaluating skin surface gradients using GOES-8 CH04 imagery. Finding periods which would allow for optimal sensing of skin surface temperatures proved to be a real challenge. As discussed in chapter 3, the conditions of 6 Aug 95 and 31 Aug 95 were not as favorable as those of 26 July 95.

Imagery of the early morning hours (UTC) of 31 Aug 95 was used to evaluate all valley sectors except the Yampa River valley and the Colorado River valley segment between Parachute and GJT. The Yampa area was excluded due to the weak surface cold front which had invaded Northern Colorado and the intermittent patchy cloudiness occurring over the region. Imagery from 6 Aug 95 was used only to evaluate the Yampa River valley sector as satellite imagery indicated that patchy cloudiness was occasionally present over the western region early in the period. Although an effort was made to ensure the absence of cloud cover, some contamination was apparent during the analysis as will be discussed in the following chapter.

5.3 Data Processing

Utilizing an IDL routine called MAP_PATCH, CH04 image data on the selected nights were converted into distinct - earth oriented - latitude, longitude, and image array files. IDL, developed by Research Systems Inc., is a powerful array-oriented graphics package utilized by CIRA to enhance, display, and manipulate satellite and GIF imagery on computer workstations, Dean et al. (1996). IDL is a high level, transportable language having raster image and map coordinate conversion capabilities.

Once created, the latitude, longitude, and image files were ported from IRIS to a UNIX platform, SUN SPARCstation LX. Plotsat was created to map and manipulate the respective GOES-8 channel 04 image files onto 30 second topography data created by the National Geophysical Data Center.

5.4 Code Development

Plotsat, an ANSI C language executable, calls pgplot, version 5.0 (1989), a graphics subroutine library maintained by T.J. Pearson of the California Institute of Technology. Plotsat reads in and manipulates the latitude, longitude, and image file arrays of the respective satellite image and the topography array data over Colorado to be mapped. Plotsat then calls pgplot to graphically map the satellite pixels, represented as trapezoids, using the latitude, longitude, and image files to the topographical data. Pgplot provides the user with a subroutine that allows the user to specify the latitude and longitude of the region to be generated for display. A GIF driver is called to map the subsequent data manipulations onto a GIF image for visual display and analysis. Plotsat incorporates a NOAA/NESDIS look-up table which converts the radiance count to a

brightness temperature. Plotsat retrieves the brightness temperature for each pixel. Plotsat generates a color table which is used by a pgplot routine to color fill the trapezoids (satellite pixels) based on their respective brightness temperatures. Plotsat also utilizes another pgplot routine to inscribe the corresponding pixel's brightness temperature to each computer generated trapezoid. Plotsat then calls yet another pgplot routine to plot elevation contours, in 152.4 m (500 feet) increments, onto the image. Using pgplot a latitude and longitude grid is also overlaid onto the mapping. Pgplot also allows for the plotting of various symbols onto the computer generated image to allow for the emphasizing of certain locations. Once created the GIF images may be displayed or printed.

5.5 Product

The Plotsat program generates GIF image products such as that shown in figure 5.1, depicting a section of the North Fork of the Gunnison Valley extending Northeastward from the town of Paonia. The GIF image was printed in black and white so each pixel brightness temperature (Kelvin) is represented by a different gray shade. Brightness temperature values are represented in degrees Kelvin truncated to the nearest tenth of a degree.
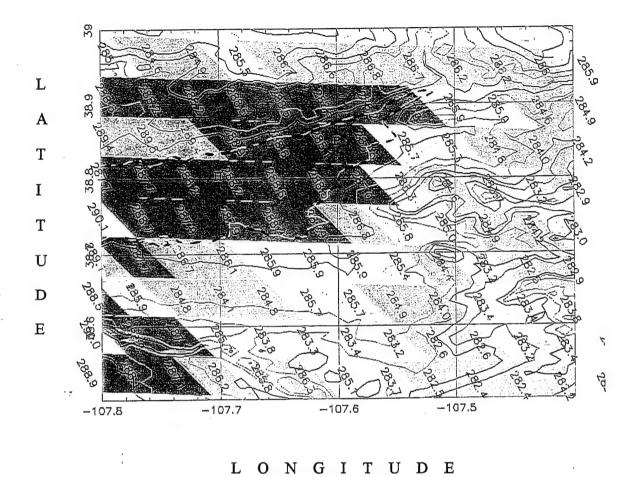
Figure 5.1 Elevation contours are in 152.4 m intervals (500 feet) from 1829 m (6,000 feet) represented by the dashed contour to 3353 m (11,000 feet). **P** and **H** represent the approximate locations of the towns of Paonia and Hotchkiss, respectively. The parallelograms represent the actual satellite pixel and the absolute temperatures inscribed within are in degrees Kelvin.

The computer generated GIF images were verified by checking the location of key terrain figures for a given image with that of the original satellite image displayed on IDL using the GVIEW function. The pixel mappings were checked by using satellite imagery in which clouds were present. A comparison in the location of the examined cloud pixels

was made between those depicted on the GIF images produced by Plotsat and the original image displayed on IDL using the GVIEW function (Dean et al., 1996). The plotted elevation contours were compared to USGS 71/2 minute maps of the selected valleys to be evaluated. Overall, no errors were found in the mapping of the topographical data nor satellite imagery.

5.6 Gradients

To determine whether or not a down-valley temperature gradient exists, these absolute temperatures needed to be transformed in some way into a potential temperature. For example, considering the atmospheric conditions discussed in chapter 3, if two pixels in a valley were examined, with the down-valley pixel having a brightness temperature of 283 K at an elevation of 1800 m while the up-valley pixel has a temperature of 280 K at 2400 m, would this imply a down gradient? If the air up-valley is colder than the air down-valley, the colder air has a higher density and in the absence of other forcings will flow downward into the warmer, less dense air regions. Neglecting the heat exchange associated with conduction, the air flowing down valley from the up valley location is expected to warm at approximately the dry adiabatic lapse rate. Hence, air moving down valley from a level of 2400 m to 1800 m would warm by approximately 6 K. Thus, the up-valley pixel in this example has a potential temperature of 286 K relative to the site at 1800 m. Hence, the up-valley air which is colder in temperature is warmer in potential temperature -- so a thermodynamically-induced down-valley gradient between the two regions doesn't exist.

The method used to place the pixel brightness temperature on an effective

horizontal plane was to convert brightness temperature to potential temperature. A function was written into Plotsat which determined the average height of each pixel.

The average height of the terrain represented in each pixel was derived by dividing the pixel into 8 equal sections. Plotsat then determined the latitude and longitude of each intersection point. Once the latitude and longitude of each point has been determined, Plotsat reads in the corresponding elevation from the topography array. The elevations of all 15 points were then summed and divided by 15 to arrive at an average pixel height.

Now that the height (z) and temperature (T) of each pixel can be derived and equivalent expression for potential temperature, θ, in terms of z and T must be applied since pressure (P) is unknown.

The potential temperature is defined as

$$\theta = T\left(\frac{P_s}{P}\right)^{\frac{R}{c_p}}$$ where R is the gas constant for dry air, c_p is the specific   (5.1)

heat at constant pressure, T is temperature, P is pressure, and P_s is 100kPa (1000 mb).

A relationship between the lapse rate of temperature (the rate of change of temperature with height) and the rate of change of potential temperature can be obtained by taking the logarithm of equation 5.1 and then differentiating with respect to height. Employing the hydrostatic equation and the ideal gas law to simplify the result gives

$$\frac{T}{\theta}\frac{\partial \theta}{\partial z} = \frac{\partial T}{\partial z} + \frac{g}{c_p}$$ (5.2)

In an atmosphere where θ is constant with height

$$\frac{\partial T}{\partial z} = -\frac{g}{c_p}$$ (5.3)

Integrating equation 5.3 from some height z downward to a height of zero gives

the following equation:

$$T(0) = T(z) + \frac{gz}{c_p}.$$

(5.4)

T(0) = θ and is the temperature at an elevation of zero and T(z) is the brightness temperature associated with the respective satellite pixel.

Once Plotsat has determined the average height of each pixel, Plotsat reads the temperature of each pixel and then converts the temperature to potential temperature using equation 5.4. Figure 5.2 depicts the absolute temperatures converted to potential temperature.
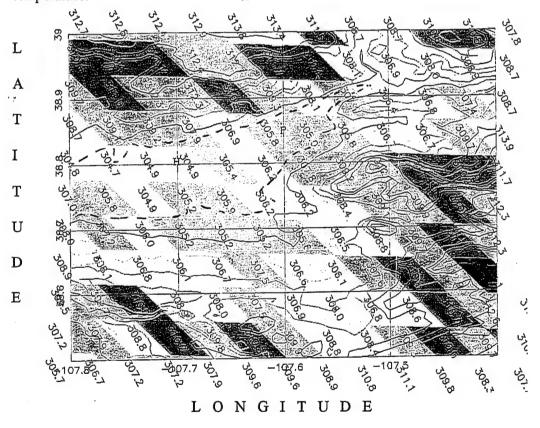
Figure 5.2 The brightness temperatures depicted in figure 5.1 have been converted to potential temperature.

Chapter 6

Analysis

6.1 Method of Analysis

As previously discussed, the resolution of GOES-8 CH04 satellite imagery greatly reduces the number of valleys which can meaningfully be evaluated in Colorado. Furthermore, if a down-valley gradient exists it must be fairly extensive, extending for at least 2 satellites pixels, to be discerned. Even if topographical data indicated that a valley is wide enough to discern, the orientation of the satellite pixels may result in more radiance being sensed from the slopes rising up from the valley floor than from the valley floor itself. An examination of the pixels along the valley floor in figure 5.2 illustrates this problem. Although the valley floor from Paonia westward appears wide enough to allow for sensing of the radiance being emitted from the valley floor, only a couple of the pixels are centered along the valley floor. The rest are sensing, at least partially, radiance along the side slopes. Therefore, care must be taken in choosing pixels which approximate the valley floor when trying to determine whether or not drainage exists in a region. Since colder, denser air, sinks - temperatures along a given valley floor should generally be colder than those along the slopes; thus, the potential temperatures of the pixels partially overlying the slopes will have a warm bias to them. All analysis was performed using the potential temperatures derived in chapter 5, unless otherwise stated.

To allow for the best selection of pixels to evaluate the along valley gradients, two new GIF images , utilizing Plotsat, were created for each valley region being analyzed. These GIF images depict the mean elevation of each pixel and the temperature adjustment made to each pixel, respectively. The two GIF images were created for each valley segment analyzed on 26 July 95 and 31 Aug 95. This was necessary due to a subtle shift in the location of the GOES-8 satellite. Hence, the slight change in the viewing angle resulted in a different representation of the pixels over the region being evaluated. The viewing angle on 26 July 95 was the same as that on 6 Aug 95.

The initial strategy was to produce and analyze GIF images, using Plotsat, for a minimum of two different nights offering favorable meteorological conditions as described in chapter 3. Images from 0315 UTC to 0745 UTC would be produced and analyzed in 1/2 hour time steps. By 0315 UTC, cooling along the valley should be well under way , and by 0745 UTC areas of pooling and draining should be evident.

However, the original plan had to be modified due to a number of the satellite images not being received between 0315 UTC and 0745 UTC on 6 Aug 95 and 31 Aug 95. Thus GIF images produced and analyzed between 0315 UTC and 0745 UTC for 6 Aug 95 were 0315, 0515, 0615, 0715, and 0745 UTC, and on 31 Aug 95 they were 0315, 0345, 0615, 0645, 0715, and 0745 UTC. All the images were available for 26 July 95. Another modification to the initial strategy resulted from the fact that out of the three data sets only one offered clear sky viewing of the Colorado river valley section between Parachute and GJT. Further discussion is provided with the analysis of this region.

Two valley segments along the Gunnison, and one each along the Uncompaghre, Colorado, Yampa, and Arkansas river systems were examined.

In each analysis the GIF images produced by Plotsat from 0315 UTC to 0745 UTC are presented. From these images pixels were chosen along the valley to represent the along valley gradient. A graph is then made depicting the different temperature trends of the selected areas. In a region where draining occurs the up-valley temperature will be colder and vice versa for a region of pooling. The graphs allowed a visualization of the temperature trends. Details of this process are provided in the analysis of each valley section.

6.2 Analysis

Attached to the back of this paper are six appendices. Appendix I contains the GIF images depicting the elevation contours and temperatures of each of the six valley segments analyzed for 26 July 95 from 0315 UTC to 0745 UTC (figures I.1 thru I.60). Appendix II depicts the equivalent GIF images created for 6 Aug 95 and 31 Aug 95 (figures II.1 thru II.29). The GIF images showing the mean elevation derived for each pixel for each of the valley regions evaluated are provided in appendix III for 26 July 95 (figures III-1 thru III-6) and appendix IV for 31 Aug 95 (figures IV-1 thru IV-4). GIF images depicting the temperature adjustment made to each pixel for each of the areas examined are provided in appendix V for 26 July 95 (figures V-1 thru V-6) and appendix VI for 31 Aug 95 (figures VI-1 thru VI-4). Details of the GIF image features such as elevation contour interval, town locations etc. are described at the beginning of each

appendix except in appendices I and II where the description precedes the GIF images representing a particular valley segment.

6.2.1 Gunnison River Valleys

6.2.1.1 Paonia to Delta

Three areas were selected along the valley floor to assist in evaluating whether the valley segment was indicative of pooling or blocking. These three areas are outlined and annotated as X1, X2, and X3 on each of the GIF images presented in this analysis. X1 represents the furthest up valley location, while X2 is down valley from X1 and X3 is the bottom most area along the valley floor.

The valley region extending from Paonia to Orchard City is suspected of being a draining region due to the orchard industry existing within this region. A pooling region is expected to form near the town of Delta as the Uncompahgre river valley and the Gunnison river valley merge and a very narrow constriction in the valley occurs downstream of Delta. Constrictions have been identified as causing areas of pooling to form upstream of them, McKee and O'Neal (1989).

Unfortunately, the resolution of the sensor and the orientation of the satellite pixels prevented an evaluation of the skin surface temperatures near Paonia and further up the valley floor.

6.2.1.1.1 26 July 95 0315 to 0745 (UTC)

In figures I.1 thru I.10, the GIF images depicting the elevation contours and temperatures from 0315 thru 0745 for 26 July 95 are presented. Figures III.1 and V.1 depict the mean elevation of each pixel and the temperature adjustment, respectively. A

graphic representation of the temperature trend of the three outlined areas is depicted in figure 6.1. In figure 6.1, a drainage flow is suggested to occur from near the town of Hotchkiss (X1) down valley to near the Orchard City region (X2). Pooling appears to occur between X2 and the down valley Delta (X3) area. The temperatures at X2 remained warmer than those at X1 throughout the period.

North Fork of the Gunnison Valley Segment Temperature Trend - 26 July 95

Figure 6.1 Temperature trends from 0315 UTC thru 0745 UTC for the Paonia to Delta valley segment.

X2 showed a slight rise in temperature from 0645 to 0745. Between X2 and X3, temperatures along the valley tend to cool, indicative of pooling. By 0745 the cooling rate along the valley appears to be bottoming out. A review of figures I.1 thru I.10 shows the cold pool near Delta expanding throughout the period. The satellite data then suggested

68

draining occurs down valley to near the Orchard City region, while extensive pooling occurs near the town of Delta. A down valley absolute temperature gradient of approximately -0.21 K km^{-1} developed from X1 to X2 during the period.
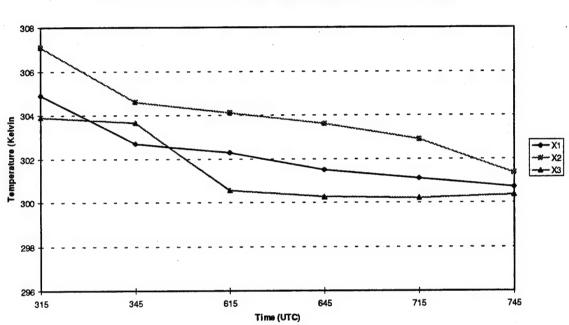
6.2.1.1.2 31 Aug 95 0315 to 0745 (UTC)

In figures II.1 thru II.6, the GIF images depicting the elevation contours and temperatures from 0315 thru 0745 for 26 July 95 are presented. Figures IV-1 and VI-1 depict the mean elevation of each pixel and the temperature adjustment, respectively. An attempt was made to choose three areas corresponding to the areas selected on 26 July 95. However, the location of X1, X2, and X3 differ slightly from those used on 26 July 95 due to the differing pixel orientations. For example, the pixel labeled as X1 on 26 July 95 is oriented in such a way on 31 Aug 95 as to be more representative of the temperature along the slope than that of the valley floor.

A graphic representation of the temperature trend of the three outlined areas is depicted in figure 6.2. Again a drainage flow is suggested to occur down to near the X2 region. Pooling still appears to occur between the X2 and the X3 area.

The analysis indicates a general agreement with the analysis conducted on 26 July 95 as X1 remains colder than X2 and X2 remains warmer than X3. A down valley absolute temperature gradient of approximately -0.21 K km^{-1} developed from X1 to X2 during the period. However, there are some significant differences in the temperature trend. The difference in pixel orientation from that of 26 July 95 and the resulting change in pixel selection could be a contributing factor. The temperature trend indicates that the cooling at X3 bottomed out around 0615 UTC while the cooling continued at X1 and X2.

However, the cooling at X1 appears to be leveling off at 0745, while the cooling rate at X2 accelerates from 0715 to 0745 which suggest that the drainage flow has either abated or weakened substantially.

North Fork of the Gunnison Valley Segment Temperature Trend - 31 Aug 95

Figure 6.2 Temperature trends from 0315 UTC thru 0745 UTC for the Paonia to Delta valley segment.

A review of figures II.1 thru II.6 suggests that the pooling region near Delta has expanded far enough up valley that by 0745 UTC the temperatures at X2 are becoming more characteristic of the cold pool. It's interesting that the cooling at X3 leveled out while the cold pool appears to be expanding further up valley. In later analysis surface temperature gradients from Delta to GJT and from Montrose to Delta are evaluated and perhaps the reason the cooling ended at X3 will become more apparent. Figures II.5 and II.6 suggest some drainage into X3 from the Uncompahgre river valley to the South.

6.2.1.1.3 Summary

In summary, evaluation of the gradient upstream near Paonia is not possible due to the limitations imposed by the satellite's resolution and the narrowness of the valley. The analysis suggests draining occurring along the valley from Hotchkiss to near Orchard City. If draining is occurring through this region, by the law of mass continuity the air that is moving down the valley must be replaced which implies that draining is also occurring upstream towards the Paonia region. However, it appears as though the drainage occurring near X2 on 31 Aug 95 weakened late in the period as the analysis suggested the temperature of the area was becoming more characteristic of the cold pool expanding upstream from the Delta region. The region near Delta, X3, is certainly characteristic of pooling; however, some draining may occur into the southern flank of X3 from the Uncompahgre River Valley.

6.2.1.2 Delta to Grand Junction

Three areas were selected along the valley floor to assist in evaluating whether the valley segment was indicative of pooling or blocking. These three areas are outlined and annotated as X1, X2, and X3 on each of the GIF images presented in this analysis. Again, X1 represents the furthest up valley location while X3 represents the furthest down valley area.

Little is documented about the valley region extending from Delta to GJT. However, as discussed and suggested in the previous analysis, the Delta region is suspected of being one of pooling. Unfortunately, the resolution of the sensor and the

71

orientation of the satellite pixels prevented an evaluation of the skin surface temperatures along the constriction west of Delta.

6.2.1.2.1 26 July 95 0315 to 0745 (UTC)

In figures I.11 thru I.20, the GIF images depicting the elevation contours and temperatures from 0315 thru 0745 for 26 July 95 are presented. Figures III.2 and V.2 depict the mean elevation of each pixel and the temperature adjustment, respectively. A graphic representation of the temperature trend of the three outlined areas is depicted in figure 6.3.

Gunnison River Valley, Delta to GJT, Temperature Trend - 26 July 95

Figure 6.3 Temperature trends from 0315 UTC thru 0745 UTC for the Delta to GJT valley segment.

Figure 6.3 shows X2 remained significantly warmer than the other two regions throughout the period of evaluation. One might expect draining at X2 based on valley

geometry per O'Neil and McKee(1989). The temperature trend of X2 exhibits rises and falls in the temperature profile which may be indicative of periodic draining. A down valley absolute temperature gradient of approximately -0.19 K km^{-1} developed from X1 to X2 during the period.

The rising temperature oscillations which occurred twice at X3 between 0645 through 0745 are not supported by a gradient upstream towards X2. The upstream gradient towards X2 are indicative of pooling at X3. Yet, the temperature of the area rose by nearly half a degree. It's possible smaller scale drainage is occurring which is not detectable by GOES-8; however, a possible draining gradient is apparent to the east (figures I.18 thru I.20), perhaps, originating from the Colorado River Valley which will be examined in a later analysis.

On the other hand, no significant warming, outside the noise threshold of the sensor, occurred at X3. Thus, again, the region near Delta is characteristic of a pooling region.

Figures I.11 thru I.20 suggest some drainage may occur into the Delta region from the Uncompahgre river valley to the south. This valley segment will also be evaluated later in this analysis. On a smaller scale, an area of possible drainage occurs west of Delta, figures I.18 to I.20 suggesting an east to west gradient develops in X1 and extends at least to the pixel located just west of X1 -- west of this region the narrow constriction prevents evaluation of the skin surface gradient. An examination of the mean pixel elevations in figure III.2 shows that westward the average elevation of the pixels increase initially by 22 m. Thus, the pixels west of this region are certainly not representative of the valley floor.

6.2.1.2.2 31 Aug 95 0315 to 0745 (UTC)

In figures II.7 thru II.12, the GIF images depicting the elevation contours and temperatures from 0315 thru 0745 for 31 Aug 95 are presented. Figures IV.2 and VI.2 depict the mean elevation of each pixel and the temperature adjustment, respectively. A graphic representation of the temperature trend of the three outlined areas is depicted in figure 6.4.

Gunnison River Valley, Delta to GJT, Temperature Trend - 31 Aug 95
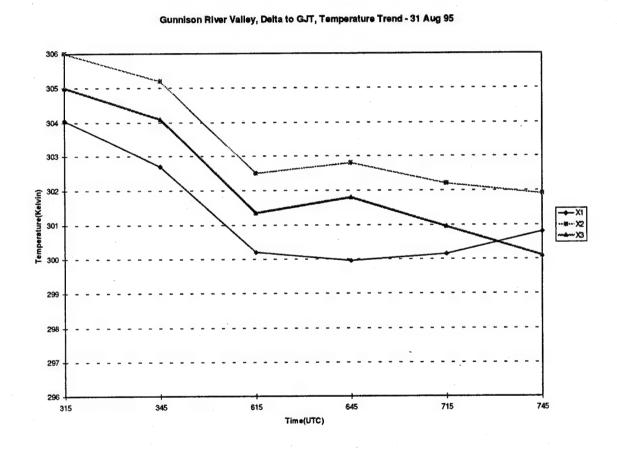
Figure 6.4 Temperature trends from 0315 UTC thru 0745 UTC for the Delta to GJT valley segment.

Once again, X2 remains warmer than X1 and X3 throughout the period, and the temperature warms slightly between 0615 and 0645. A down-valley absolute temperature

gradient of approximately -0.12 K km^{-1} developed from X1 to X2 during the period. X3 also warms between 0615 and 0645; however, no draining originating from the valley to the east of the area is evident during this time. After 0645 the temperature drops steeply at X3 becoming colder than X1. Temperatures actually increased at X1 from 0645 to 0745, significantly, 0.65 degrees, from 0715 to 0745. This rise in temperatures is supported by the apparent stronger drainage from the south at 0715 and 0745, originating from the Uncompahgre river valley (figures II.11 and II.12). Also much like that of 26 July 95, the possibility of drainage is apparent in the gradient just west of Delta, as can be seen in figures II.11 and II.12.

The temperature trend is vastly different from 26 July 95. The cooling rates of X1, X2, and X3 depicted are approximately the same from 0315 thru 0615. Furthermore, the temperature trends at X2 and X3 follow nearly the same pattern from 0315 thru 0715. From 0715 to 0745 the temperatures at X3 become more characteristic of a pooling region perhaps developing downstream towards the town of Fruita.

6.2.1.2.3 Summary

The disparities between the two days could not be completely resolved by the satellite sensor. The differing pixel orientations between the two days and the poorer time scale resolution of 31 Aug 95 could be contributing factors. Another key element perhaps contributing to the temperature trend at X3 is cloud cover apparently existing along the Colorado river valley between Parachute and GJT on 31 Aug 95 -- this will be discussed later in the analysis of this region.

The analysis of both days suggests drainage may develop into the GJT(X3) region from the Colorado river valley. GJT appears to become more characteristic of pooling if this flow isn't established. No drainage is apparent between X2 and GJT. The temperature trend of X2 is suggestive of a region receiving a drainage flow. It appears the area near Delta can receive drainage from the valley to its south; however, upstream of this region along the North Fork of the Gunnison previous analysis indicated this to be a region of pooling which the gradients to the east of Delta (X1) still supports. A possible draining gradient apparently develops from X1 and extends some distance westward into the narrow constriction formed by the Gunnison River. The Gunnison River Valley downstream of this area is far too narrow to be analyzed with GOES-8 imagery. The narrowness of this valley appears to act as a constriction which prevents the efficient drainage of the cold air pool which forms near Delta.

6.2.2 Uncompaghre River Valley - Montrose to Delta

In this section the Uncompaghre River Valley from near Montrose to close to the town of Delta, where the Uncompaghre River merges with the Gunnison River, is analyzed. Five areas were selected along the valley floor to assist in evaluating whether the valley segment was indicative of pooling or blocking. These five areas are outlined and annotated as X1, X2, X3, X4, and X5 on each of the GIF images presented in this analysis.

The wind flow regimes of this valley are unknown except as pointed out in the Paonia to Delta analysis and discussion which stated that the region near Delta is

suspected of being a pooling region. What prompted the evaluation of this valley segment was the draining suggested to occur into Delta from the previous analysis.

6.2.2.1 26 July 95 0315 to 0745 (UTC)

In figures I.21 thru I.30, the GIF images depicting the elevation contours and temperatures from 0315 thru 0745 for 26 July 95 are presented. Figures III.3 and V.3 depict the mean elevation of each pixel and the temperature adjustment, respectively. A graphic representation of the temperature trend of the five outlined areas is depicted in figure 6.5. Figure 6.5, suggests that above Montrose (X1) the temperatures remained warmer than the region just below Montrose (X2) and X2 remained warmer than areas further down the valley throughout the period. Furthermore, after 0345 the region below X2, X3, remained warmer than X4 and the region near Delta (X5). Hence, the along valley gradient from X1 to X3 indicates an absence of draining. The temperatures at X4 are colder than those at X5 from 0315 to 0345 and again from 0545 to 0745 which suggests draining occurred into the valley segment west of Delta during these times. A down valley absolute temperature gradient of approximately -0.17 K km^{-1} developed from X4 to X5 during the period.
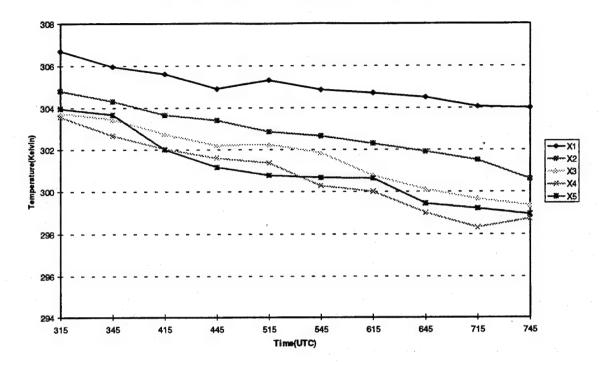
Figure 6.5 Temperature trends from 0315 UTC thru 0745 UTC for the Montrose to Delta valley segment.

The temperature trend suggests a slight warming, 0.4 K, occurred at X1 between 0445 and 0515. The temperature gradients do not suggest draining. However, draining whose detection is beyond the resolution of the sensor to detect could have occurred. The cooling trend at X2 is quite gradual throughout most of the period but accelerates between 0715 and 0745 while the cooling trend at X1 appears to flatten out during this time frame.

The cooling trends of X3 and X4 closely follow the same pattern except between 0715 and 0745 where X4 shows a 0.4 K warming. A down-valley absolute temperature gradient of approximately -0.20 K km^{-1} developed from X4 to X5 during the period. By

mass continuity, air which is departing X4 into X5 must somehow be replaced, perhaps by a draining flow which is undetectable by the sensor.

The cooling trend at X5 from 0345 thru 0445 is suggestive of a pooling region as the temperature drops fairly rapidly; however, the draining suggested by the data to occur between X4 and X5 is responsible for modifying this cooling trend.

In figure 6.5, a large departure between the temperatures at the top of the valley and those near the bottom of the valley is evident. At 0315, the difference was 3.1 K and by 0745 the difference has increased to 5.3 K an increase of 71%.

6.2.2.2 31 Aug 95 0315 to 0745 (UTC)

In figures II.13 thru I.18, the GIF images depicting the elevation contours and temperatures from 0315 thru 0745 for 26 July 95 are presented. Figures IV.3 and VI.3 depict the mean elevation of each pixel and the temperature adjustment, respectively. A graphic representation of the temperature trend of the five outlined areas is depicted in figure 6.6. Figure 6.6 again shows that above Montrose (X1) the temperatures remained warmer than the region just below Montrose (X2) and X2 remained warmer than areas further down the valley throughout the period. However, during this period of evaluation X3 becomes colder than both X4 and the region near Delta (X5) between 0715 to 0745. A down-valley absolute temperature gradient of approximately -0.20 K km^{-1} developed from X4 to X5 during the period. The temperatures at X4 and X5 appear to respond to the subsequent drainage flow by rising 0.7 K and 0.8 K between 0715 and 0745. The temperature trends of X1 and X2 are again suggestive of an undetected drainage flow.

Figure II.18 shows a region up valley to the southwest of X2 which is colder; hence,

drainage from this region could result
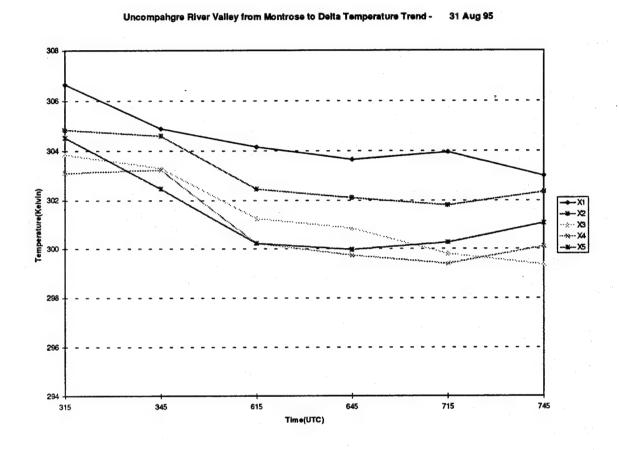
Figure 6.6 Temperature trends from 0315 UTC thru 0745 UTC for the Montrose to Delta
valley segment.

and account for the 0.55 K warming which occurred between 0715 to 0745. However,

no cooler temperatures are seen upstream of X1. The temperature difference between the

upper valley and the lower valley region is not as great as at 0745 as on 26 July as a result

of the warming experienced at X4 and X5 and the temperature drop of 0.95 K

experienced at X1 between 0715 and 0745.

6.2.2.3 Summary

This analysis coupled with the previous Gunnison River evaluations suggests that although pooling exists east of Delta, a drainage does indeed develop into the region south of Delta which originates from the Uncompahgre river valley. Although, it wasn't discussed in this section, it is also apparent that an east to west drainage develops in area X5 leading into the downstream constriction. On the large scale, along the major axis of the river valley between X1 and X3 the gradient is suggestive of a pooling region. However, the temperature trend suggests smaller scale drainages may be occurring which are not detectable due to the resolution of the satellite.

6.2.3 Colorado River Valley - Parachute to GJT

In this section the Colorado River Valley from around the town of Parachute to near GJT where the Gunnison River merges with the Colorado River is analyzed. The draining suggested to occur into the GJT region from the Colorado River valley during the Delta to GJT analysis prompted the evaluation of this region. Unlike the other valley segments in which two days were evaluated, only one day was evaluated, 26 July 95. For the reasons discussed in chapter 3, 6 Aug 95 couldn't be evaluated due to cloud cover. Although a review of the satellite images from 31 Aug 95 displayed on IRIS with GVIEW appeared clear the GIF images created utilizing Plotsat, see figure 6.7, indicated that clouds were indeed present.
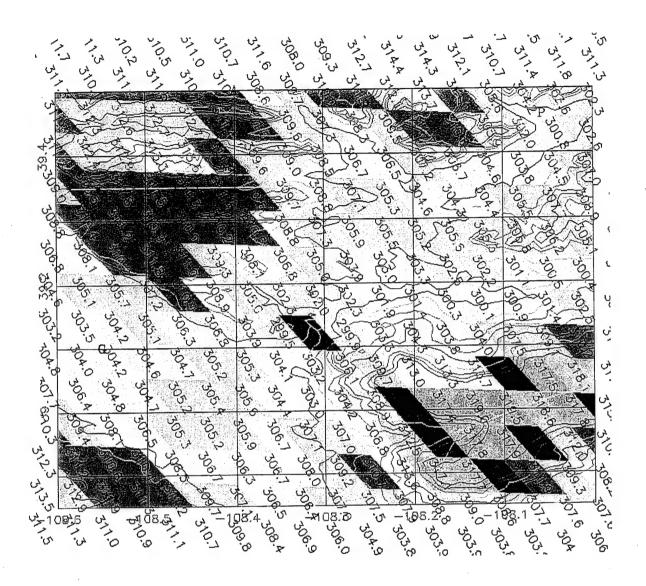
Figure 6.7 Depicts the valley segment evaluated between GJT(G) and Parachute(P) on 31 Aug 95 at 0345 (UTC). From this figure it is clear that the satellite is sensing radiance from some medium other than just the earth's surface. Note the temperatures along the constriction east of GJT -- these temperatures are 10K colder than they were at 0315. The temperatures further eastward and along the ridges are also far cooler than they should be.

Three areas were selected along the valley floor to assist in evaluating whether valley segments are indicative of pooling or draining. The three areas are outlined on each of the images presented in this analysis and annotated as X1, X2, and X3.

The research of Neff and King(1989) shows the region above DeBeque Canyon, evaluated as X1 in this paper, to be one of pooling. The narrow constriction between X1 and X2 in this analysis is known as DeBeque Canyon. Their research shows that the pooling region eventually reaches a depth where it flows over the downstream topography, into the Grand Junction area.

6.3.1 26 July 95 0315 to 0745 (UTC)

Figures I.31 thru I.40, the GIF images depicting the elevation contours and temperatures from 0315 thru 0745 for 26 July 95 are presented. Figures III.4 and V.4 depict the mean elevation of each pixel and the temperature adjustment, respectively. A graphic representation of the temperature trend of the three outlined areas is depicted in figure 6.8.

A review of figures I.31 thru I.40 strongly suggests that the up valley region (X1) is a region of pooling; whereas X2 and the region near GJT (X3) are regions which experience draining. The temperature trends in figure 6.9 indicate that although X3 and X2 were initially cooler than X1, the rapid cooling rate of X1 made it the coldest region along the valley segment sometime between 0515 and 0545. By the end of the period a down valley temperature gradient is apparent. A down valley absolute temperature gradient of approximately -0.16 K km^{-1} and -0.22 K km^{-1} developed from X1 to X2 and between X2 and X3, respectively, during the period.

Colorado River Valley Between Parachute and GJT Temperature Trend - 26 Jul 95
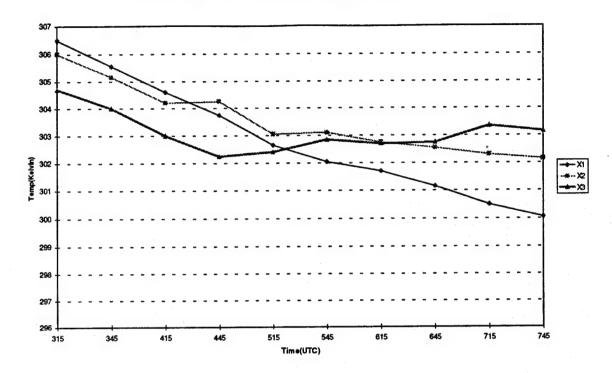
Figure 6.8 Temperature trends from 0315 UTC thru 0745 UTC for the Parachute to GJT valley segment.

6.2.3.2 Summary

The analysis suggests that pooling occurs near X1 and that a draining flow develops from this region downstream through X2 and X3.

6.2.4 Yampa River Valley

In this section the Yampa river valley from near the town of Steamboat westward past the town of Milner is examined. Four areas were selected along the valley floor to assist in evaluating whether the valley segment was indicative of pooling or blocking.

These four areas are outlined and annotated as X1, X2, X3, and X4 on each of the GIF images presented in this analysis.

The only documented evidence of this region applies to the area near the town of Steamboat. Research conducted by Whiteman (1980) and McKee and O'Neal (1989) both found this region to be one in which the air pools.

6.2.4.1 26 July 95 0315 to 0745 (UTC)

In figures I.41 thru I.50, the GIF images depicting the elevation contours and temperatures from 0315 thru 0745 for 26 July 95 are presented. Figures III.5 and V.5 depict the mean elevation of each pixel and the temperature adjustment, respectively. A graph of the temperature trend of the four outlined areas is depicted in figure 6.9.
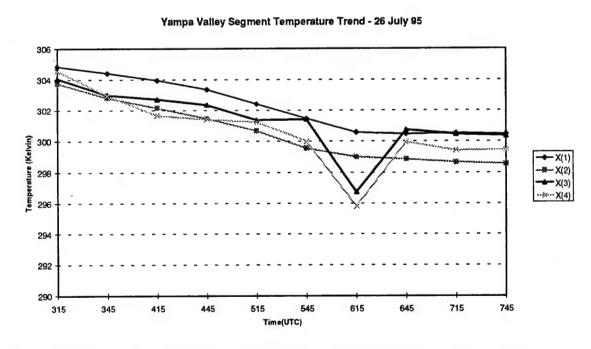
Figure 6.9 Temperature trends from 0315 UTC thru 0745 UTC for the Yampa valley segment.

A review of figures I.41 through I.50 indicate the entire region to be one of pooling with the possible exception of X3, located to the west of Milner, where some minor drainage may occur through the constriction from the cold pool near Milner. The temperature trend depicted on figure 6.9 indicates impairment of the sensor's ability to measure the skin surface temperature at 0615 over areas X3 and X4. This is probably due to some airborne smoke or thin or small cloud elements within the pixel area. Other than this anomaly no significant oscillations in the temperature occurred. X2 generally had the coldest temperatures while X1 had the warmest temperatures throughout the period.

6.2.4.2 6 Aug 95 0315 to 0745 (UTC)

In figures II.19 thru I.23, the GIF images depicting the elevation contours and temperatures from 0315 thru 0745 for 6 Aug 95 are presented. Figures IV.4 and VI.4 depict the mean elevation of each pixel and the temperature adjustment, respectively. A graph of the temperature trend of the four outlined areas is depicted in figure 6.10.

The same trend of 26 July 95 is apparent in the 6 Aug 95 analysis. Overall, the temperature at X1 again tended to be the warmest, followed by X3 then X4, while the temperature at X2 tended to be the coldest. A down-valley absolute temperature gradient of approximately -0.17 K km^{-1} developed from X2 to X3 during the period.

Yampa Valley Segment Temperature Trend - 6 Aug 95
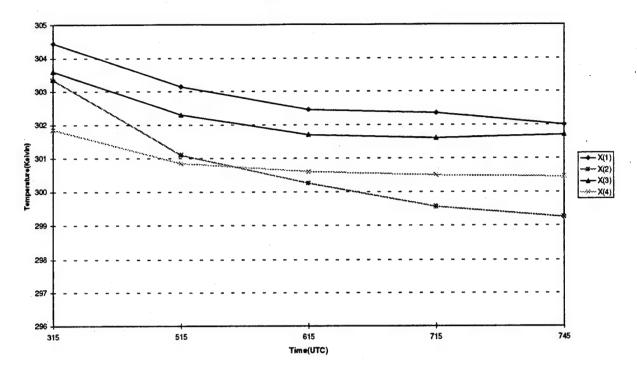
Figure 6.10 Temperature trends from 0315 UTC thru 0745 UTC for the Yampa valley segment.

6.2.4.3 Summary

The data clearly suggests that this region is a pooling region with perhaps a weak drainage flow making it through the constriction west of Milner into X(3); however, since the elevation difference between X(2) and X(3) is slight, approximately 46 m, significant warming wouldn't occur.

6.2.5 Arkansas River Valley - Leadville to Salida

In this section the Arkansas River Valley from near the town of Leadville down valley to near the town of Salida is evaluated. Five areas were selected along the valley floor to assist in evaluating whether the valley segment was indicative of pooling or

87

draining. These three five are outlined and annotated as X1, X2, X3, X4, and X5 on each of the GIF images presented in this analysis.

Little is documented about the valley region extending from Leadville to Salida. However, the flow path of the Arkansas River for up valley near the town of Leadville down stream to near Buena Vista is relatively straight suggesting, by the research of McKee and O'Neal, the occurrence of drainage flow along this segment of the valley. However, downstream from Buena Vista the river forms two bends, one just below Buena Vista and one above Salida as the river flows southeastward. These bends may induce a regions of pooling by restricting the rate in which the air up-valley can flow downward.

6.2.5.1 26 July 95 0315 to 0745 (UTC)

The GIF images depicting the elevation contours and temperatures from 0315 thru 0745 for 26 July 95 are presented in figures I.51 thru I.60. Figures III.6 and V.6 depict the mean elevation of each pixel and the temperature adjustment, respectively. A graphic representation of the temperature trend of the five outlined areas is depicted in figure 6.11.

A review of figures I.51 through I.60 suggests draining occurs from near Leadville (X1) down valley to near Buena Vista(X2) while pooling appears to occur between X2 and the region further down valley at X3. Draining is suggested between X3 and the area above Salida, X4 while pooling again occurs between X4 and the Salida region (X5).

Arkansas River Valley from Leadville to Salida Temperature Trend, 26 Jul 95
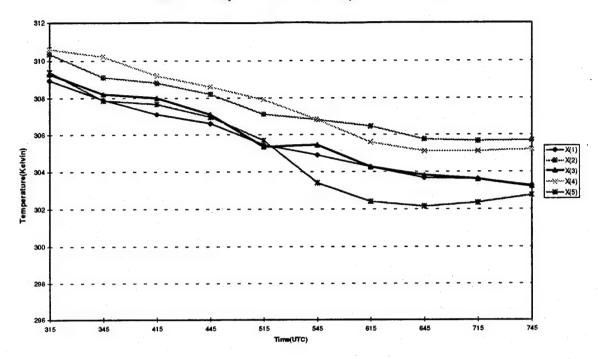
Figure 6.11 Temperature trends from 0315 UTC thru 0745 UTC for the Leadville to Salida valley segment.

The temperature trends of figure 6.11 suggests the same scenario. The temperature of X1 decreases relatively steadily through 0645, from 0645 the cooling rate tends to flatten out. The temperature at X1 remains colder than X2 throughout the period. The two areas, X2, near Buena Vista, and X4, above Salida, where the gradients suggested draining, remain potentially the warmest regions along the valley throughout the period.
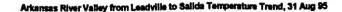
The area down valley from Buena Vista, X3, where pooling is suggested becomes more characteristic of the temperature trend of X1 after 0545. The coldest region, in terms of potential temperature, was the Salida area, X5, where temperatures fell approximately 7 K

from 0315 to 0645. However, the temperature trend does show a slight warming of this area from 0645 thru 0745. Perhaps the slight increase in temperature is due to a weakening or shifting of the cold pool. A down valley absolute temperature gradient of approximately -0.26 K km^{-1} and -0.25 K km^{-1} developed from X1 to X2 and between X3 and X4, respectively, during the period.

6.2.5.2 31 Aug 95 0315 to 0745 (UTC)

The GIF images depicting the elevation contours and temperatures from 0315 thru 0745 for 31 Aug 95 are presented in figures II.24 thru II.29. Figures IV.5 and VI.5 depict the mean elevation of each pixel and the temperature adjustment, respectively. A graphic representation of the temperature trend of the five outlined areas is depicted in figure 6.12.

Again, due to the different orientation of the pixels on 31 Aug 95 from 26 July 95 different pixels had to be selected to represent the valley floor. At 0315, there appears to be some type of contamination occurring between the satellite sensor and the earth's surface preventing the satellite from accurately sensing the skin surface temperature as the temperature at X5 is far colder than would be expected. A review of figures II.24 through II.29 suggest the regions of pooling and draining are more sporadic than on 26 July 95. Draining from X1 to X2 is suggested to occur from 0315 thru 0615 and 0715 thru 0745 only. X3 remains cooler than X2 throughout the period. X4 is occasionally colder than X3. In general, X5 remains colder than the upstream locations; however, the temperature trend again shows warming between 0715 to 0745.
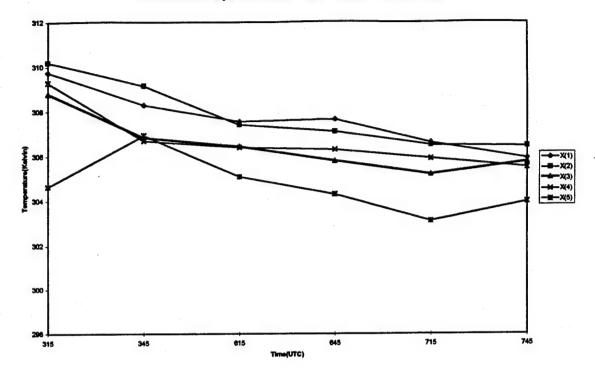
Figure 6.12 Temperature trends from 0315 UTC thru 0745 UTC for the Leadville to Salida valley segment.

6.2.5.3 Summary

It's apparent that the 26 July 95 data were cleaner than that of the 31 Aug 95. Although in general, the trend of the two days were in agreement. Specifically, draining tends to occur between X1 and X2, pooling is evident between X2 and X3, draining is suggested between X3 and X4 and pooling appears to occur between X4 and X5.

6.3 Discussion

Although this analysis suggests that GOES-8 imagery can be used to infer regions of pooling and draining, an accurate measure of the gradients which form along the valley floor cannot be discerned. These gradients were much smaller (-0.12 K km^{-1} to

91

-0.26 K km^{-1}) than those found along the Brush Creek Valley (0.5 K km^{-1} to 0.9 K km^{-1}) axis. Although the temperature gradients observed at Brush Creek may indeed be larger than those of the valleys evaluated in this paper due to differences in valley geometry, smoothing of the gradient could be expected due to the oversampling performed by the satellite. Furthermore, biases to the temperature gradients were also likely imparted as a result of the methodology employed. For example, although relatively wide Colorado valleys were selected for the analysis, and regions along the valley floor were carefully chosen to represent the gradient, a warm bias in the narrower upper valley reaches was likely imparted to the pixels representing the valley floor. The warm bias was due to the pixels overlapping the valley slopes, whereas at the bottom of the valleys, the valley floor was generally wide enough so no overlap occurred.

Although it's apparent that the method employed is limited in the sense that the gradients observed along the valley floors evaluated cannot be accurately quantified, the satellite inferred regions of draining and pooling are consistent with the available documented evidence.

The evidence that is available suggests pooling occurs near Delta due to the downstream constriction (McKee and O'Neal, 1989); in the Yampa Valley near the town of Steamboat, (Whiteman, 1980 and McKee and O'Neal, 1989); and above the De Beque Canyon east of GJT (Neff and King, 1989). Also, the two bends occurring along the Arkansas River, one below Buena Vista and the other above Salida would be suggestive of pooling (McKee and O'Neal, 1989). This evidence supports the analysis conducted in chapter 6 indicating that pooling occurred in all these regions.

Evidence suggests that draining occurs from above De Beque Canyon into the GJT area when overflow occurs as observed by Neff and King (1989), along the North Fork of the Gunnison from Paonia downstream to near Orchard City as suggested by the orchard industry which exists in this region, and along the Arkansas River from near Leadville downstream to Buena Vista as suggested by the topography of the region (McKee and O'Neal, 1989). The satellite derived temperature gradients presented in this chapter are consistent with this evidence.

Although the resolution of the satellite limits the valleys which can be evaluated, and reduces the discernible detail of the down valley gradients which form, the above evidence suggests that the process employed may be useful in determining large scale regions of pooling and draining in valleys which are wide enough to be discerned by the satellite sensor.

Chapter 7

Conclusion and Suggestions for Future Research

7.1 Conclusions from Research

The focus of this research was to assess the feasibility of employing GOES-8 satellite imagery to infer regions of pooling and draining along inner-mountain valley floors.

Utilizing a computer model, an analysis using the radiative transfer equation was performed. This analysis demonstrated that during the night, under stable conditions, clear skies, and weak large scale forcings the GOES-8 channel 04 sensor could be employed to discern these along valley temperatures. The analysis demonstrated that over a suitably defined atmosphere over Paonia, Colorado approximately 92% of the radiance sensed by the satellite originated from the earth's surface. Although 8% of the radiance originated from the atmosphere, the strongest emissions originated from within the inversion near the earth's surface. This simulation produced a satellite brightness temperature which correlated exactly with the 283 K surface temperature inputted into the model. The greatest limitation found to using the GOES-8 channel 04 satellite imagery to discern the along valley temperature gradient was its resolution of approximately 3.2 by 6.9 km over Colorado.

Three days offering favorable meteorological conditions between 0315 UTC and 0745 UTC were selected to evaluate the GOES-8 satellite sensors ability to discern

regions of pooling and draining along six relatively wide inner-mountain valley segments in Colorado.

A computer program was developed which retrieved the brightness temperatures of each satellite pixel, converted these temperatures to potential temperatures and then mapped the pixels with their respective potential temperature onto 30 second topography data of the selected valley floor. Areas representing the temperature profile along each valley floor were then selected and the temperature trends of these areas graphed from 0315 UTC through 0745 UTC.

An analysis of the potential temperature gradients and temperature trends inferred from the satellite suggested regions of draining and pooling in the six Colorado valley segments examined. In valley segments in which the temperature trend and horizontal temperature profiles suggested a draining flow, temperature gradients were much smaller (-0.12 K km^{-1} to -0.26 K km^{-1}) than those observed for the Brush Creek field study (-0.5 K km^{-1} to -0.9 K km^{-1}). Although the temperature gradients observed at Brush Creek may indeed be larger than those of the valleys evaluated in this paper due to differences in valley geometry, smoothing of the gradient could be expected due to the oversampling performed by the satellite. Furthermore, biases to the temperature gradients were also likely imparted as a result of the methodology employed. For example, although relatively wide Colorado valleys were selected for the analysis, and regions along the valley floor were carefully chosen to represent the gradient, a warm bias in the narrower upper valley reaches was likely imparted to the pixels representing the valley floor. The warm bias was

due to the pixels overlapping the valley slopes, whereas at the bottom of the valleys, the valley floor was generally wide enough so no overlap occurred.

Although it's apparent that the method employed is limited in the sense that the gradients observed along the valley floors evaluated cannot be accurately quantified, the satellite inferred regions of draining and pooling are consistent with the available documented evidence. Hence, the use of GOES-8 channel 04 satellite imagery to infer whether inner-mountain valley segments, wide enough to be discerned by the satellite, nocturnally pool or drain appears promising.

7.2 Suggestions for Future Research

Field measurements of the along valley surface temperature and wind flow of the selected valleys should be performed on nights when favorable meteorological conditions exist to quantify the gradients which develop along the valley floor. The data gathered from these field sites should then be compared with the processed satellite data to determine the extent in which smoothing occurred using this methodology. Furthermore, the incorporation of polar orbiting satellite imagery into the analysis should enhance the ability to discern smaller scale draining and pooling regions and perhaps allow for a more accurate determination of the existing surface gradients.

Chapter 8

REFERENCES

IDL User's Guide. Version 4. Research Systems Inc, Boulder, Colorado, 1995.

MODTRAN3 Beta-TEST Version 1.21 User Instructions & Comments, Air Force Geophysics Laboratory, Hanscom AFB, Massachusetts, 1995.

PGPLOT Graphics Subroutine Library, T.J. Pearson, California Institute of Technology, Pasadena, California, 1989.

User's Guide to LOWTRAN 7, Air Force Geophysics Laboratory, Hanscom AFB, Massachusetts, 1988.

Clements, William E., J. A. Archuleta and P. H. Gudikson, 1989: Experimental design of the 1984 ASCOT field study. *J. Appl. Meteor.,* **28**, 000-000.

Dean, K., K. Eis, T. Vonder Haar, 1996: GVAR image application in interactive data language. 12th International Conference on Interactive Information and Process Systems for Meteorology, Oceanography, and Hydrology, January 28 - February 2, 1996, Atlanta, Georgia, American Meteorological Society, 462-465.

Egger, J., 1987: Simple models of the valley-plain circulation. Part I: Minimum resolution model. Part II: Flow resolving model. *Meteor. Atmos. Physics,* **36**, 231-254.

McKee, T. B., R. D. O'Neal, 1989: The role of valley geometry and energy budget in the formation of nocturnal valley winds. *J. Appl. Meteor.,* **28**, 445-456.

McNider, R. T., and R. A. Pielke, 1984: Numerical simulation of slope and mountain flows. *J. Climate Appl. Meteor.,* **23**, 1441-1453.

Neff, W. D. and C.W. King, 1989: The accumulation and Pooling of Drainage Flows in a Large Basin. *J. Appl. Meteor.,* **28**, 518-529.

Petkovsek, Z., 1978: Relief meteorologically relevant characteristics of basins. *Z Meteor.,* 333-340.
_____, 1980: Additional relief meteorologically relevant characteristics of basins. *Z Meteor.,* 379-382.

Steinacker, R., 1984: Area-height distribution of a valley and its relation to the valley wind. *Contrib. Atmos. Physics*, **51(1)**, 64-71.

Vergeiner, I., 1987: An elementary valley wind model. *Meteor. Atmos. Physics*, **36**, 255-263.

____, and E. Dreiseitl, 1987: Valley winds and slope winds--Observations and elementary thoughts. *Meteor. Atmos. Physics*, **36**, 264-268.

____, ____ and C.D. Whiteman, 1987: Dynamics of katabatic winds in Colorado's Brush Creek Valley. *J. Atmos. Sci.*, **44(1)**, 148-157.

Wagner, A., 1938: Theorie and Beobachtung der peiodischen gebirgswinde. *Gerlands Beitr. Geophys.*, **52**, 408-449.

Whitcomb, D., R. Gartner, K. Eis, T. Vonder Haar, 1996: GOES I-M data collection software and algorithms. 12th International Conference on Interactive Information and Process Systems for Meteorology, Oceanography, and Hydrology, January 28 - February 2, 1996, Atlanta, Georgia, American Meteorological Society, 472-475.

Whiteman, C.D., 1980: Breakup of temperature inversions in Colorado mountain valleys, Ph. D. dissertation, Colorado State University.

____, 1982: Breakup of temperature inversions in deep mountain valleys. Part 1: Observations. *J. Appl. Meteor.*, **21(3)**, 270-289.

____, K.J. Allwine, M. M. Orgill, L. J. Fritschen and J. R. Simpson, 1989: Deep valley radiation and surface energy budget microclimates. Part II: Energy budget. *J. Appl. Meteor., 000-000*.

Yamada, T., S. Bunker, 1989: A numerical model study of nocturnal drainage flows with strong wind and temperature gradients. *J. Appl. Meteor.*, **28**, 545-554.

Appendix I

GIF IMAGES FOR 26 JULY 95 DEPICTING THE POTENTIAL TEMPERATURES AND TOPOGRAPHY OF SELECTED VALLEY REGIONS

A. Paonia to Delta
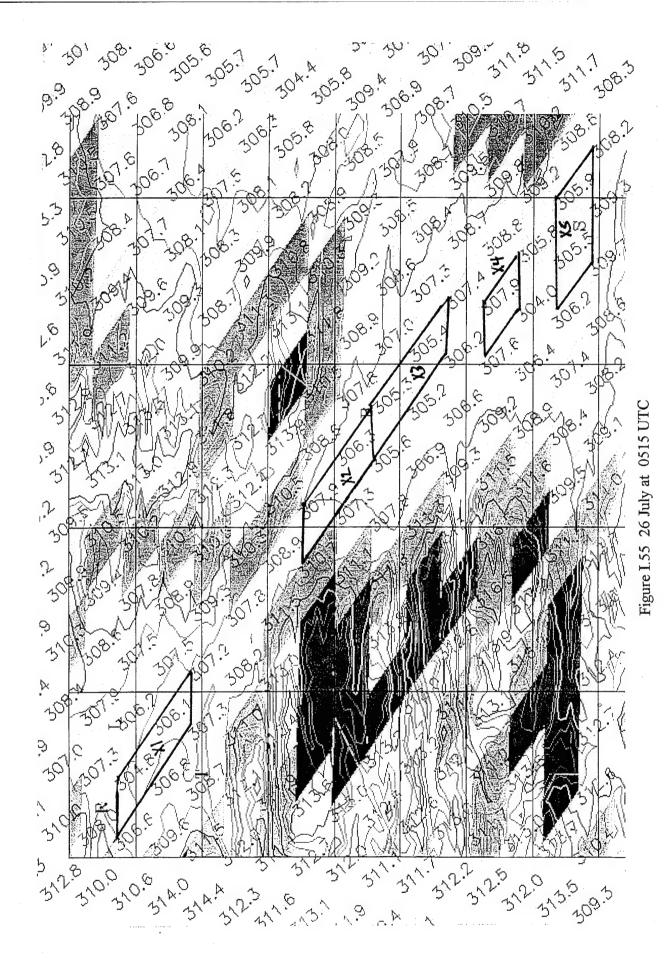
Figures I.1 through I.10 depict the potential temperatures of the Paonia to Delta region. The letters P, H, C, O and D depict the approximate locations of the towns of Paonia, Hotchkiss, Cedaredge, Orchard City , and Delta, respectively. Elevation contours are from 1524 meters (5000 feet) to 3353 meters (11000 feet) in 152.4 meter (500 feet) intervals. Three areas were selected along the valley floor to assist in evaluating whether the valley segments were indicative of pooling or draining. These regions are outlined in bold and labeled X(1) through X(3).
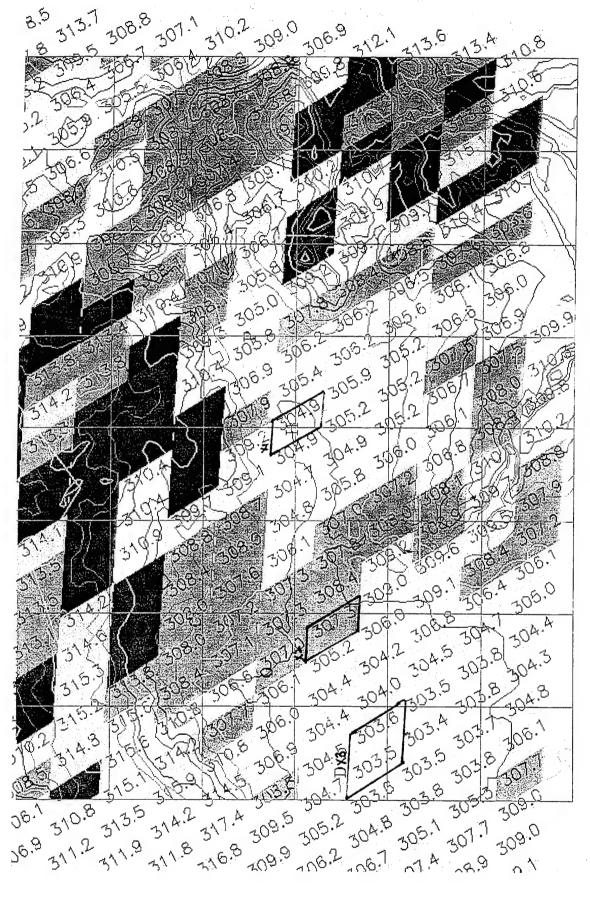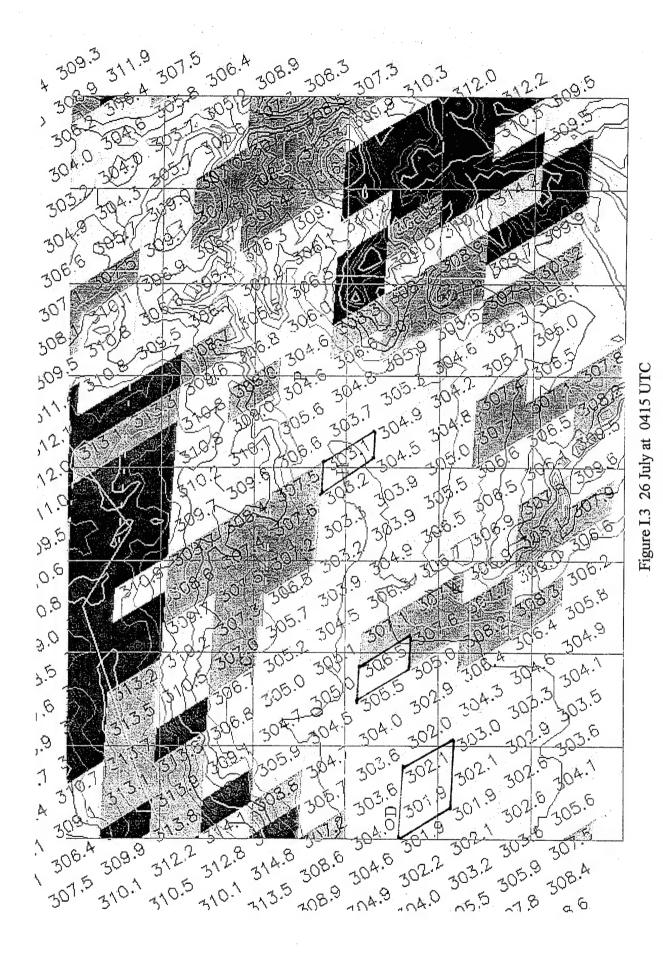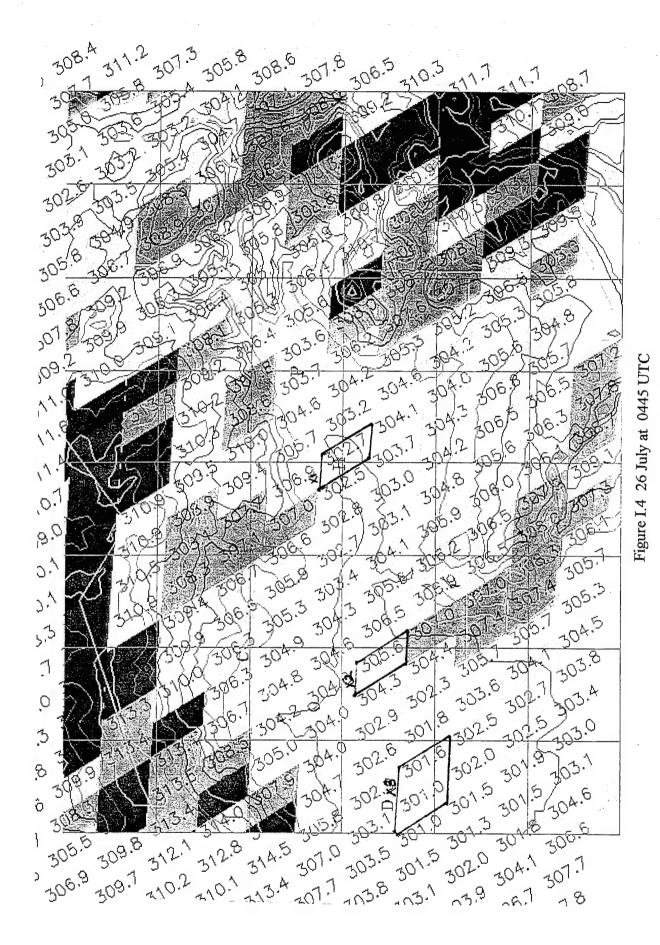
Figure I.1 26 July at 0315 UTC
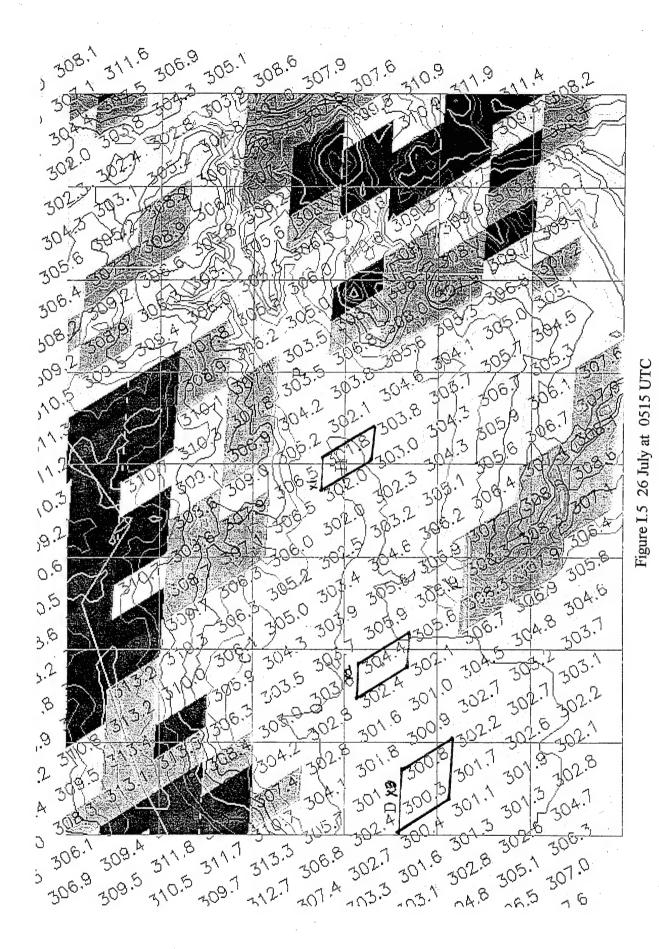
Figure I.2 26 July at 0345 UTC

Figure I.3 26 July at 0415 UTC

Figure I.4 26 July at 0445 UTC

Figure I.5 26 July at 0515 UTC

Figure I.6 26 July at 0545 UTC

Figure I.7 26 July at 0615 UTC

Figure I.8 26 July at 0645 UTC

Figure I.9 26 July at 0715 UTC

Figure I.10 26 July at 0745 UTC
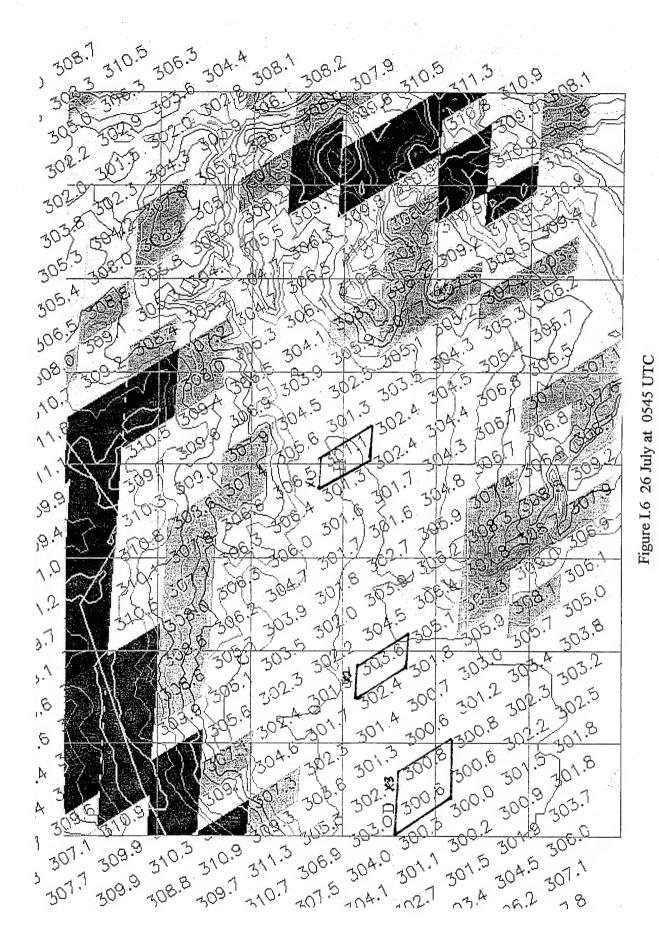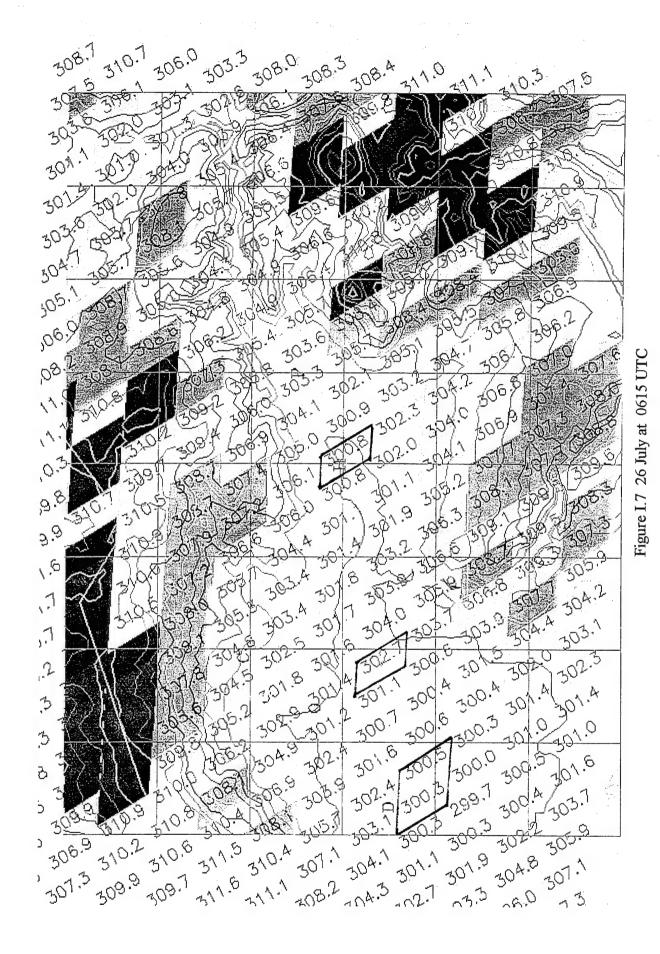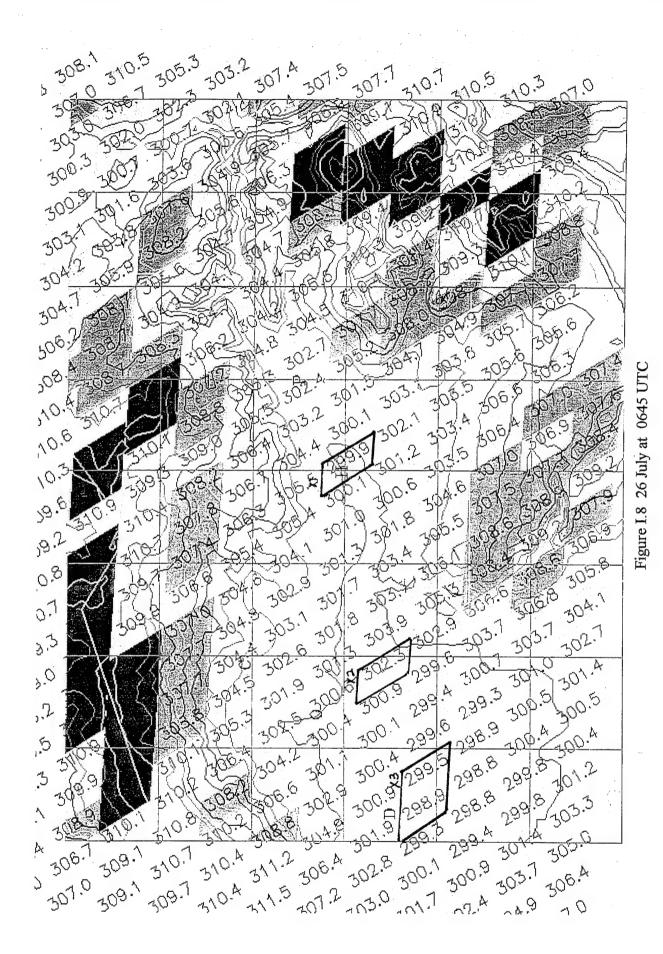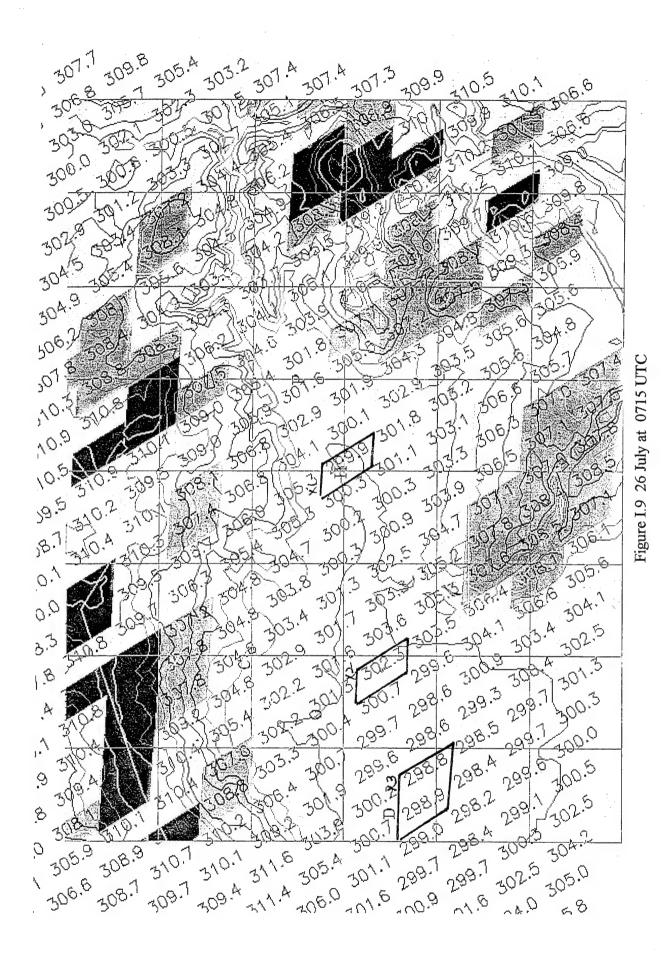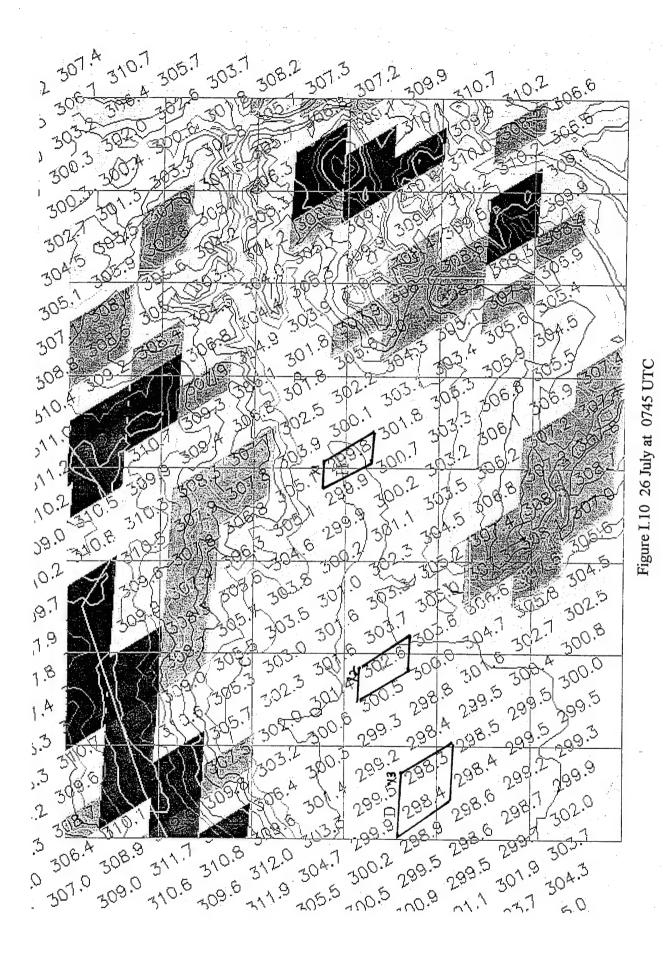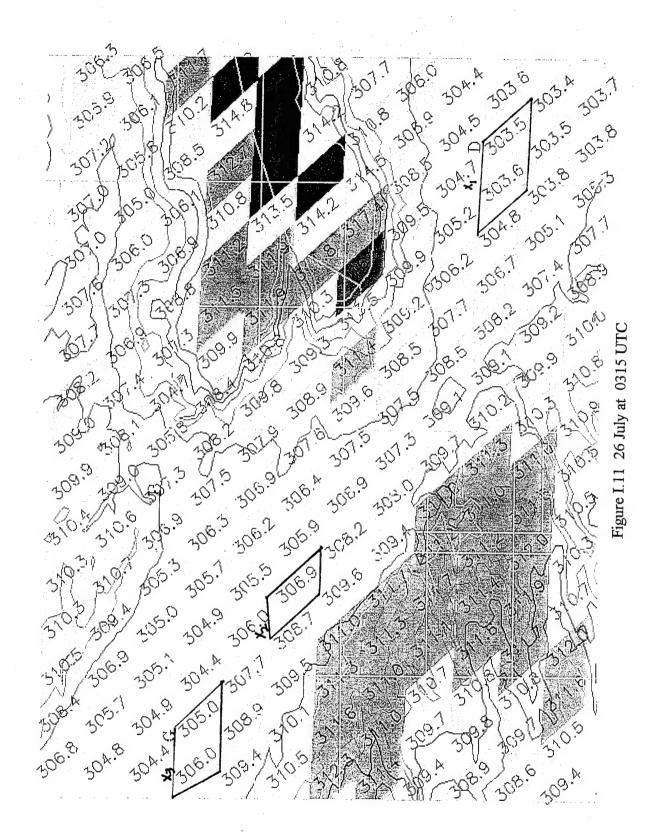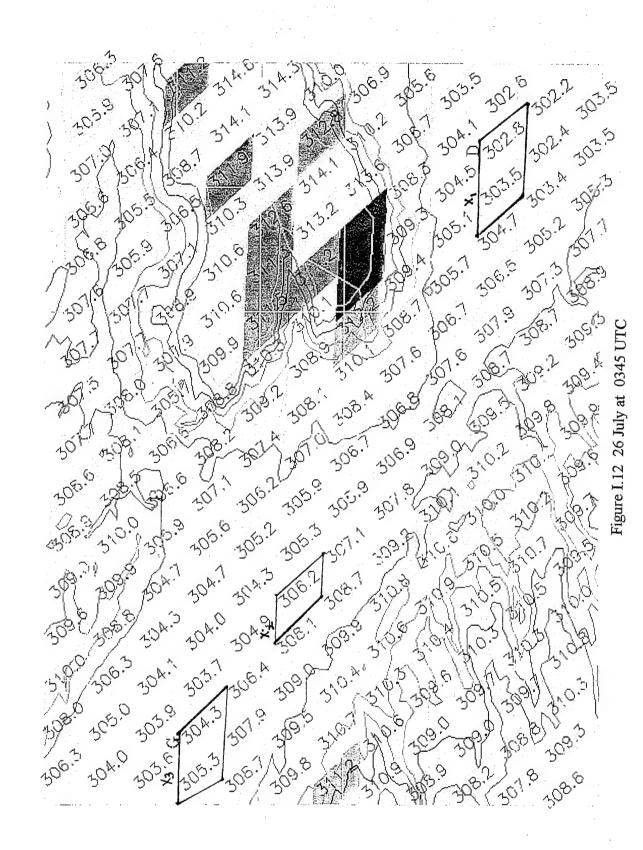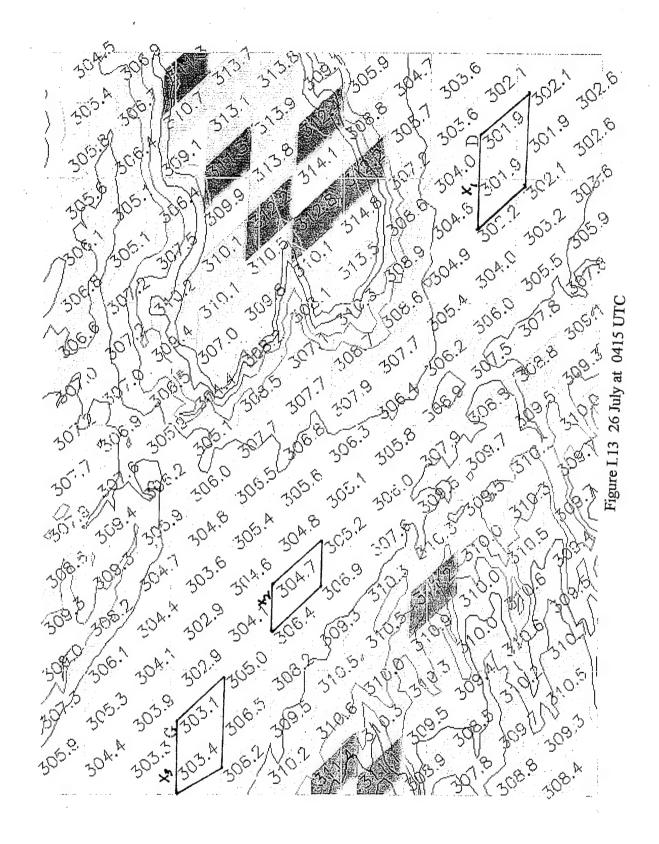
B. Delta to Grand Junction

Figures I.11 through I.20 depict the potential temperatures of the Delta to Grand Junction region. The letters D and P represent the approximate locations of the towns of Delta and Palisade, respectively. G depict the approximate location of the Grand Junction (GJT) Weather Service Office (WSO). Elevation contours are from 1524 meters (5000 feet) to 2591 meters (8500 feet) in 152.4 meter (500 feet) intervals. Three areas were selected along the valley floor to represent the along valley gradient. These regions are outlined in bold and labeled X(1) through X(3).
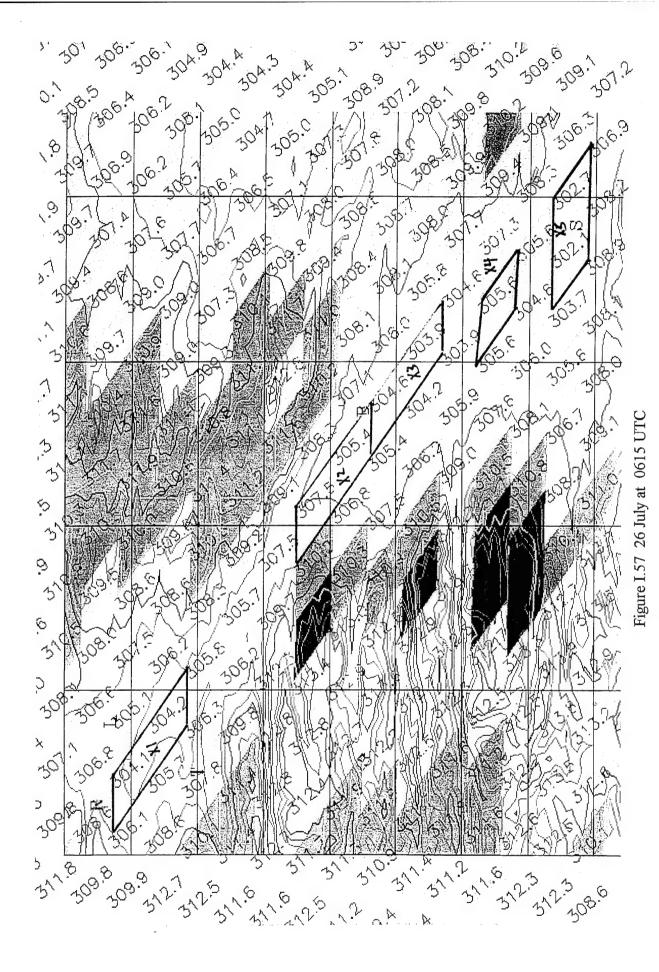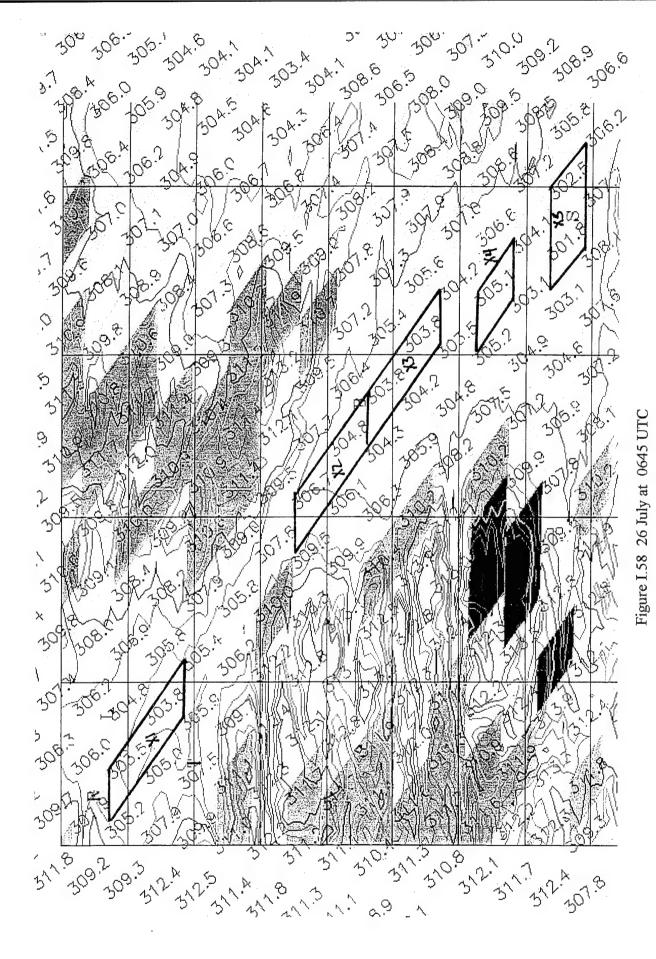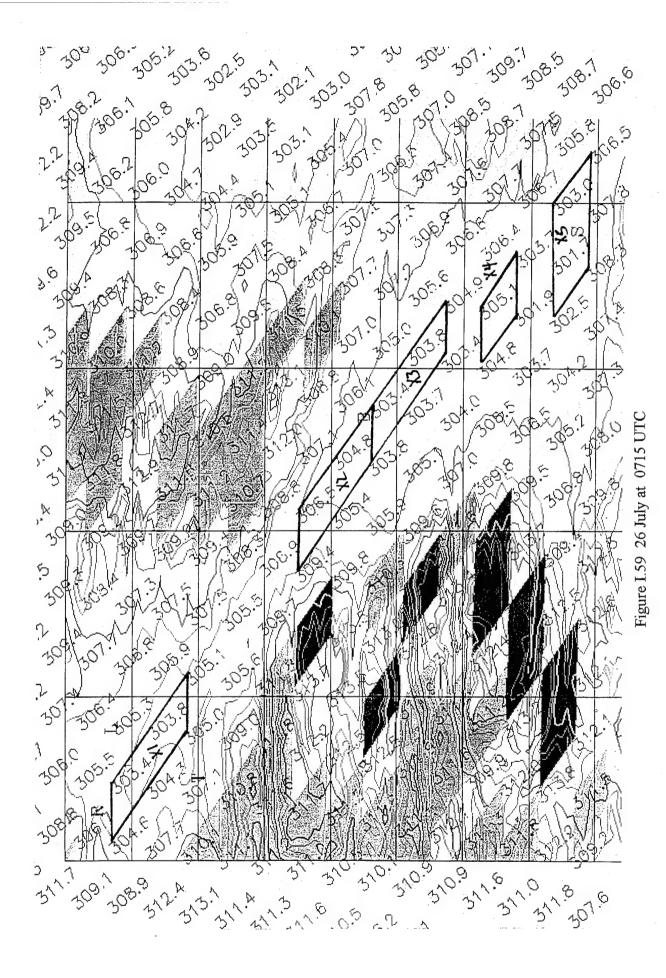
Figure I.11 26 July at 0315 UTC

Figure I.12 26 July at 0345 UTC

Figure I.13 26 July at 0415 UTC

Figure I.14 26 July at 0445 UTC
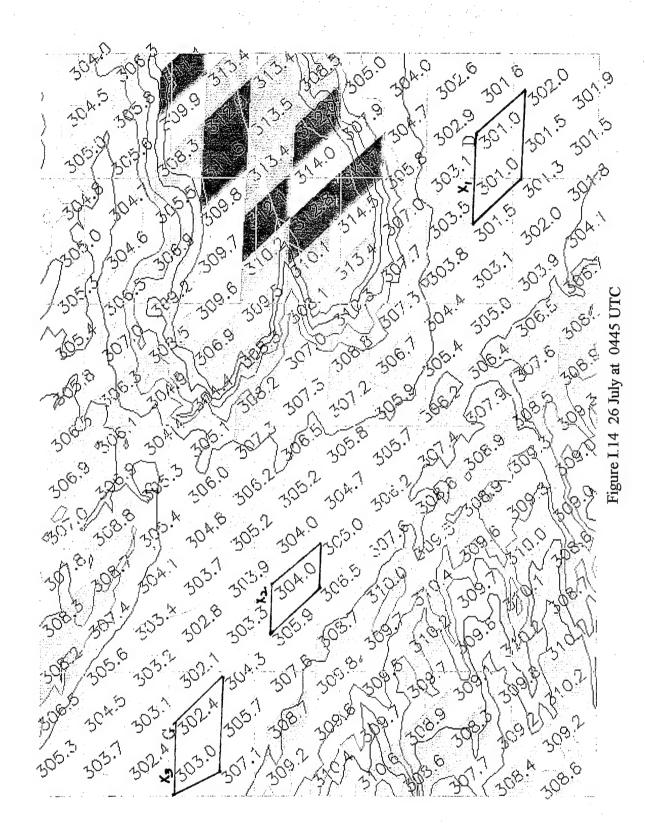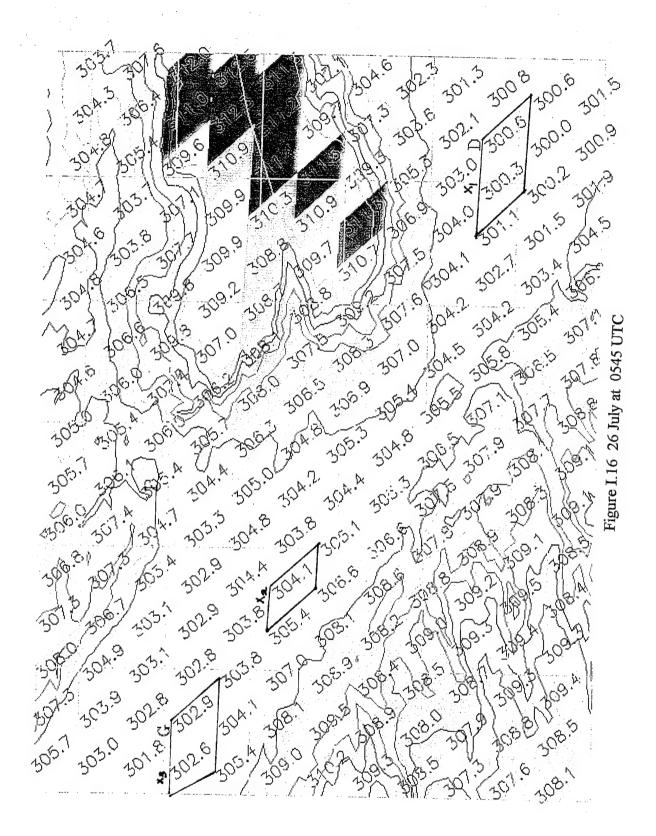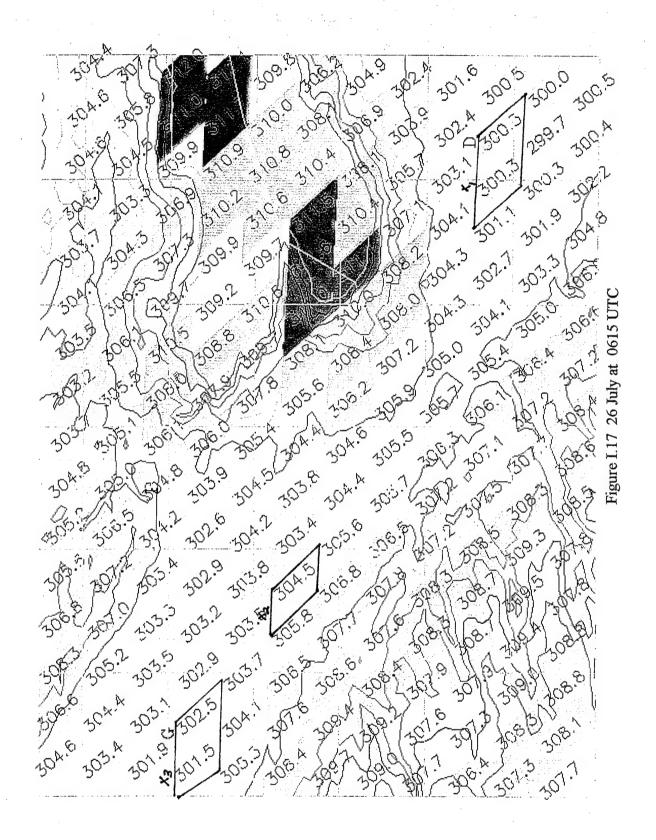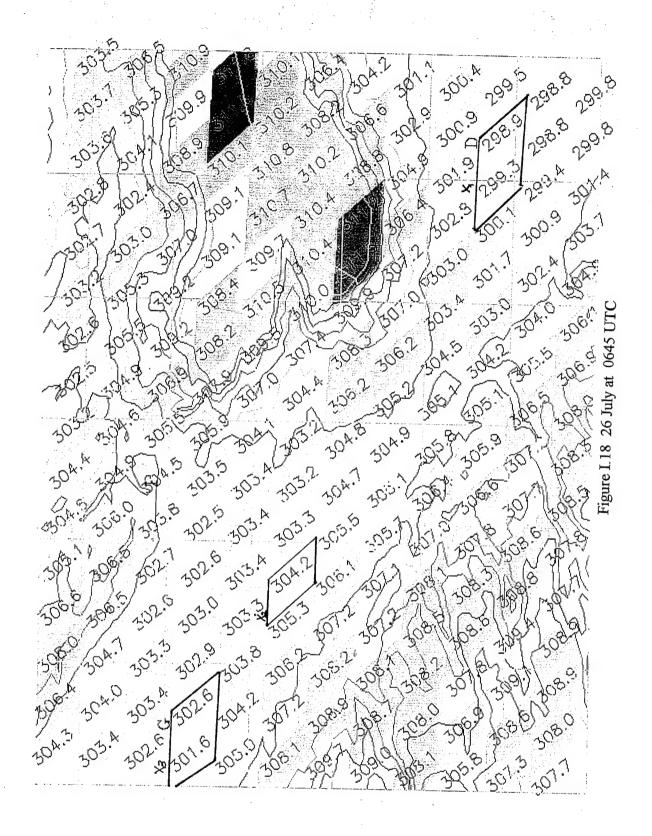
Figure I.15 26 July at 0515 UTC

Figure I.16 26 July at 0545 UTC

Figure I.17 26 July at 0615 UTC

Figure I.18 26 July at 0645 UTC

Figure I.19 26 July at 0715 UTC
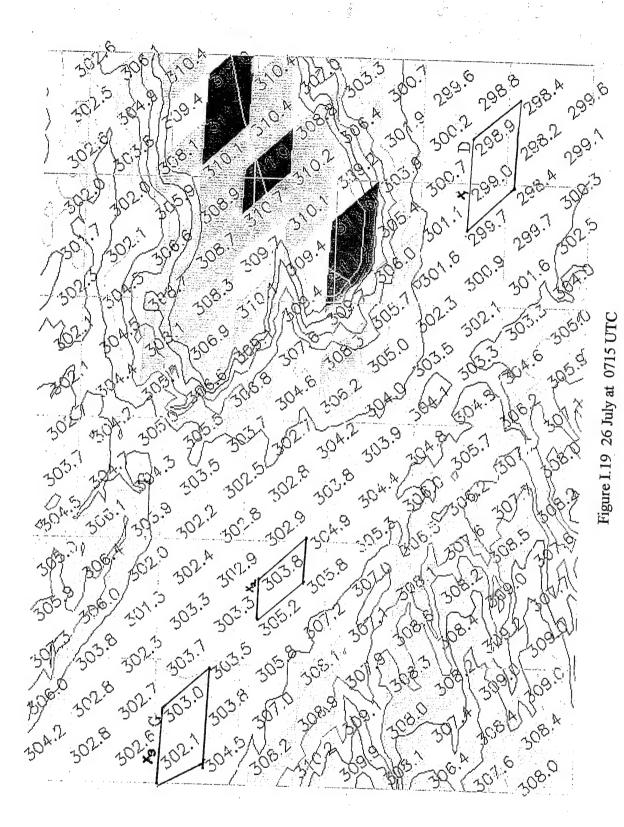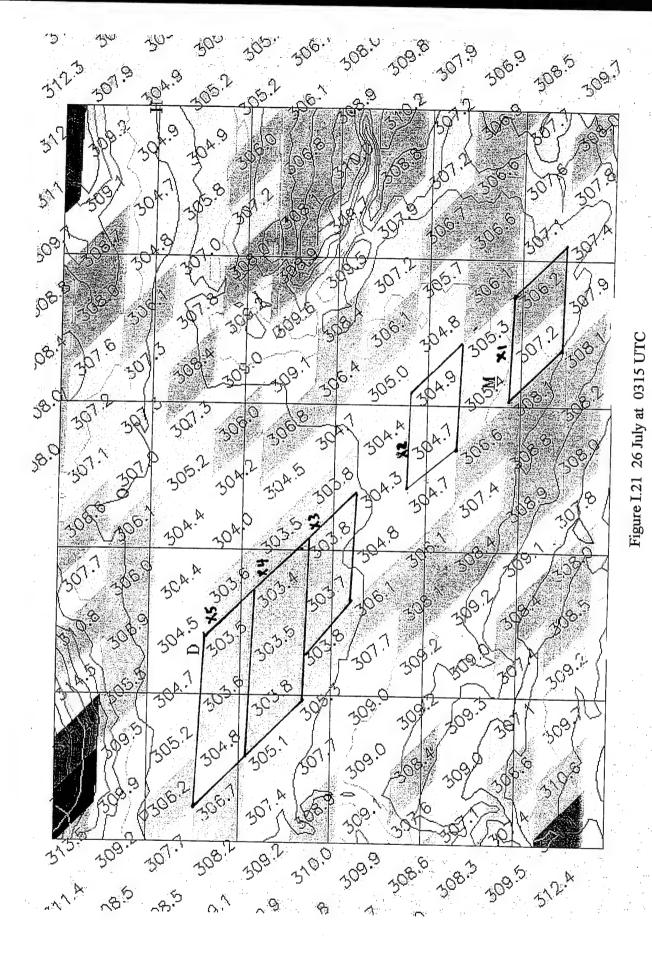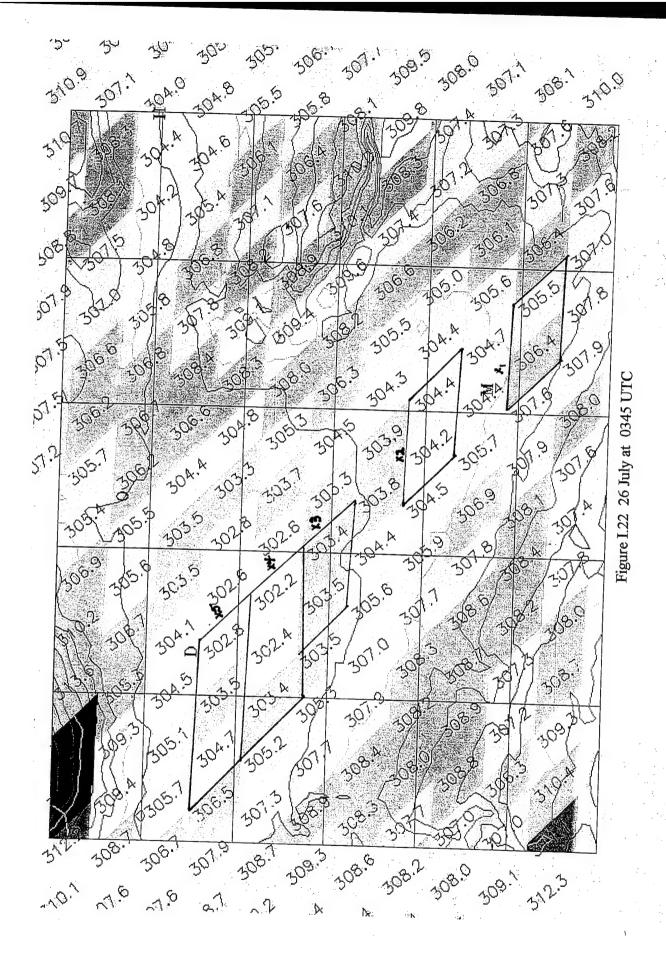
Figure I.20 26 July at 0745 UTC
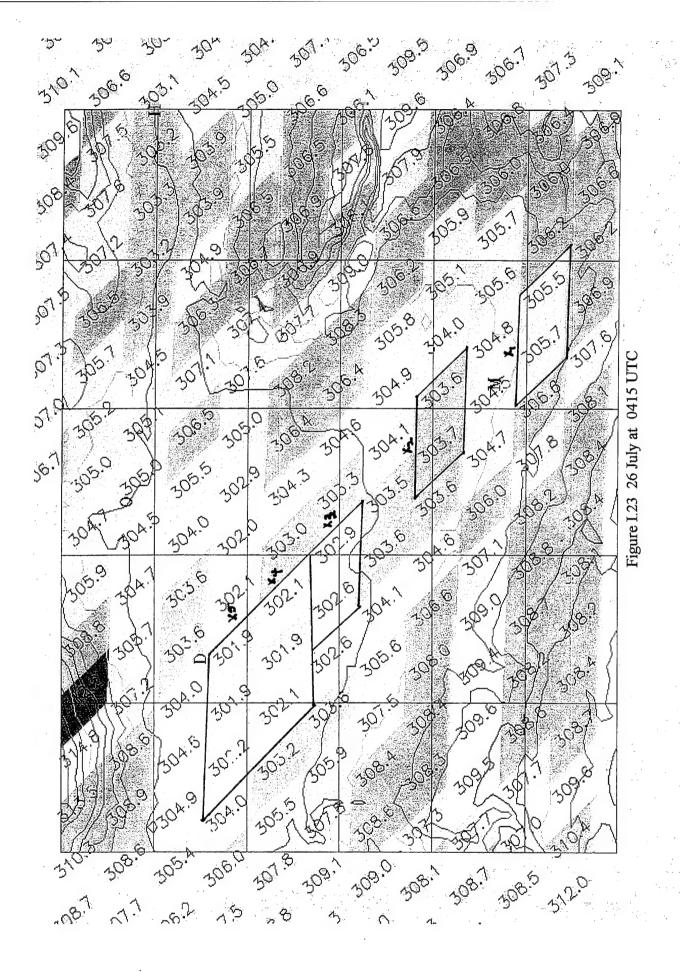
C. Montrose to Delta

Figures I.21 through I.30 depict the potential temperatures of the Montrose to Delta region. The letters M, D, O and H represent the approximate locations of the towns of Montrose, Delta, Orchard City, and Hotchkiss, respectively. Elevation contours are from 1524 meters (5000 feet) to 3048 meters (10000 feet) in 152.4 meter (500 feet) intervals. Five areas were selected along the valley floor to represent the along valley gradient. These regions are outlined in bold and labeled X(1) through X(5).
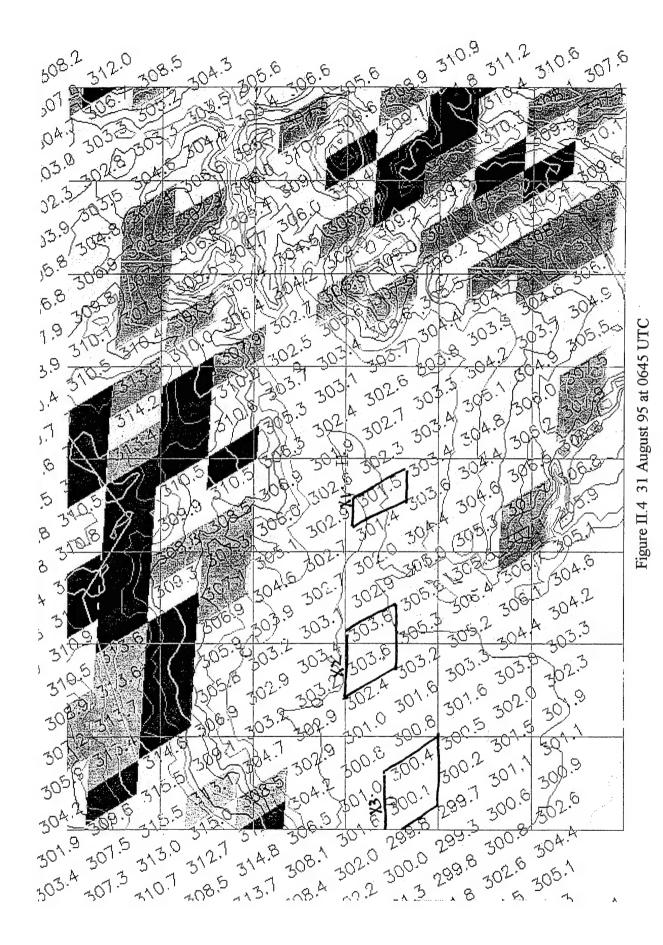
Figure I.21 26 July at 0315 UTC

Figure I.22 26 July at 0345 UTC

Figure I.23 26 July at 0415 UTC
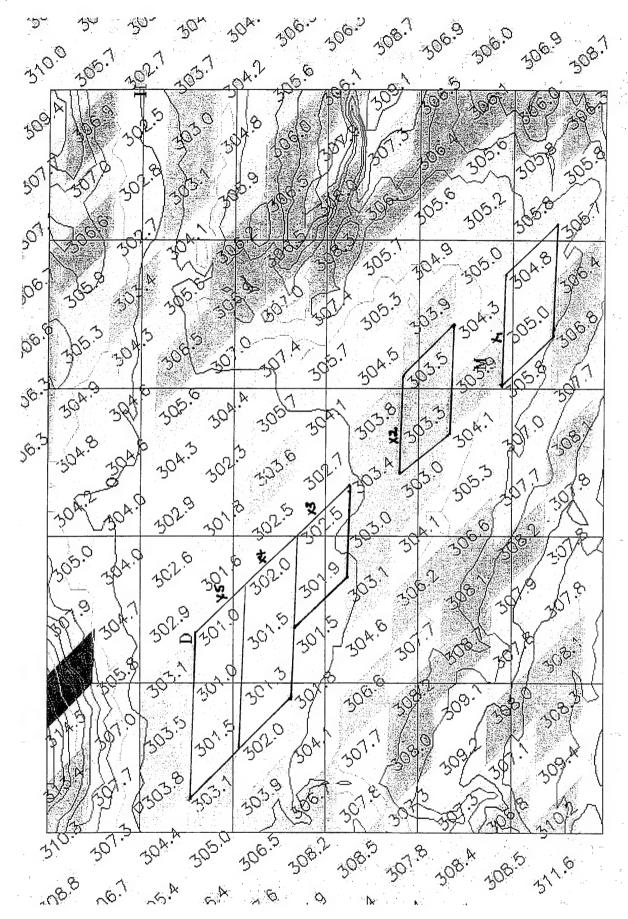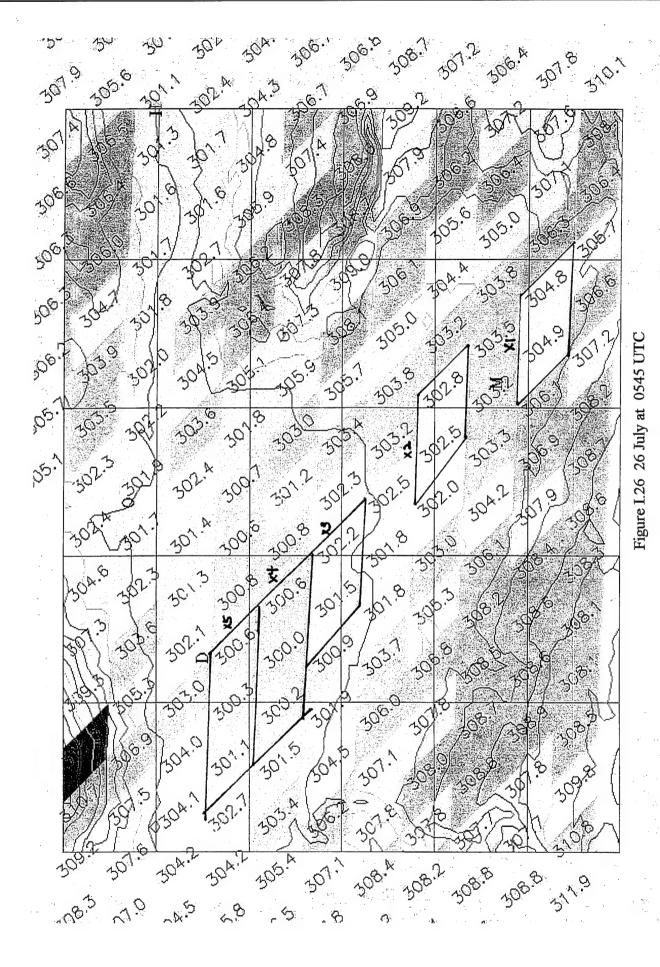
Figure I.24 26 July at 0445 UTC
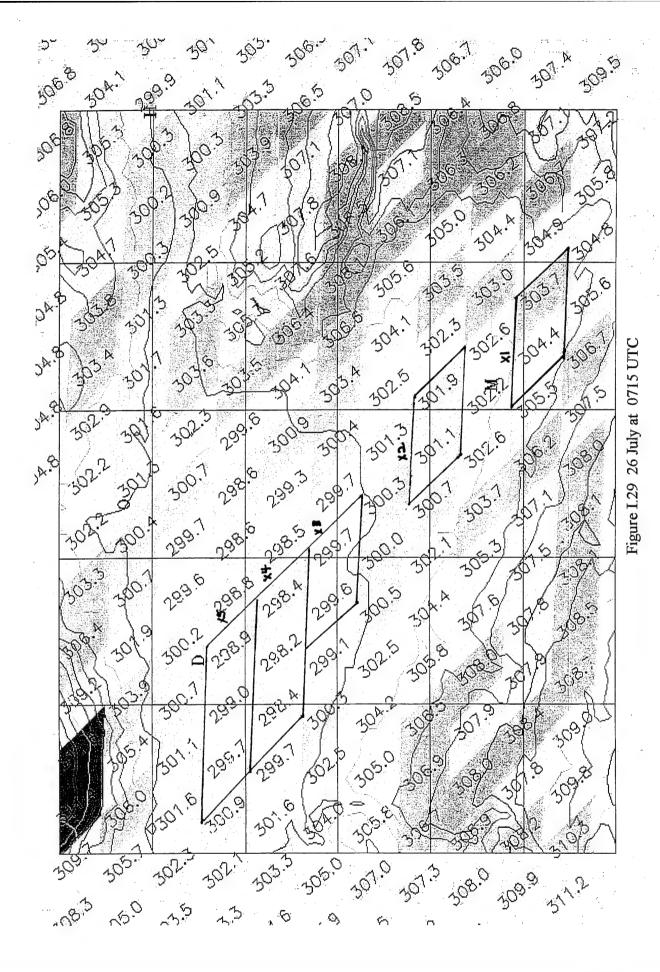
Figure I.25   26 July at 0515 UTC

Figure I.26 26 July at 0545 UTC
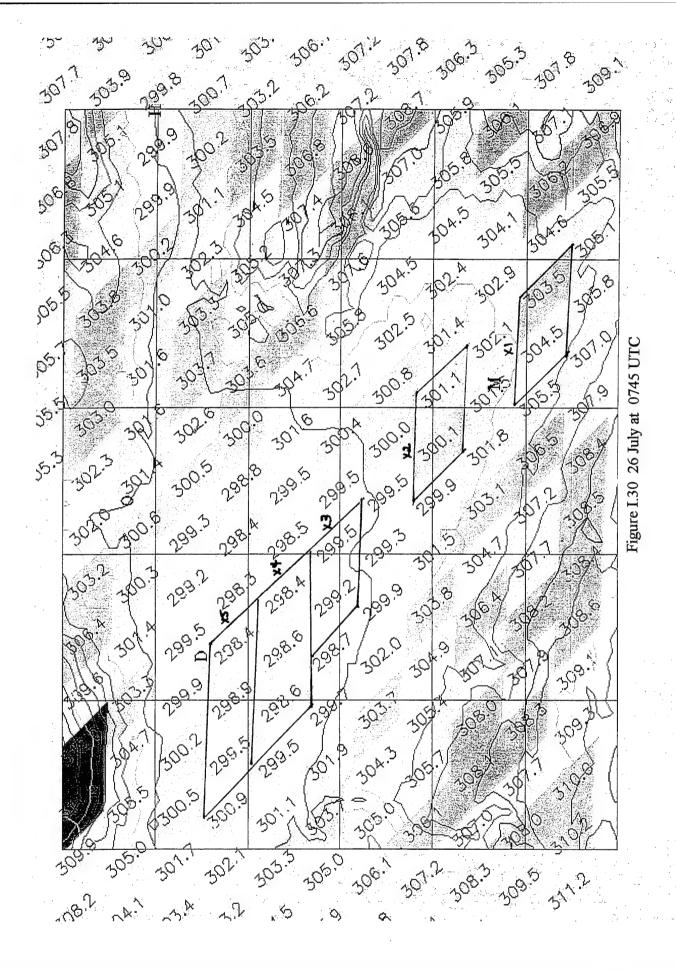
Figure I.27 26 July at 0615 UTC
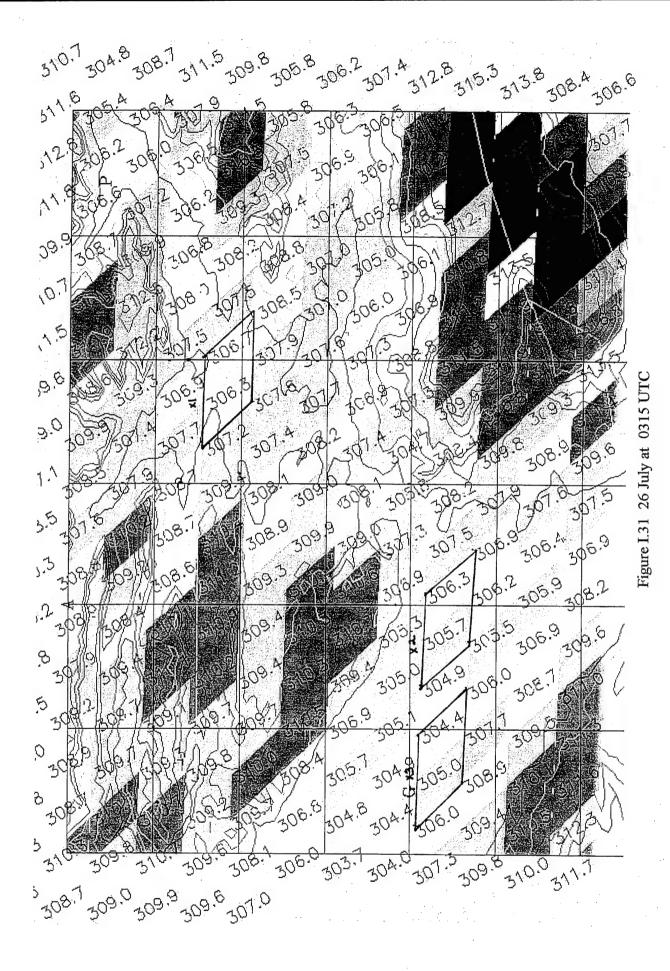
Figure I.28 26 July at 0645 UTC

Figure I.29 26 July at 0715 UTC

Figure I.30 26 July at 0745 UTC
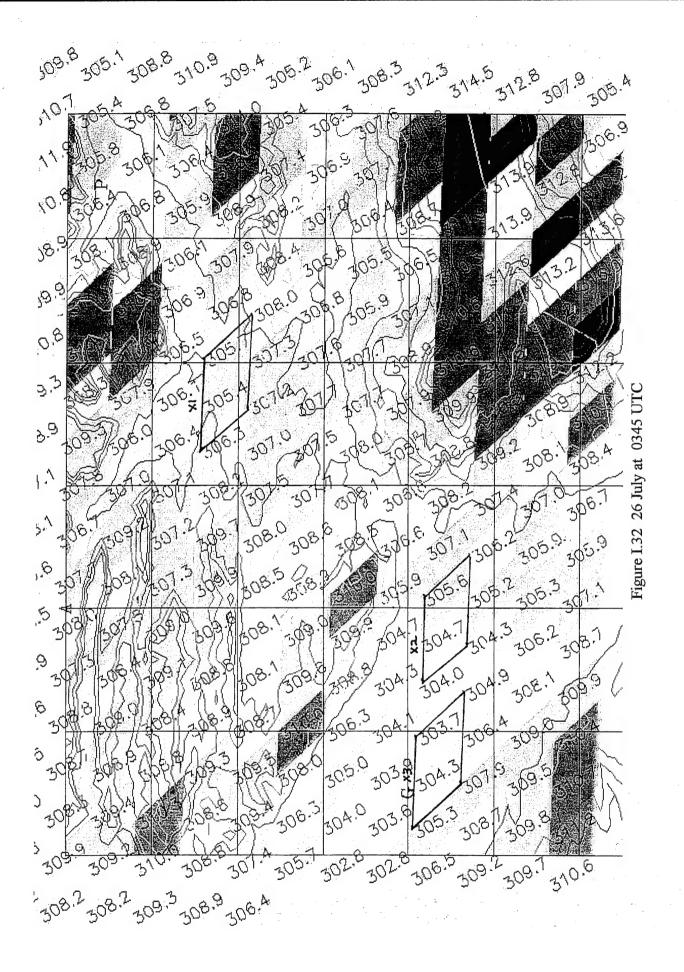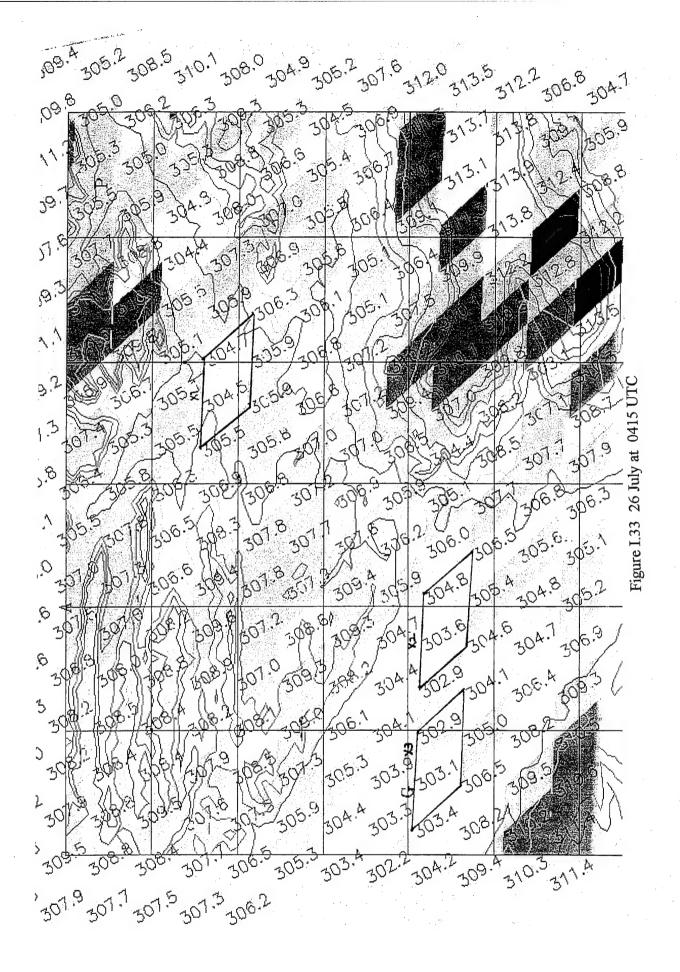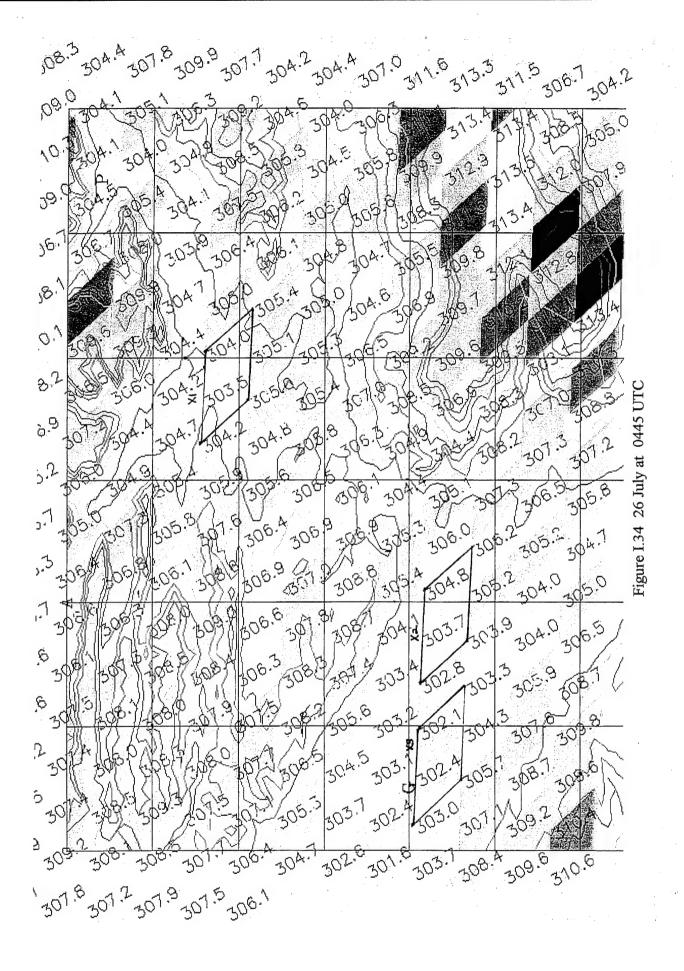
D. Parachute to Grand Junction
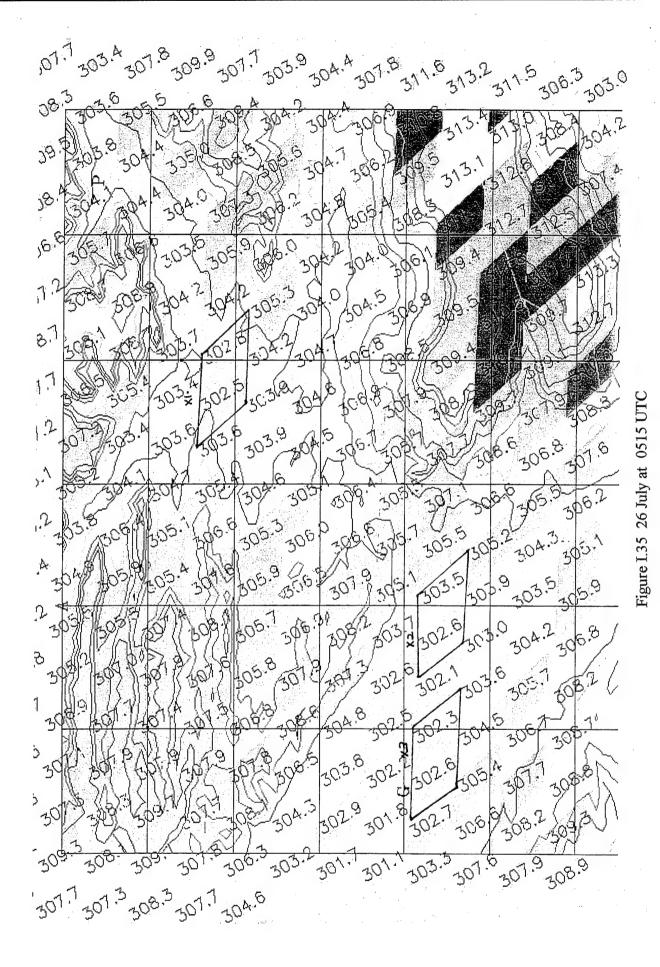
Figures I.31 through I.40 depict the potential temperatures of the Montrose to Delta region. The letters P and G represent the approximate locations of the town of Parachute and the GJT WSO, respectively. Elevation contours are from 1524 meters (5000 feet) to 2743 meters (9000 feet) in 152.4 meter (500 feet) intervals. Three areas were selected along the valley floor to represent the along valley gradient. These regions are outlined in bold and labeled X(1) through X(3).

Figure I.31 26 July at 0315 UTC

Figure I.32 26 July at 0345 UTC

Figure I.33 26 July at 0415 UTC

Figure I.34 26 July at 0445 UTC

Figure I.35 26 July at 0515 UTC

Figure I.36 26 July at 0545 UTC

Figure I.37 26 July at 0615 UTC

Figure I.38 26 July at 0645 UTC

Figure I.39 26 July at 0715 UTC

Figure I.40 26 July at 0745 UTC
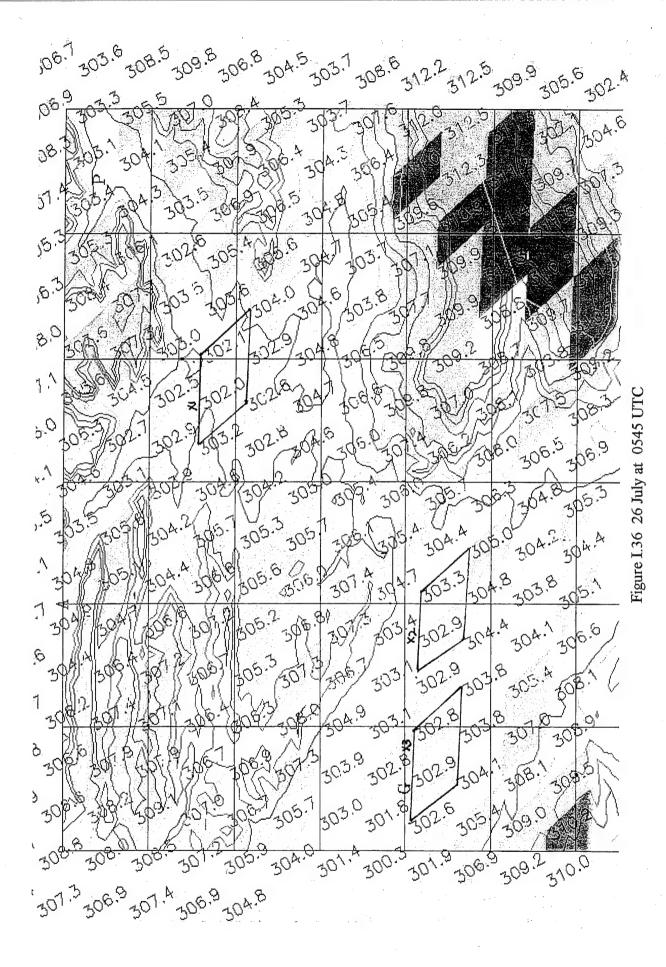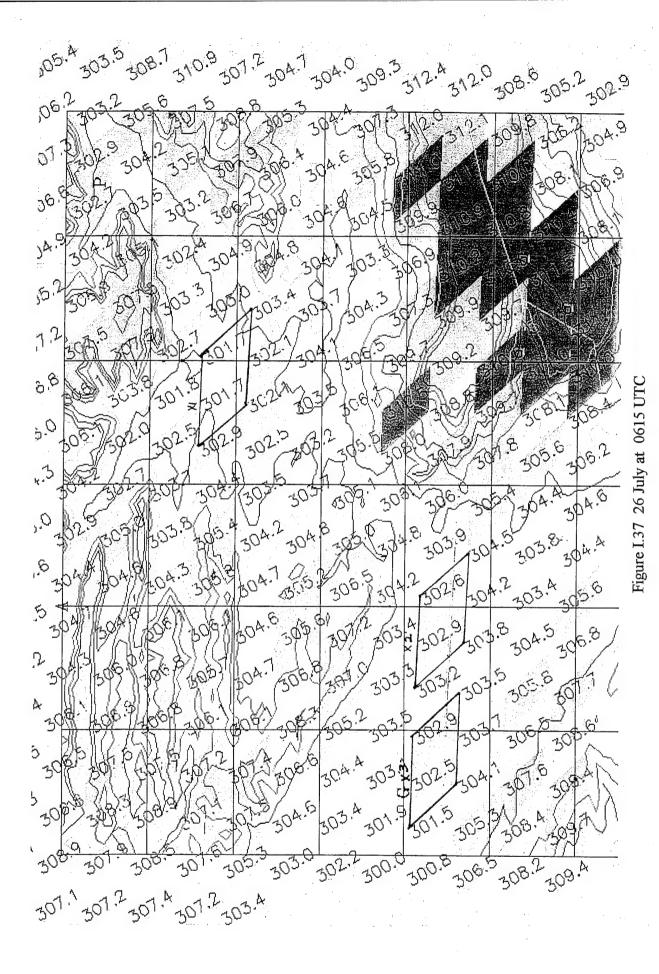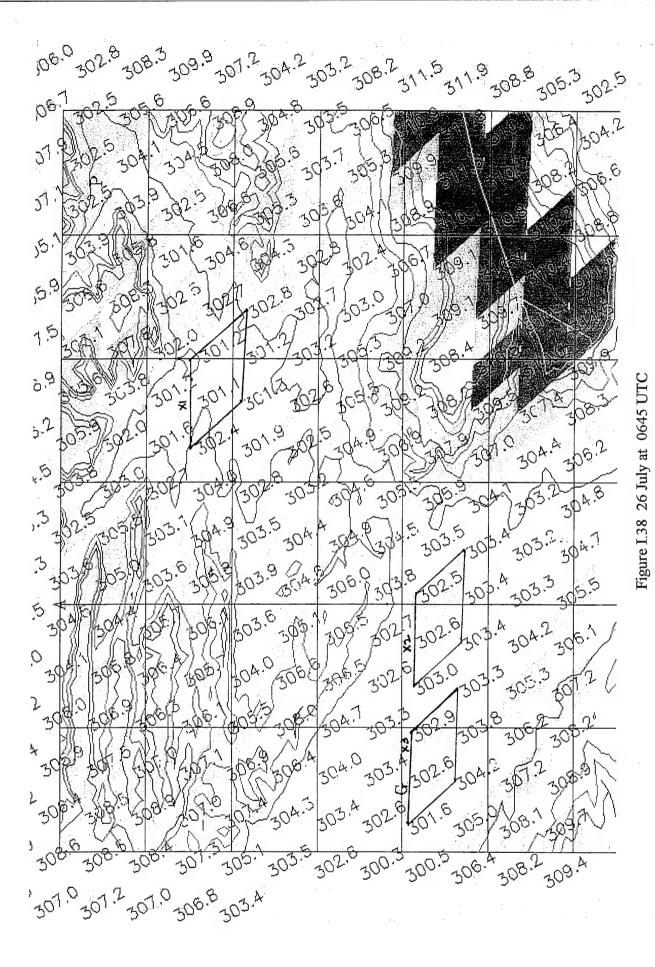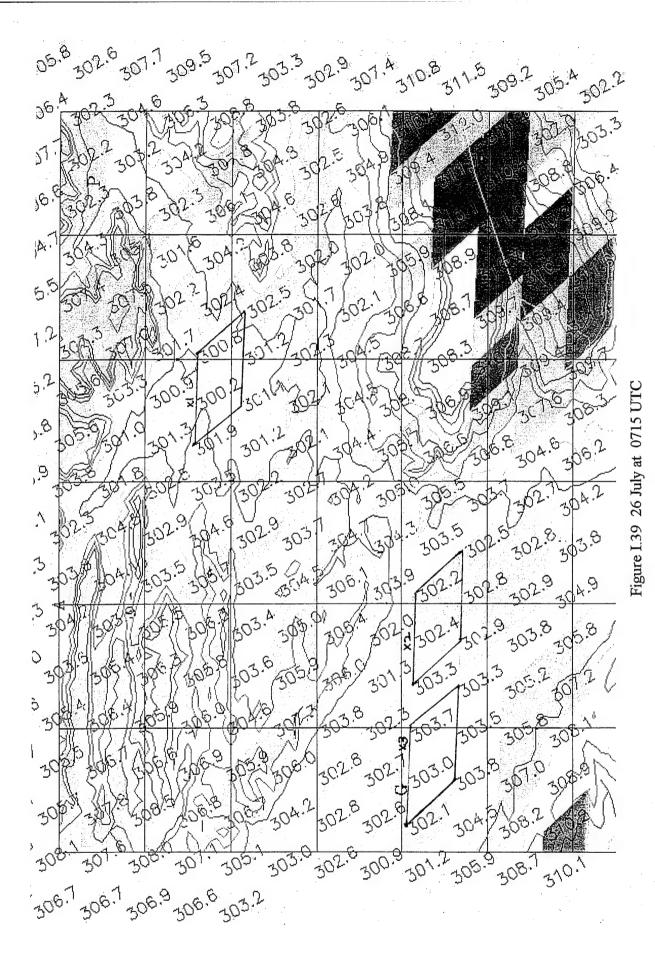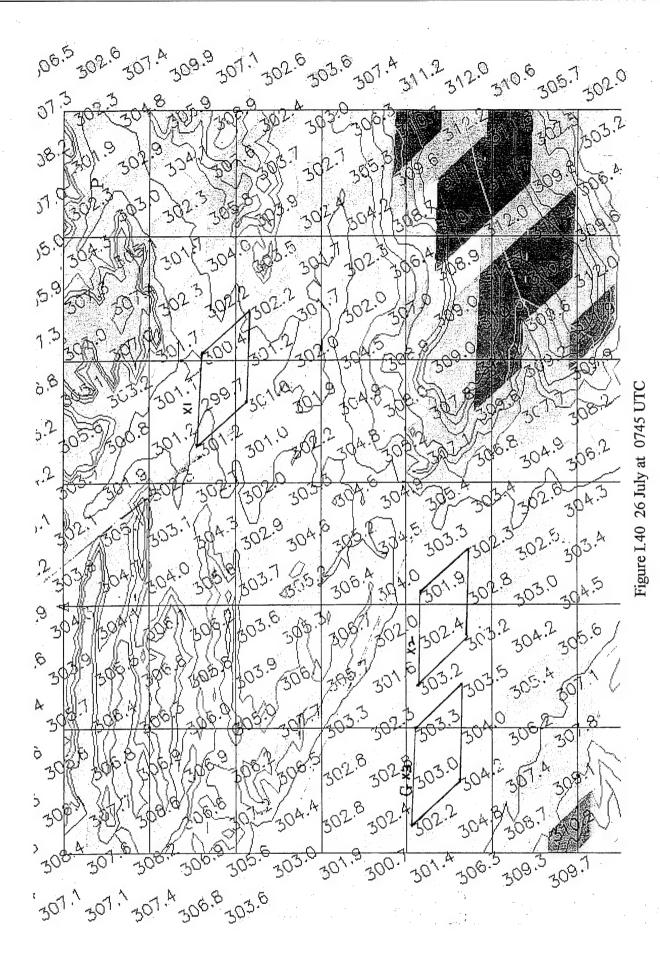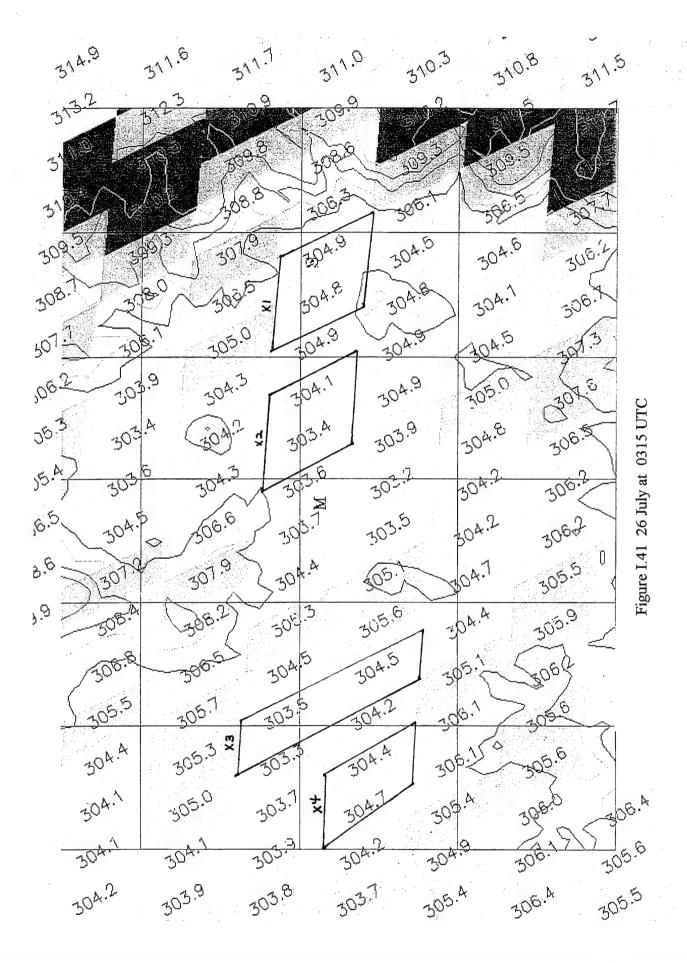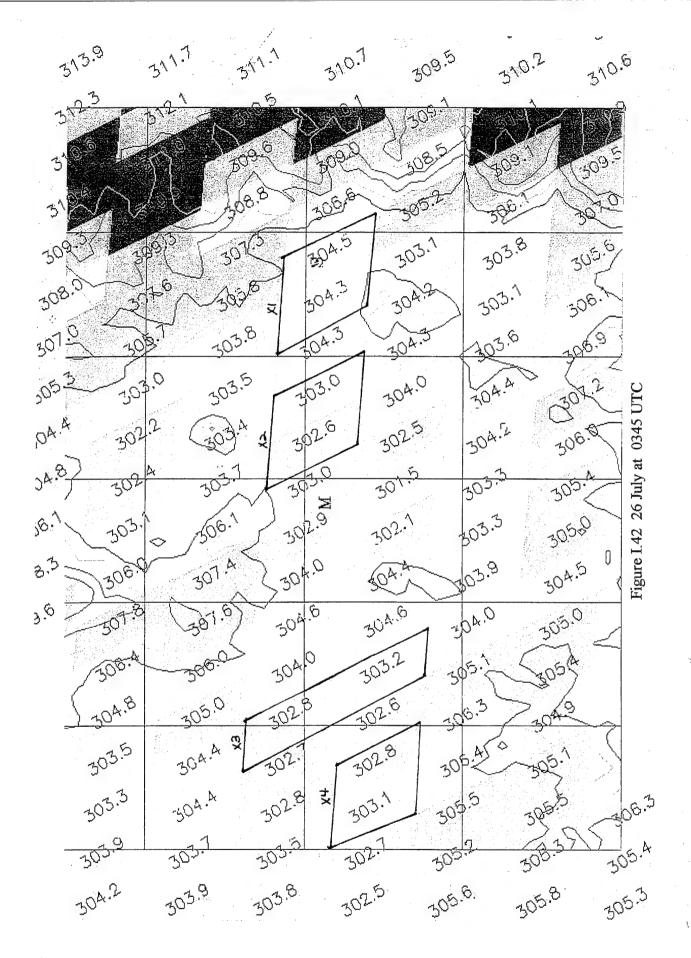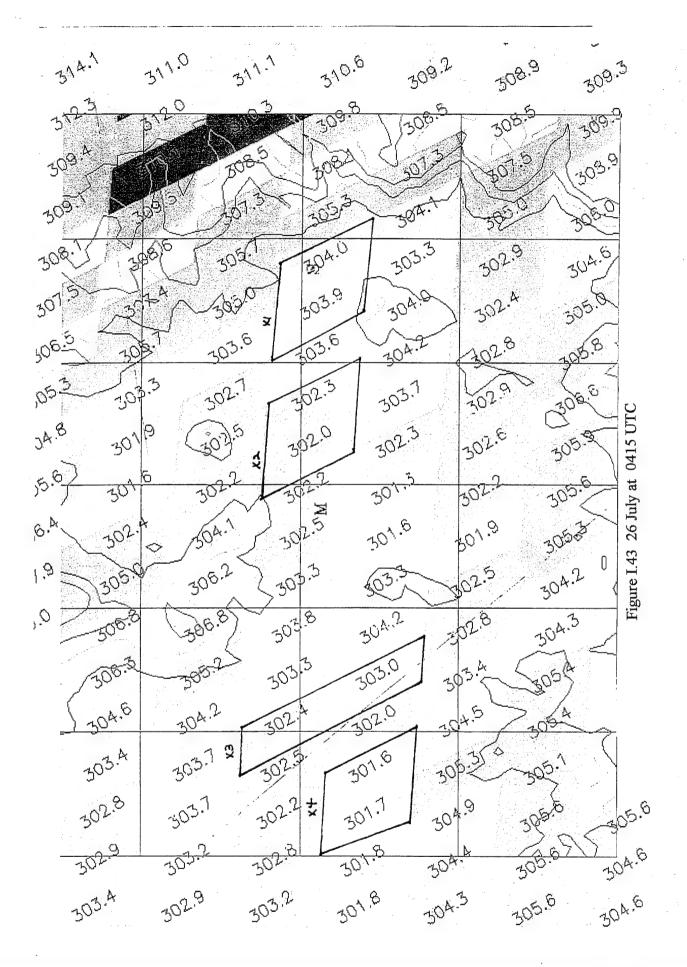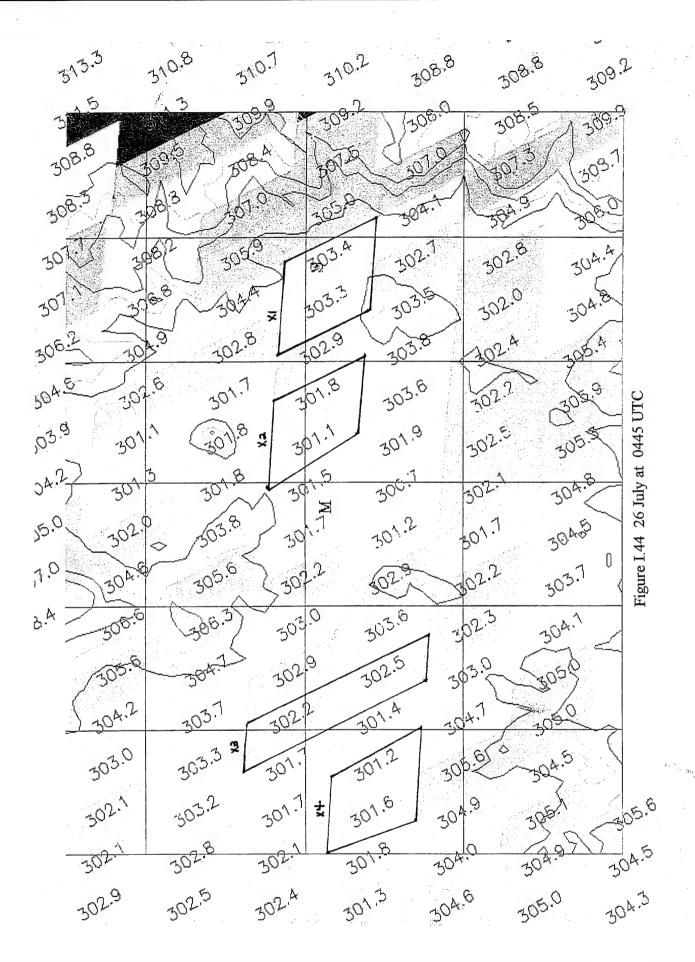
E. Yampa Valley
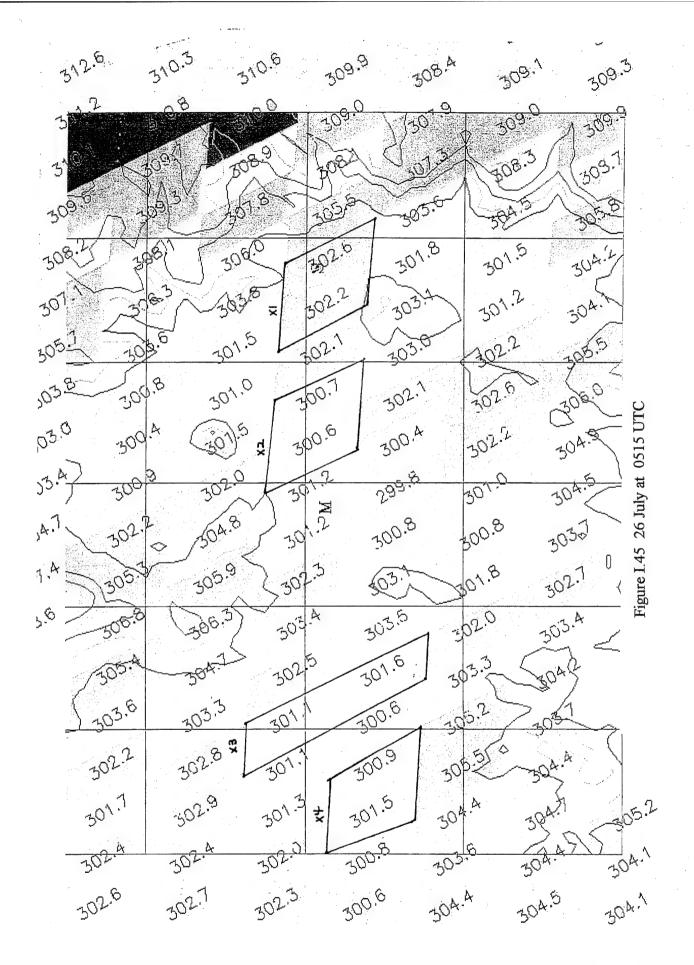
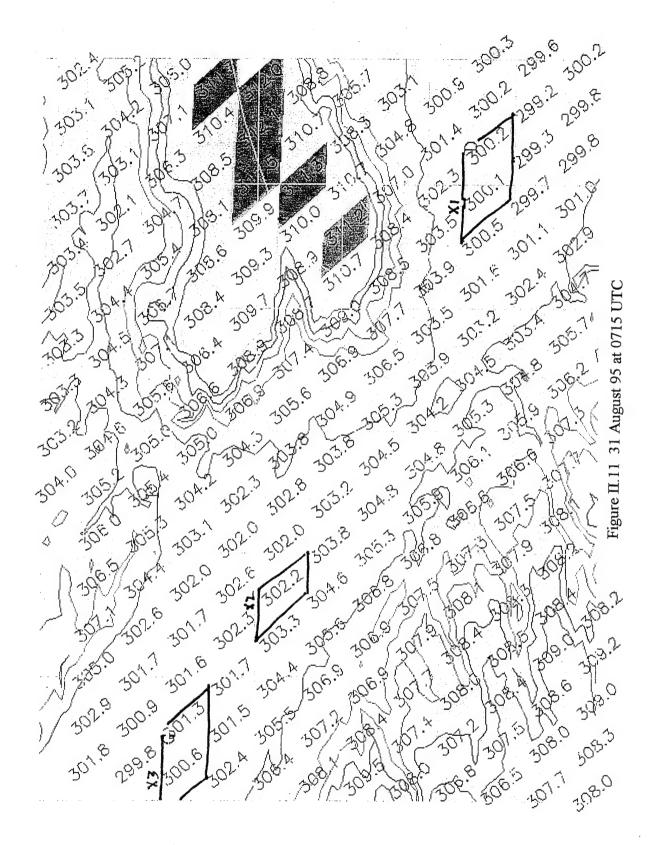Figures I.41 through I.50 depict the potential temperatures of the Montrose to Delta region. The letters S and M represent the approximate locations of the towns of Steamboat and Milner, respectively. Elevation contours are from 1829 meters (6000 feet) to 3048 meters (10000 feet) in 152.4 meter (500 feet) intervals. Four areas were selected along the valley floor to represent the along valley gradient. These regions are outlined in bold and labeled X(1) through X(4).
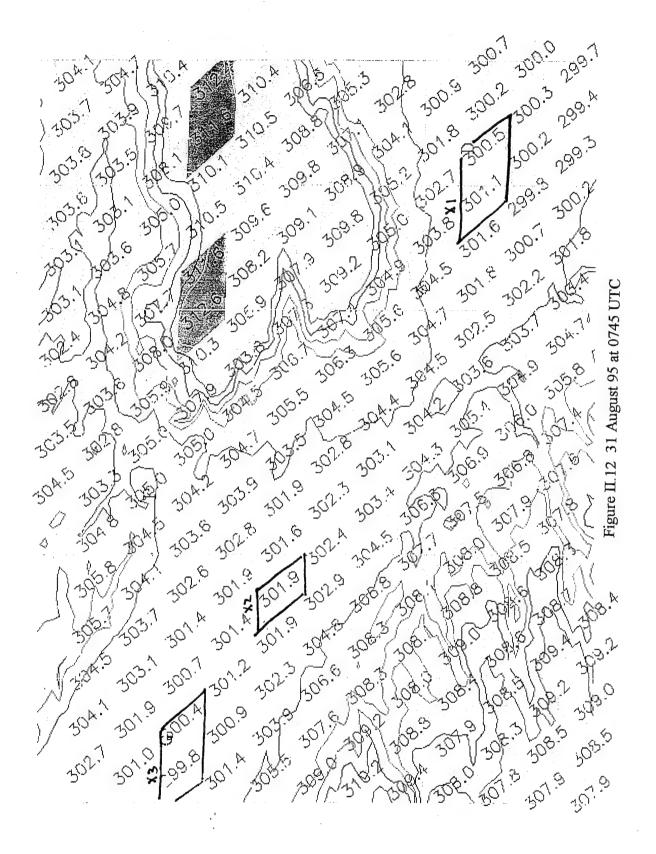
Figure I.41 26 July at 0315 UTC

Figure I.42 26 July at 0345 UTC

Figure I.43   26 July at 0415 UTC

Figure I.44 26 July at 0445 UTC

Figure I.45 26 July at 0515 UTC

Figure I.46 26 July at 0545 UTC

Figure I.47 26 July at 0615 UTC

Figure I.48 26 July at 0645 UTC

Figure I.49 26 July at 0715 UTC

Figure I.50 26 July at 0745 UTC
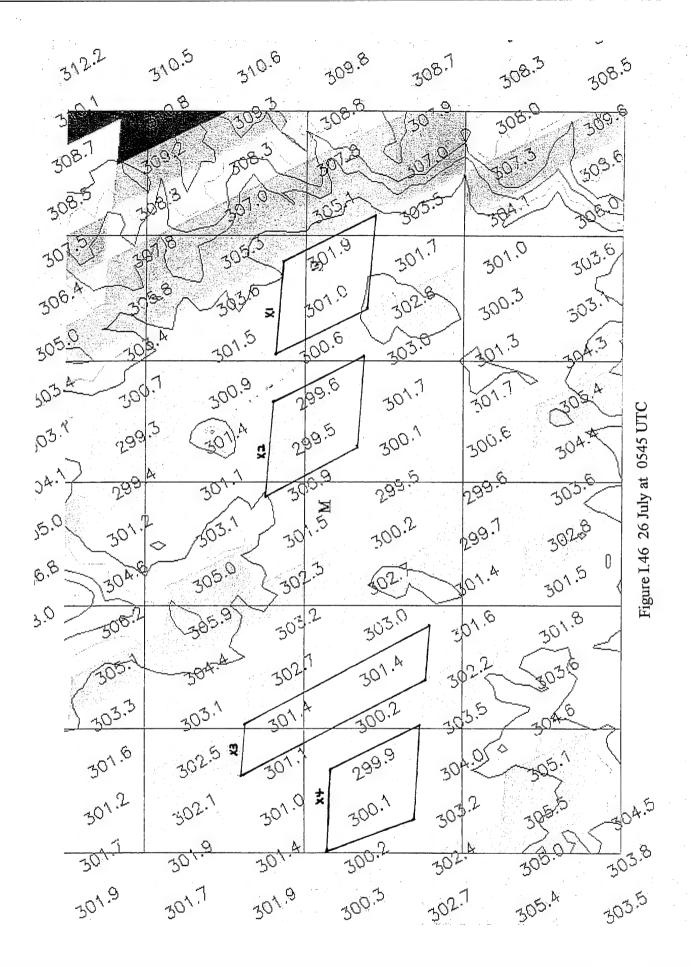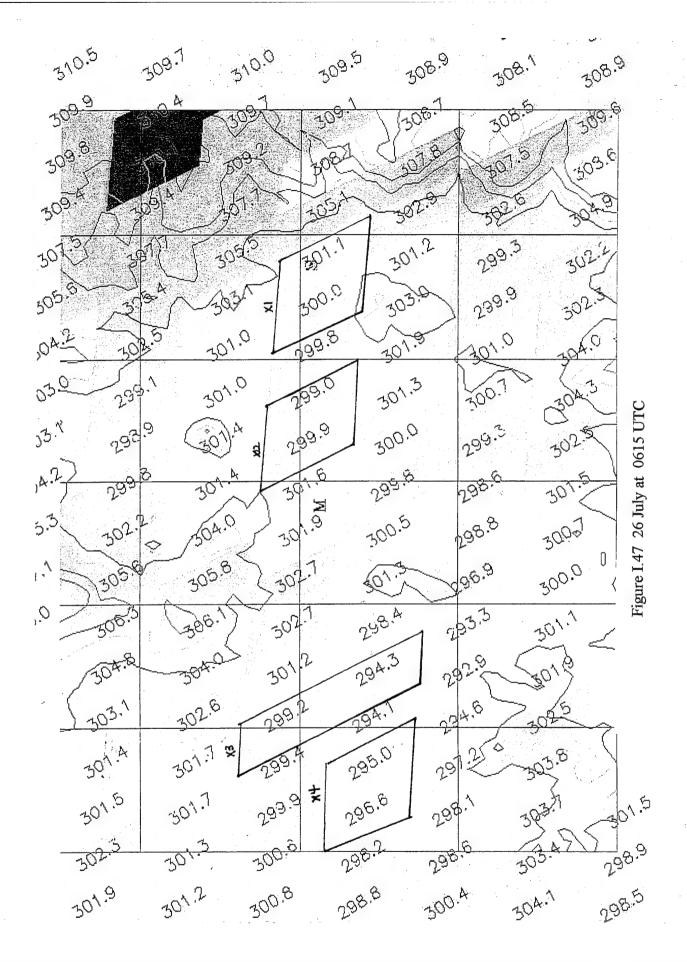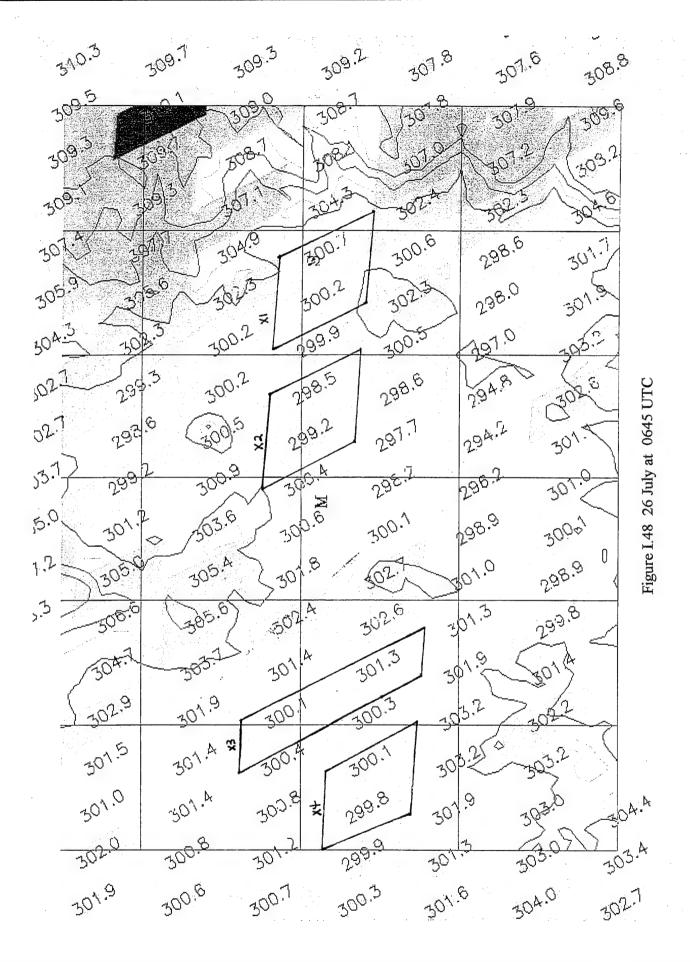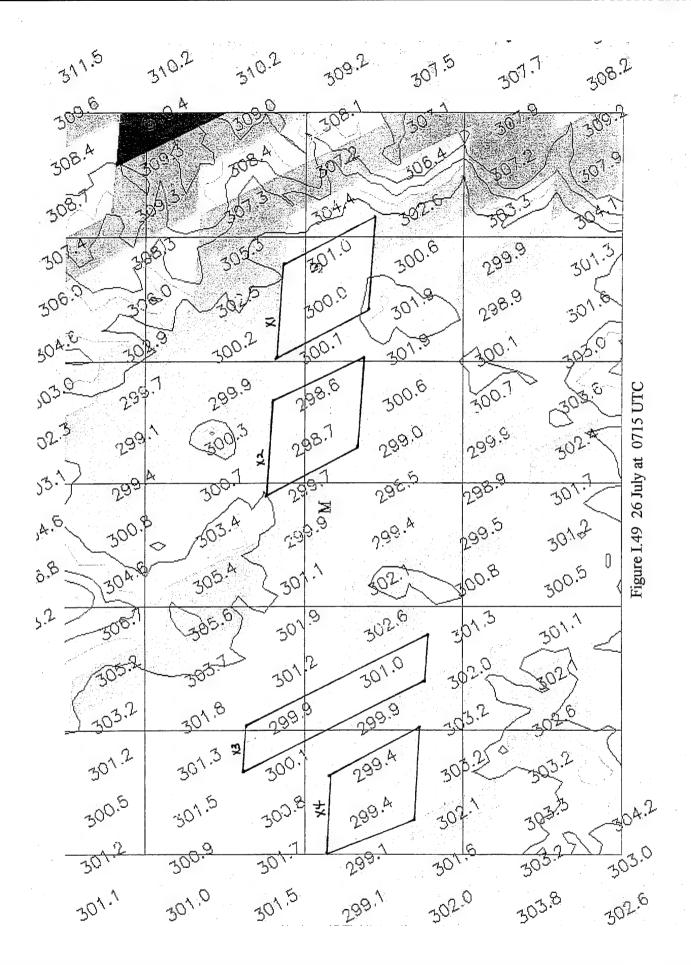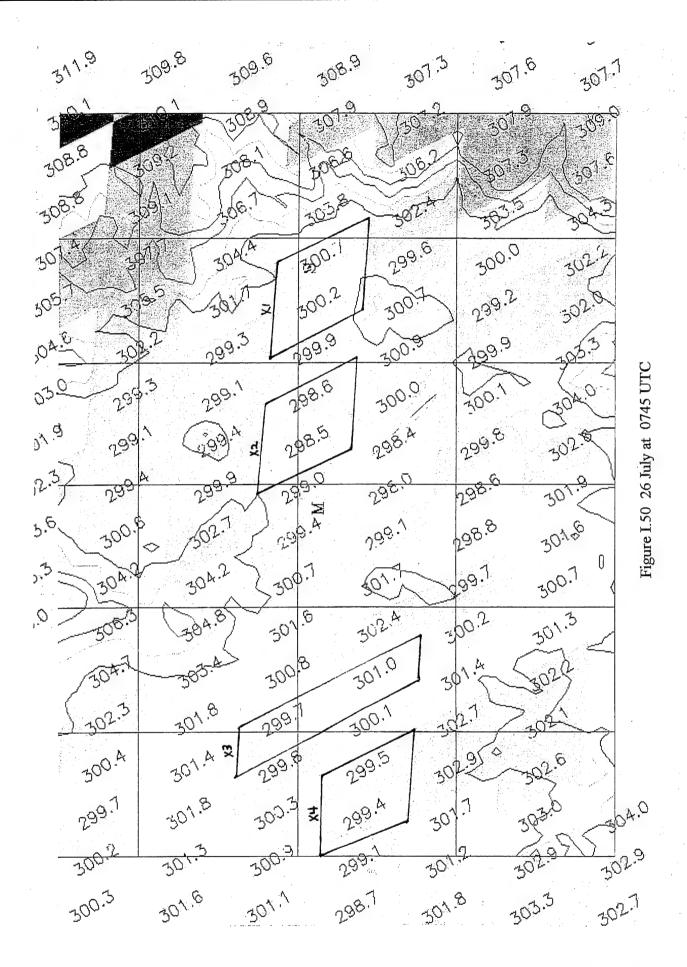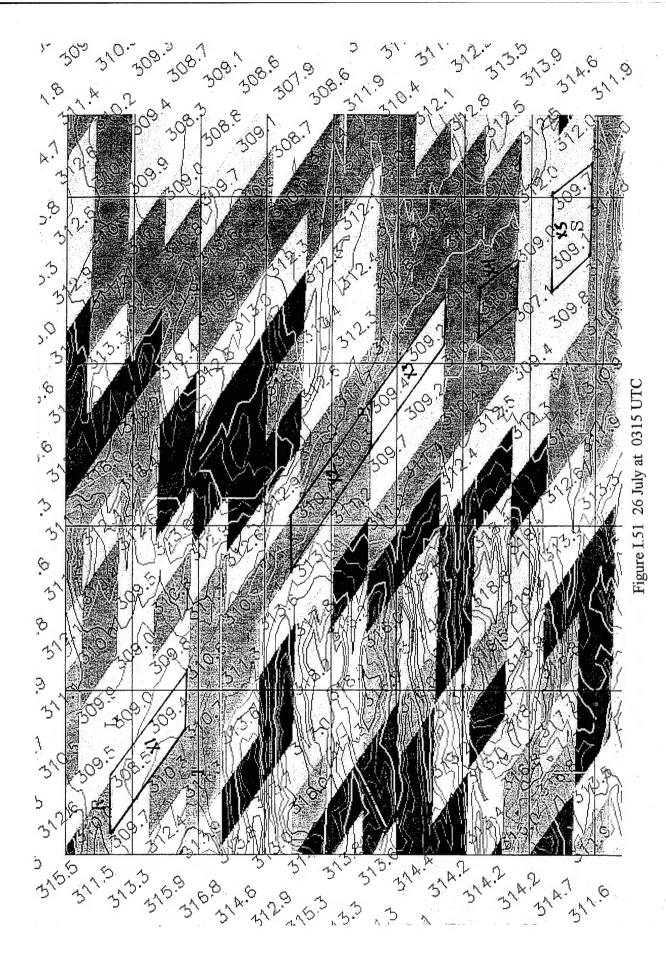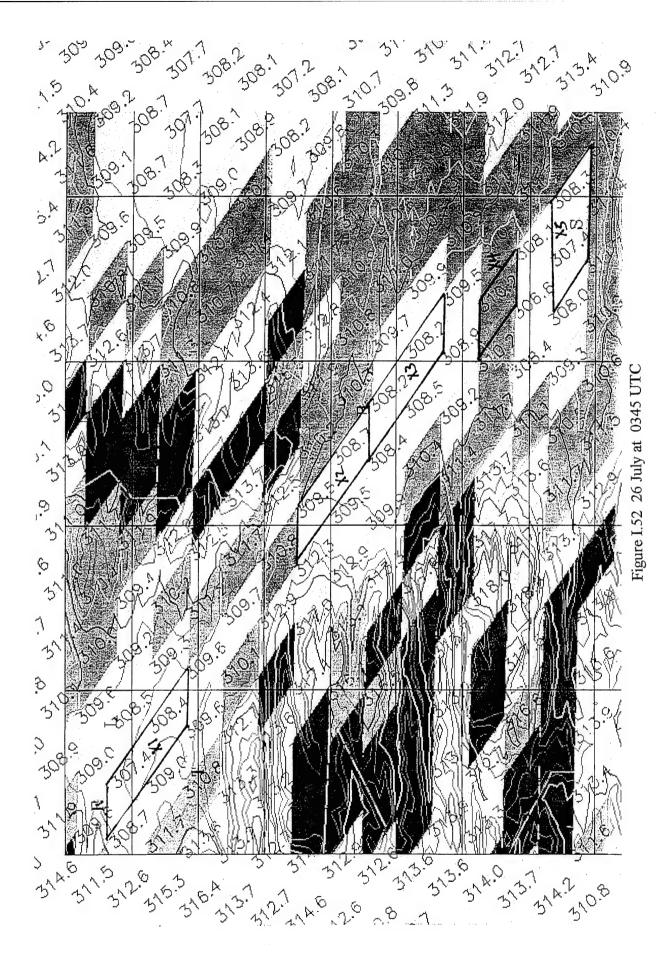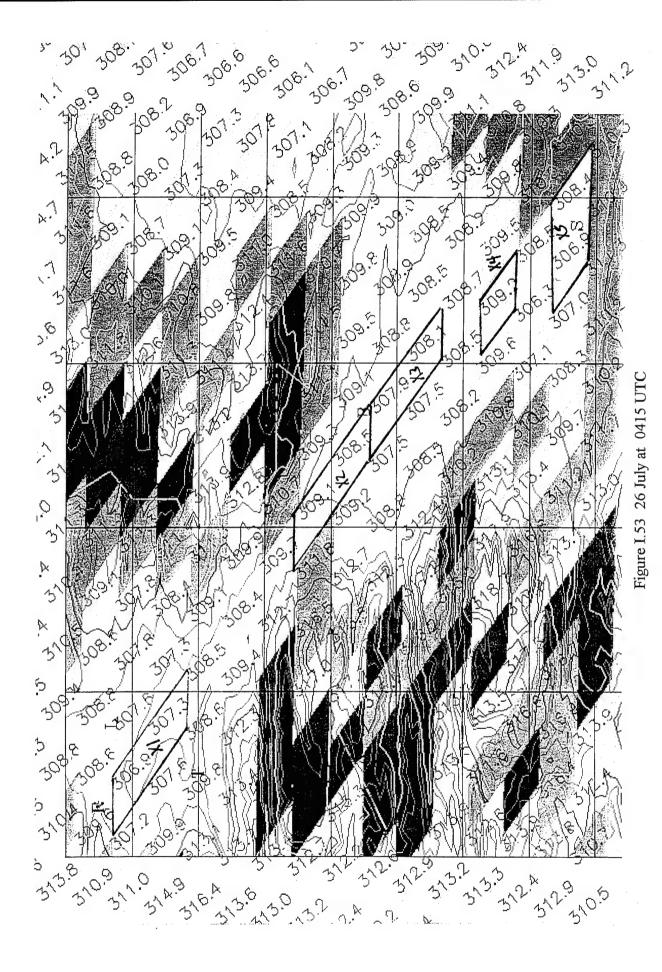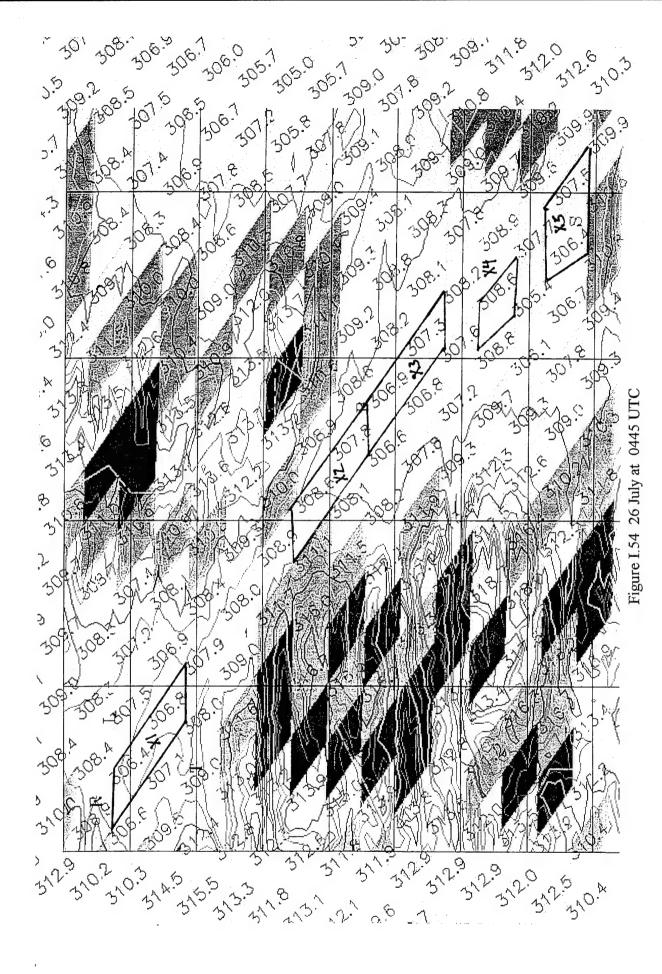
F. Leadville to Salida

Figures I.51 through I.60 depict the potential temperatures of the Leadville to Salida region. The letters R, L, T, B, and S represent the approximate locations of Sugar Loaf Reservoir, Leadville, Twin Lakes, Buena Vista, and Salida, respectively. Elevation contours are from 2438 meters (8000 feet) to 3810 meters (12500 feet) in 152.4 meter (500 feet) intervals. Five areas were selected along the valley floor to represent the along valley gradient. These regions are outlined in bold and labeled X(1) through X(5).
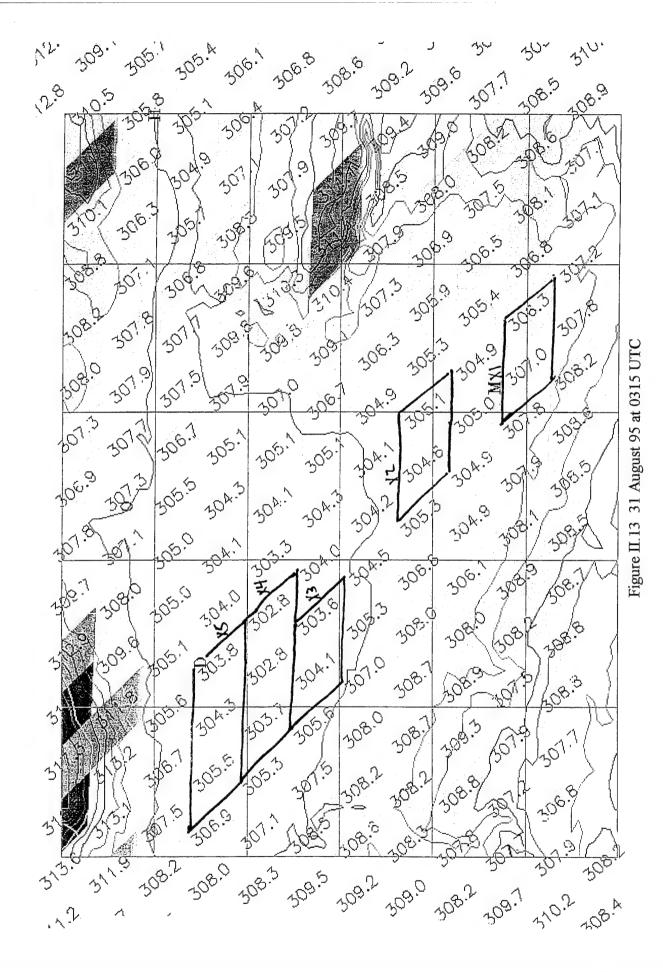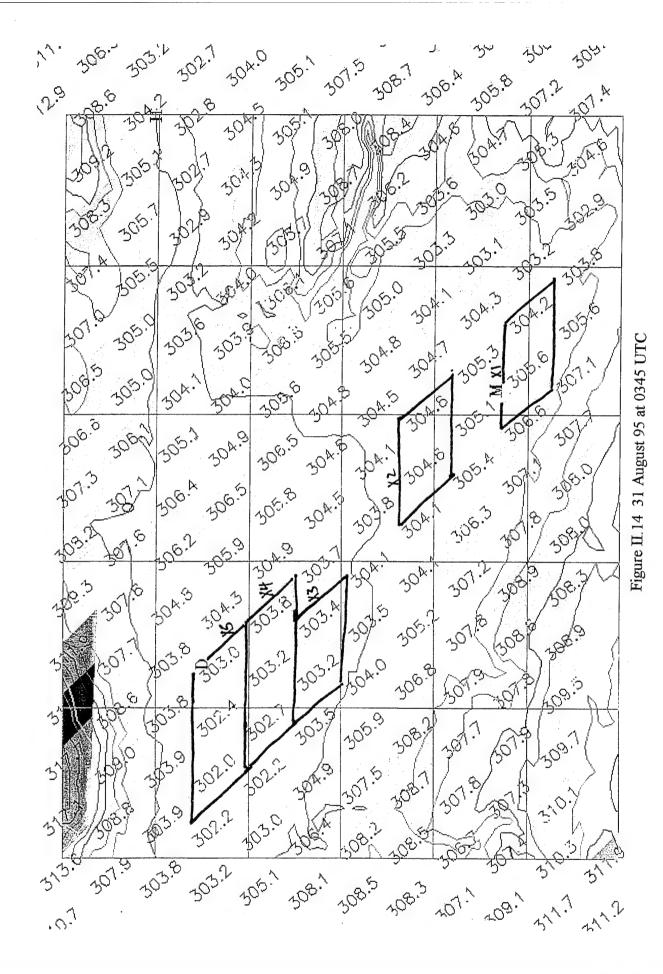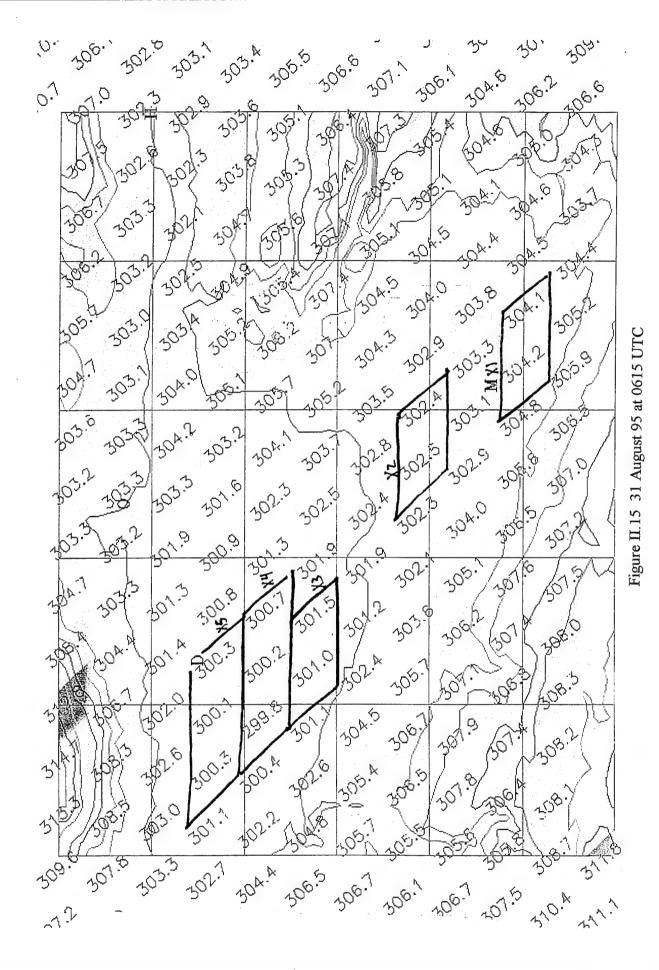
Figure I.51 26 July at 0315 UTC

Figure I.52 26 July at 0345 UTC

Figure I.53 26 July at 0415 UTC

Figure I.54 26 July at 0445 UTC

Figure I.55 26 July at 0515 UTC

Figure I.56 26 July at 0545 UTC

Figure I.57 26 July at 0615 UTC

Figure I.58 26 July at 0645 UTC

Figure I.59 26 July at 0715 UTC

Figure I.60 26 July at 0745 UTC
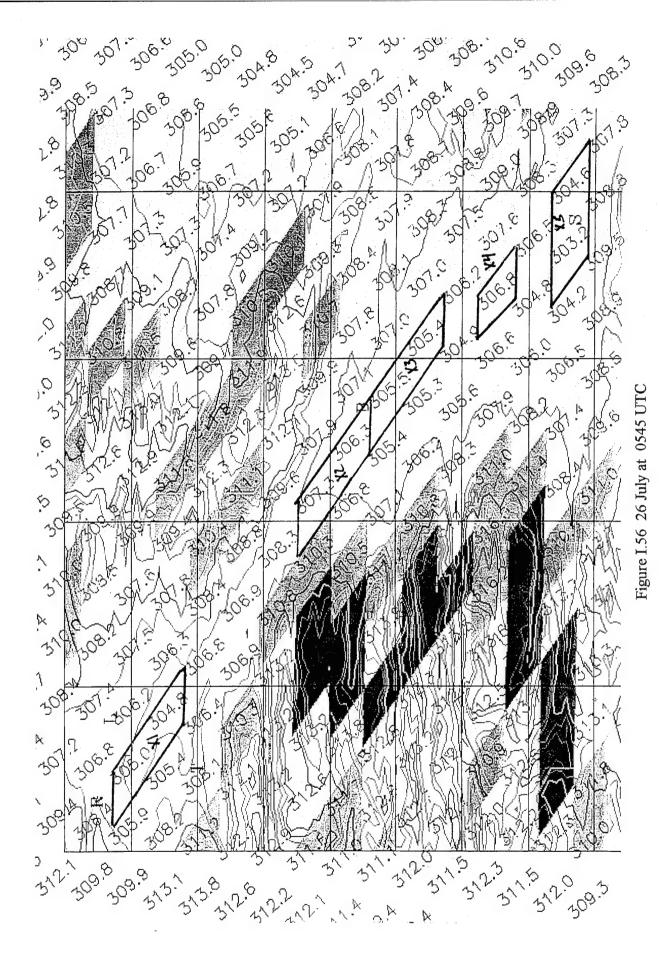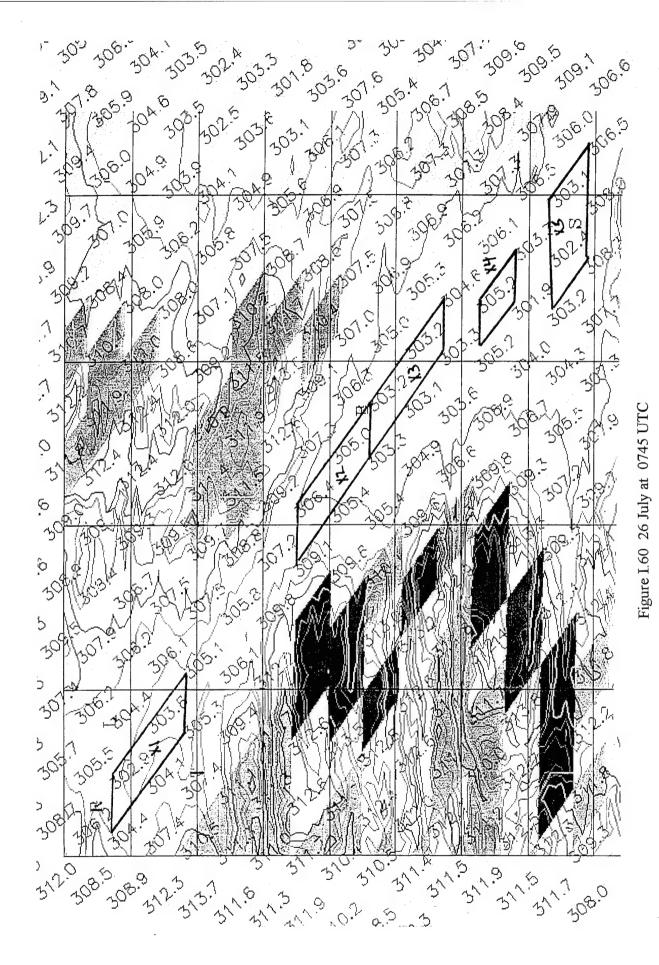
Appendix II

GIF IMAGES FOR 6 AUG AND 31 AUG 95 DEPICTING THE POTENTIAL TEMPERATURES AND TOPOGRAPHY OF SELECTED VALLEY REGIONS

A. Paonia to Delta

Figures II.1 through II.6 depict the potential temperatures of the Paonia to Delta region. The letters P, H, C, O and D depict the approximate locations of the towns of Paonia, Hotchkiss, Cedaredge, Orchard City , and Delta, respectively. Elevation contours are from 1524 meters (5000 feet) to 3353 meters (11000 feet) in 152.4 meter (500 feet) intervals. Three areas were selected along the valley floor to assist in evaluating whether the valley segments were indicative of pooling or draining. These regions are outlined in bold and labeled X(1) through X(3).
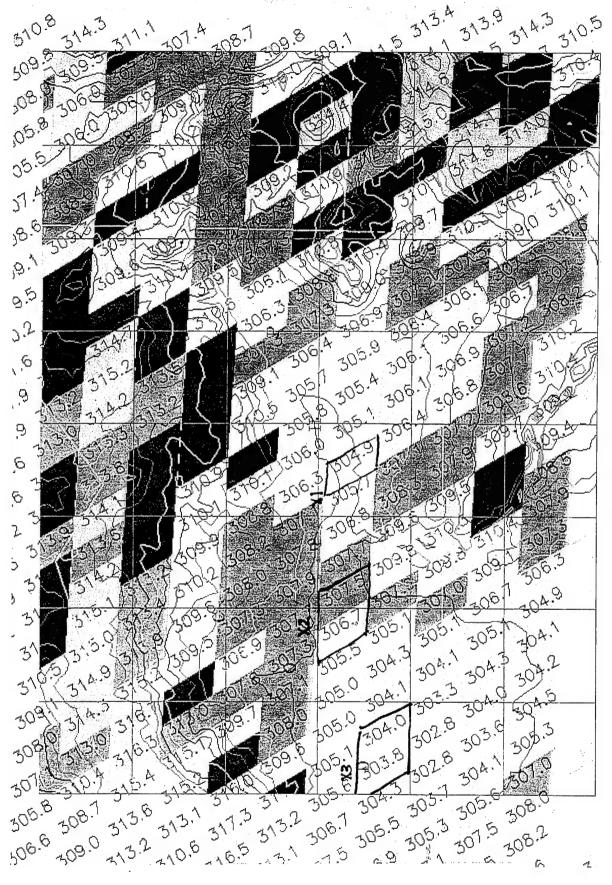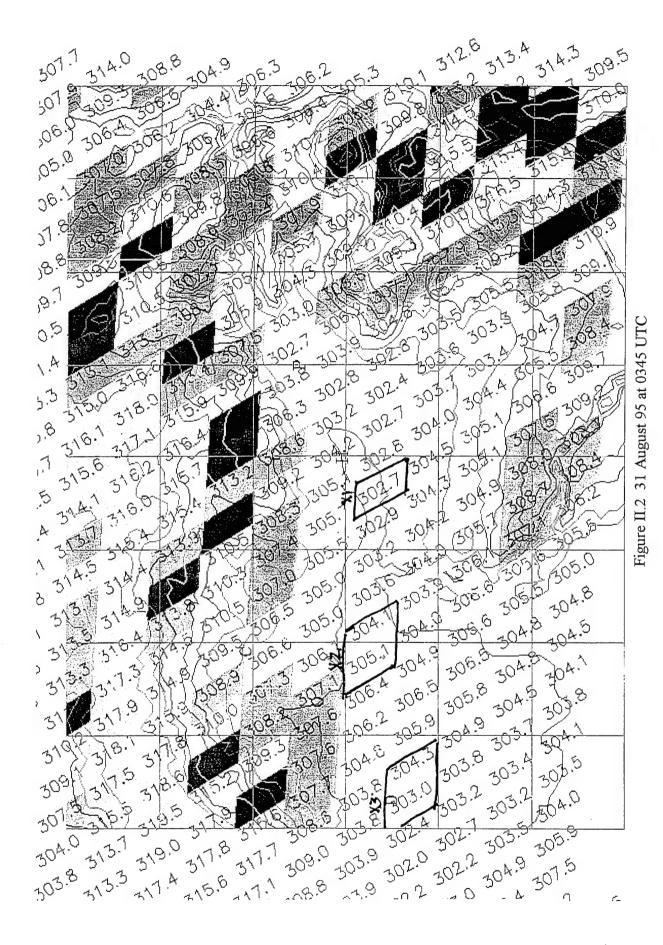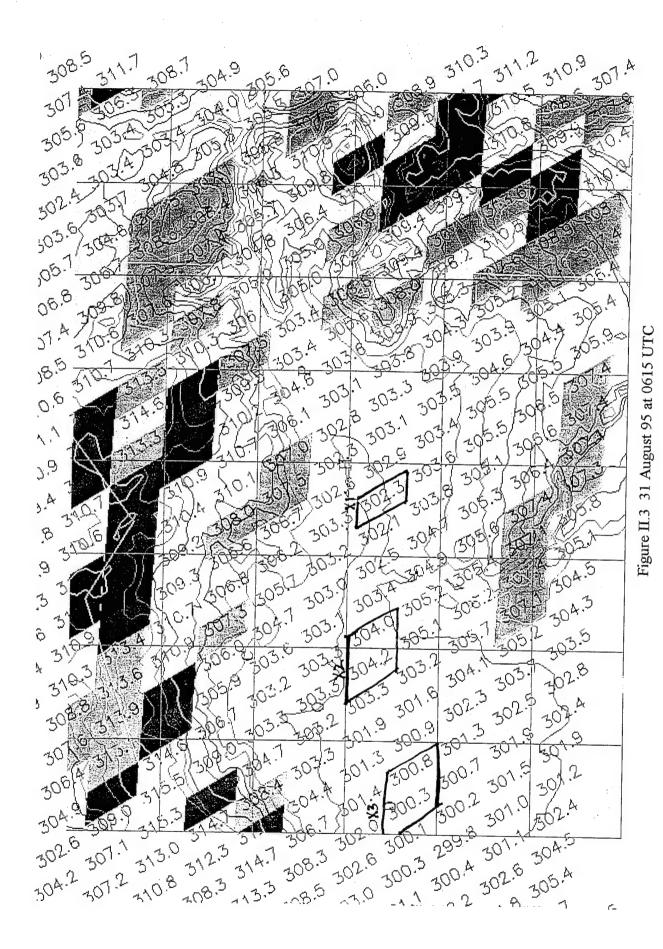
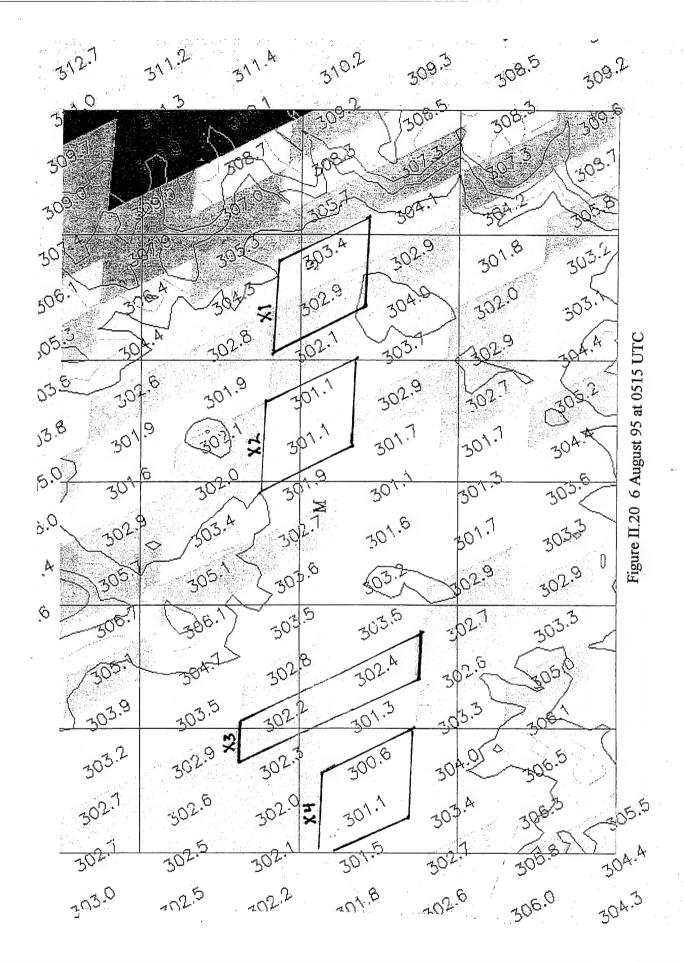Figure II.1 31 August 95 at 0315 UTC

Figure II.2 31 August 95 at 0345 UTC

Figure II.3   31 August 95 at 0615 UTC

Figure II.4 31 August 95 at 0645 UTC

Figure II.5 31 August 95 at 0715 UTC

Figure II.6 31 August 95 at 0745 UTC
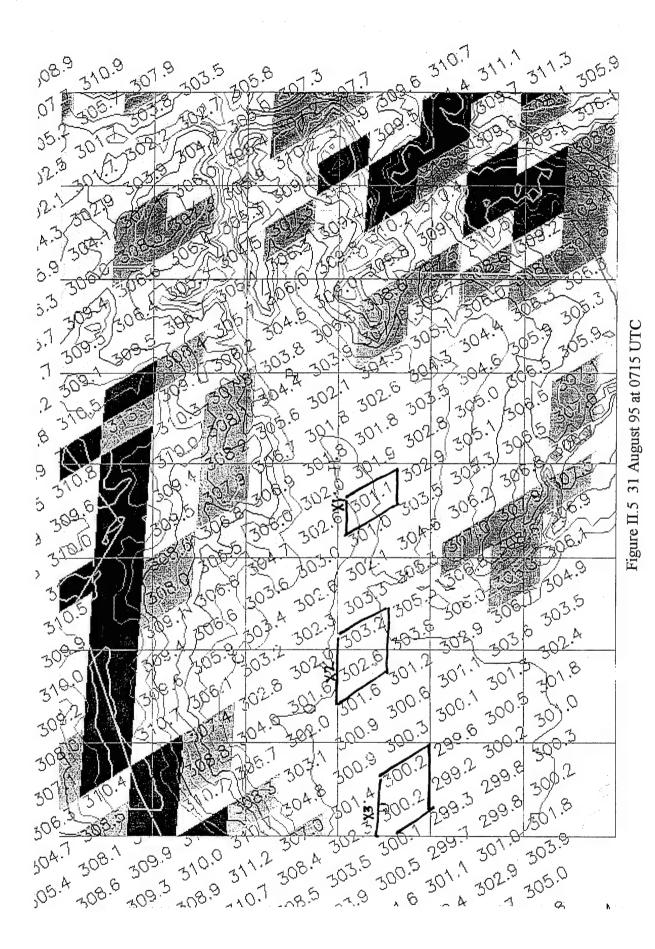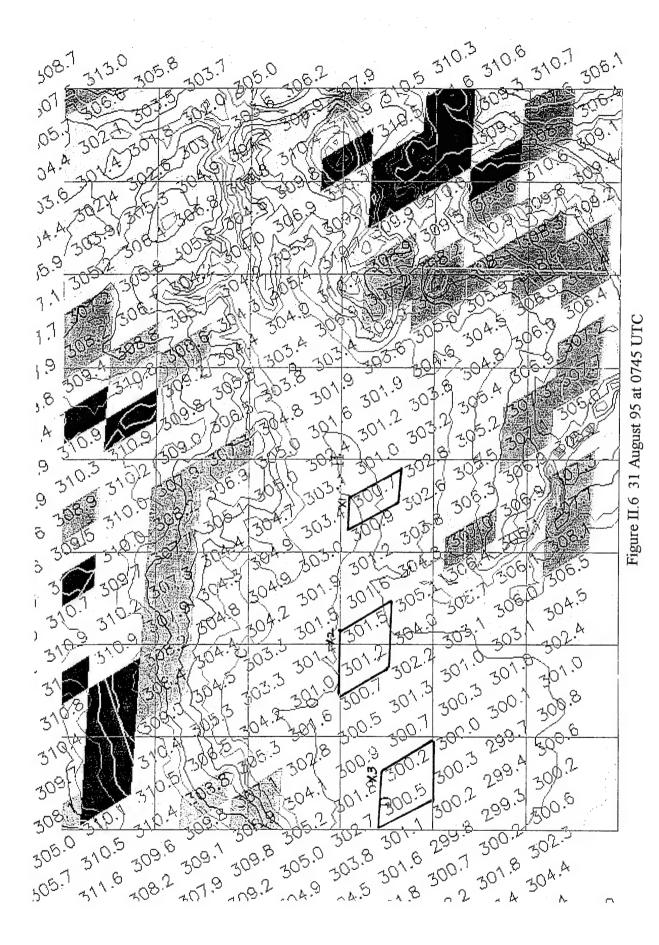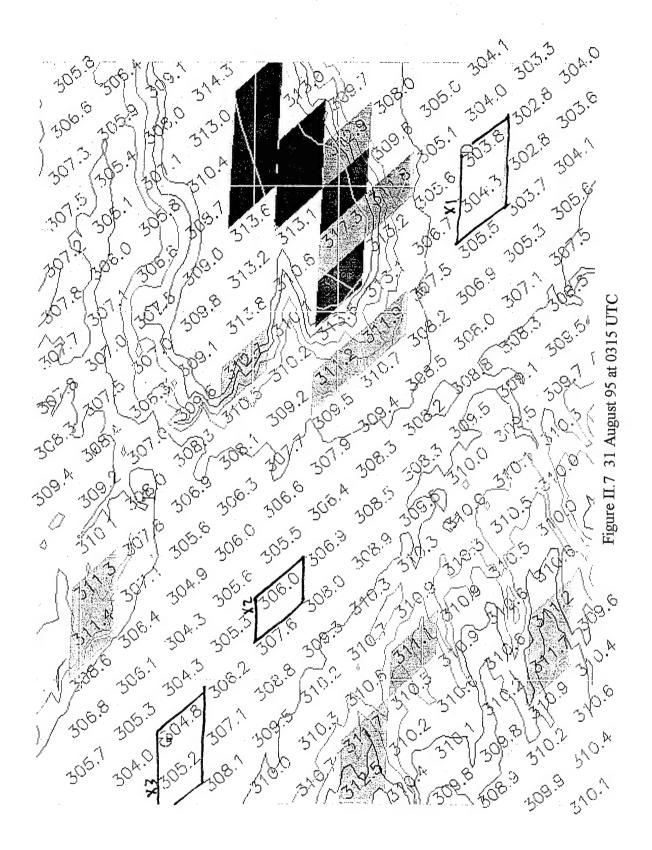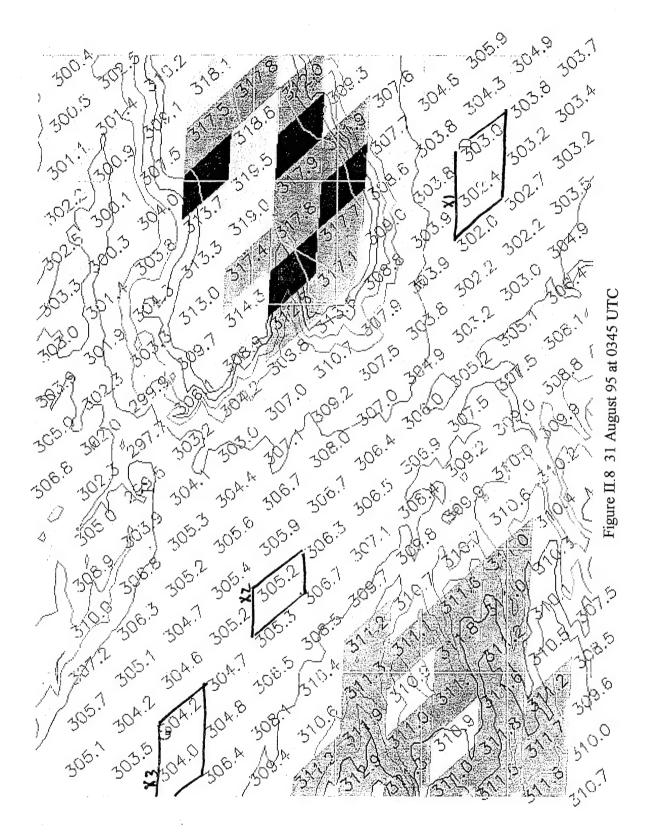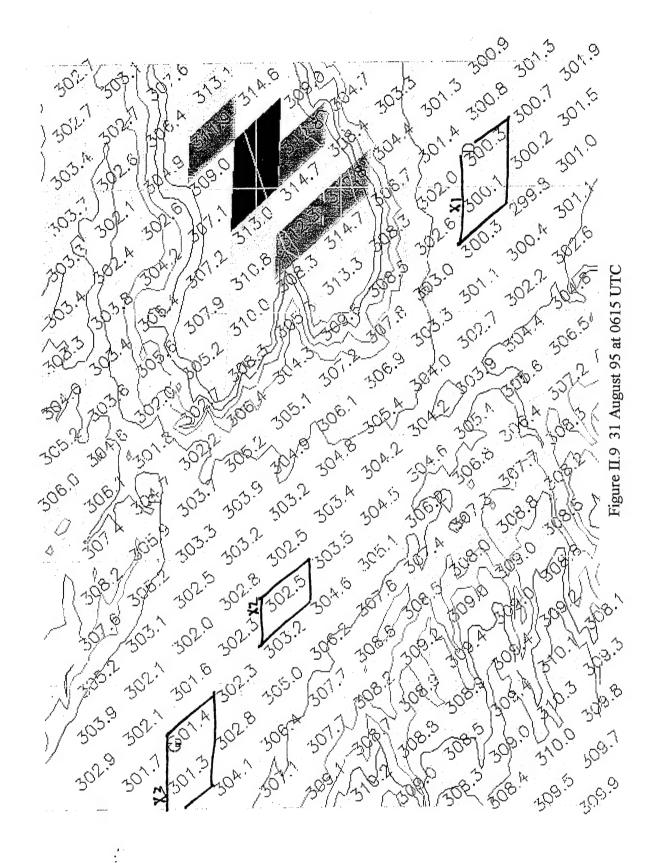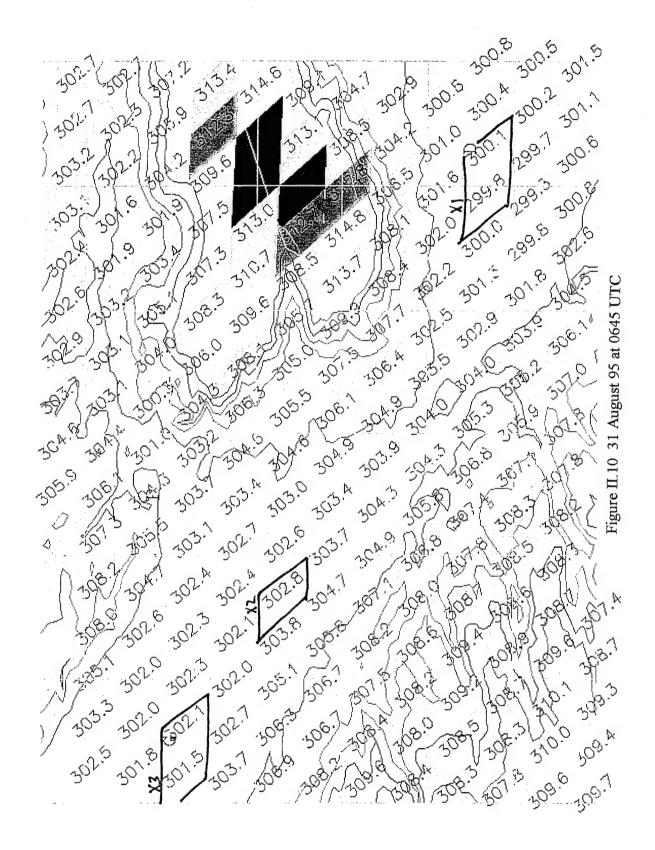
B. Delta to Grand Junction

Figures II.7 through II.12 depict the potential temperatures of the Delta to Grand Junction region. The letters D and P represent the approximate locations of the towns of Delta and Palisade, respectively. G depict the approximate location of the Grand Junction (GJT) Weather Service Office (WSO). Elevation contours are from 1524 meters (5000 feet) to 2591 meters (8500 feet) in 152.4 meter (500 feet) intervals. Three areas were selected along the valley floor to represent the along valley gradient. These regions are outlined in bold and labeled X(1) through X(3).

Figure II.7 31 August 95 at 0315 UTC

Figure II.8 31 August 95 at 0345 UTC

Figure II.9 31 August 95 at 0615 UTC

Figure II.10 31 August 95 at 0645 UTC

Figure II.11 31 August 95 at 0715 UTC

Figure II.12 31 August 95 at 0745 UTC
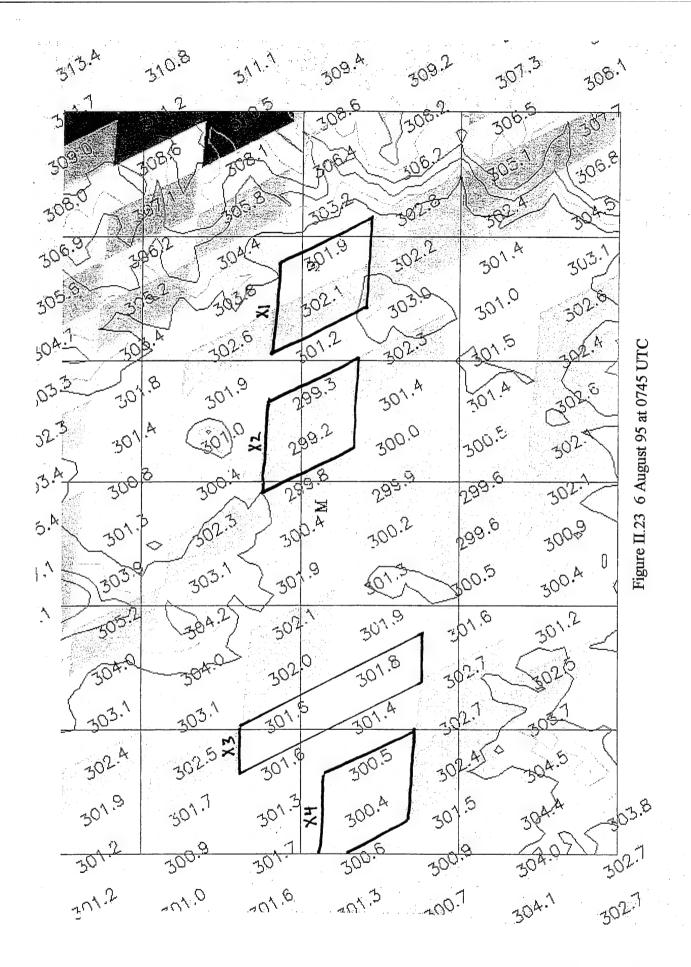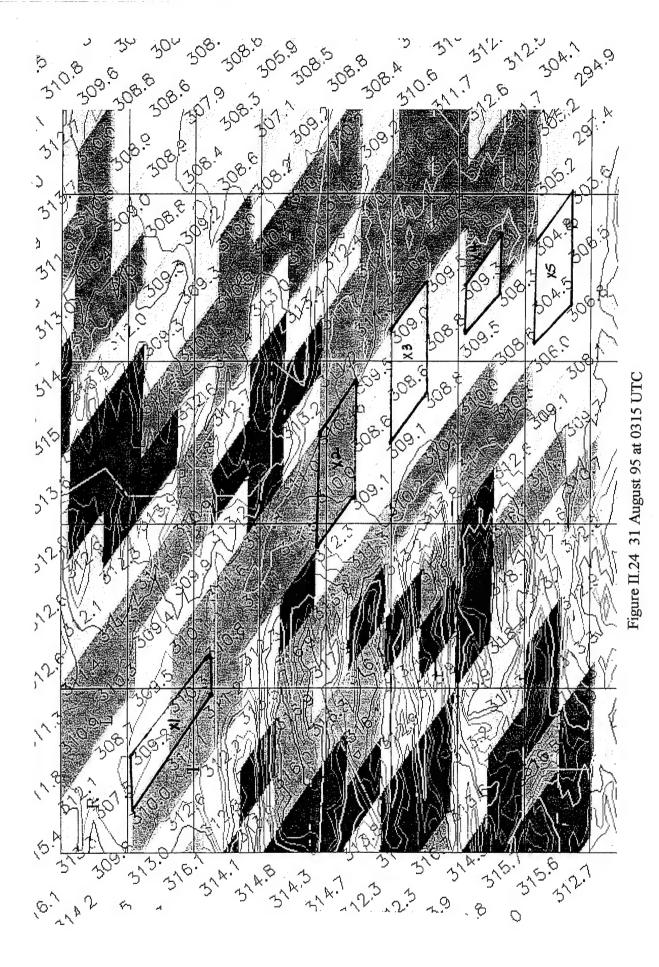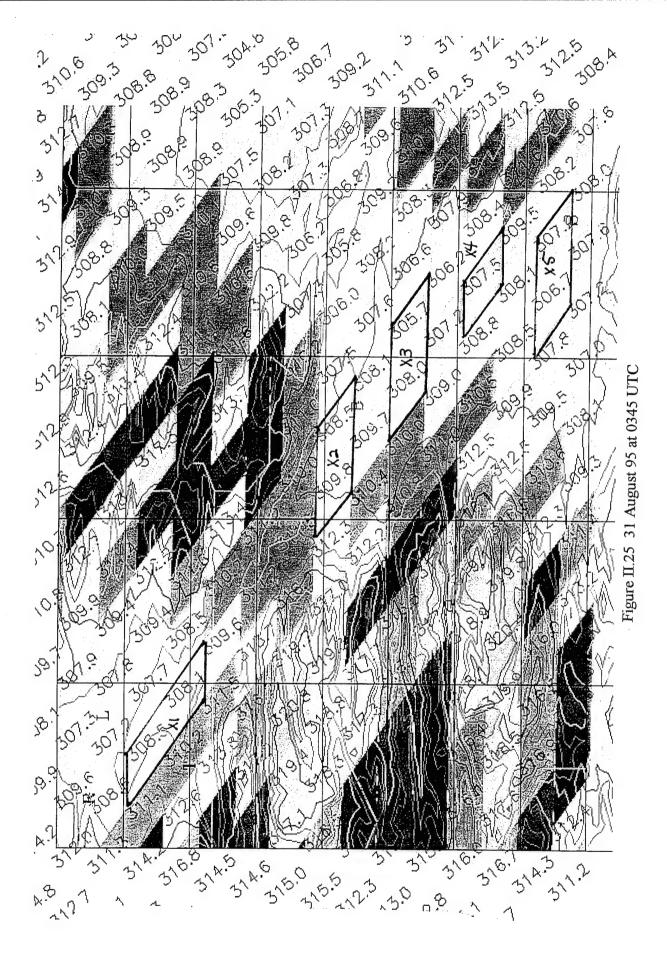
C. Montrose to Delta

Figures II.13 through II.18 depict the potential temperatures of the Montrose to Delta region. The letters M, D, O and H represent the approximate locations of the towns of Montrose, Delta, Orchard City, and Hotchkiss, respectively. Elevation contours are from 1524 meters (5000 feet) to 3048 meters (10000 feet) in 152.4 meter (500 feet) intervals. Five areas were selected along the valley floor to represent the along valley gradient. These regions are outlined in bold and labeled X(1) through X(5).
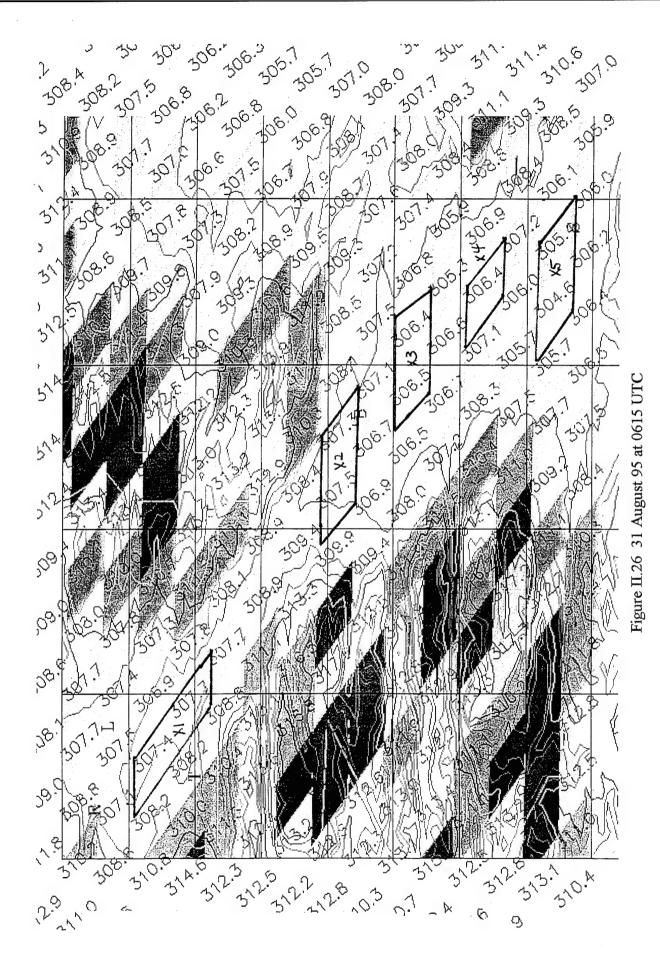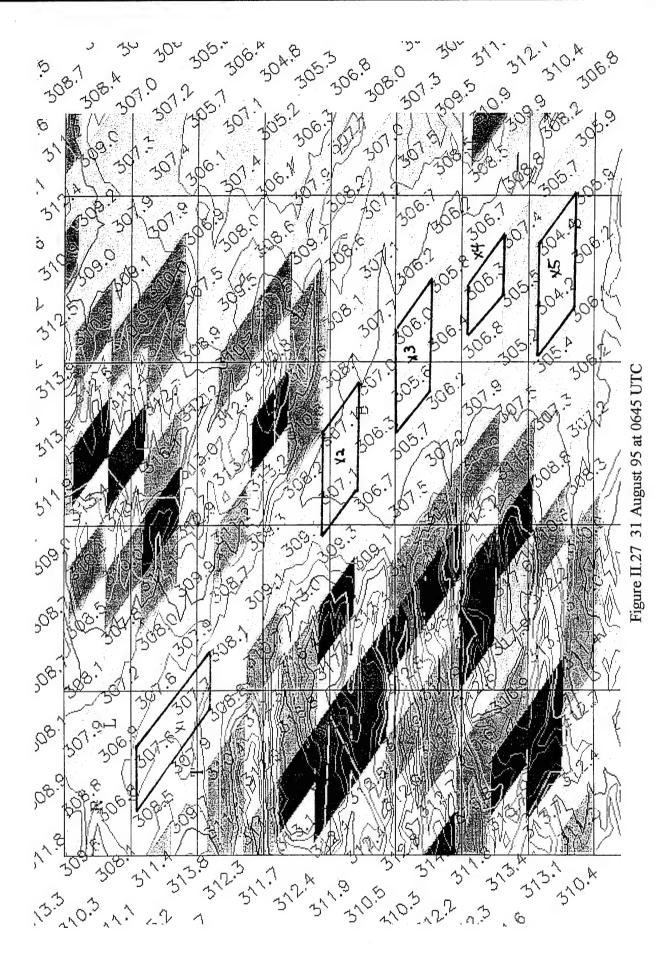
Figure II.13 31 August 95 at 0315 UTC

Figure II.14 31 August 95 at 0345 UTC

II-18

Figure II.15 31 August 95 at 0615 UTC

Figure II.16 31 August 95 at 0645 UTC

Figure II.17 31 August 95 at 0715 UTC
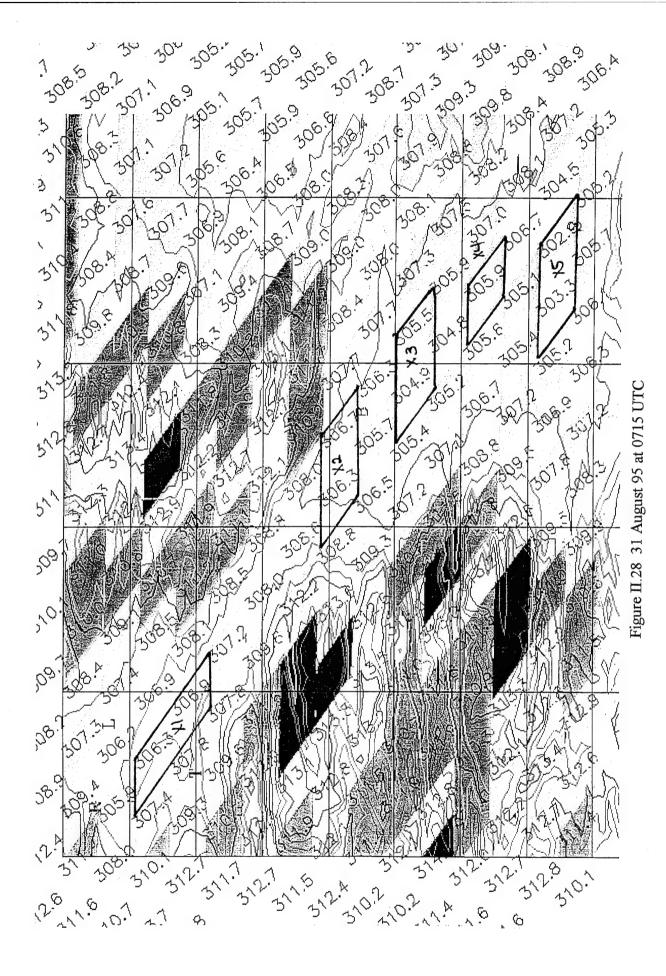
Figure II.18 31 August 95 at 0745 UTC
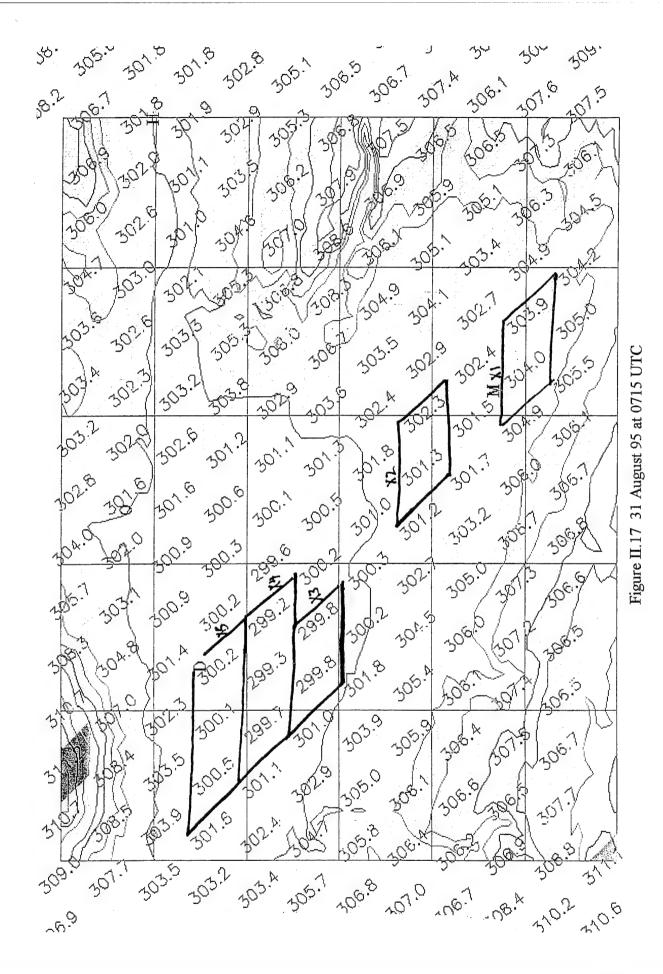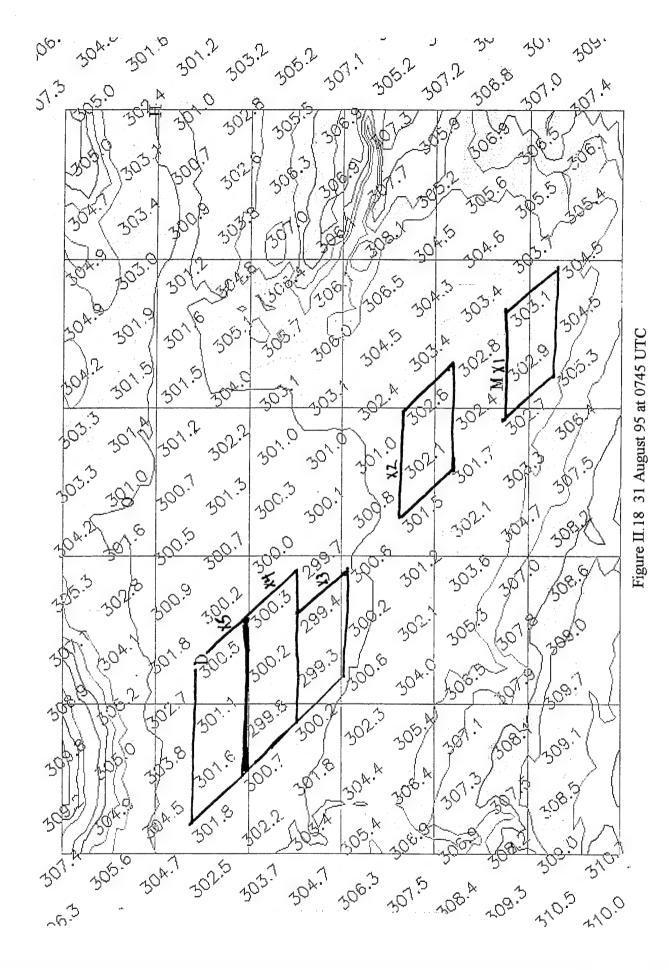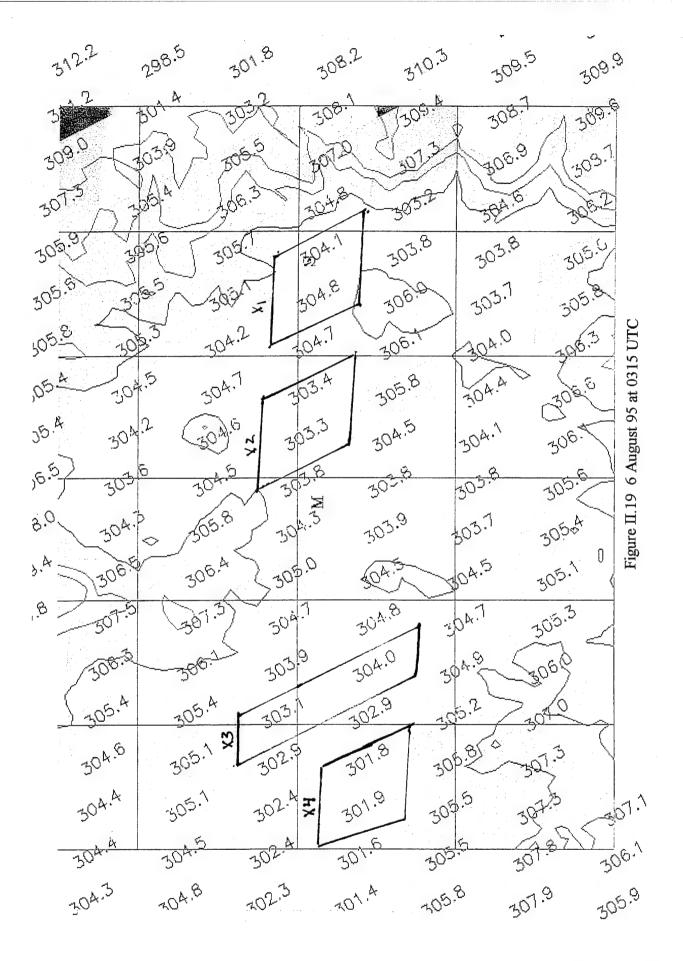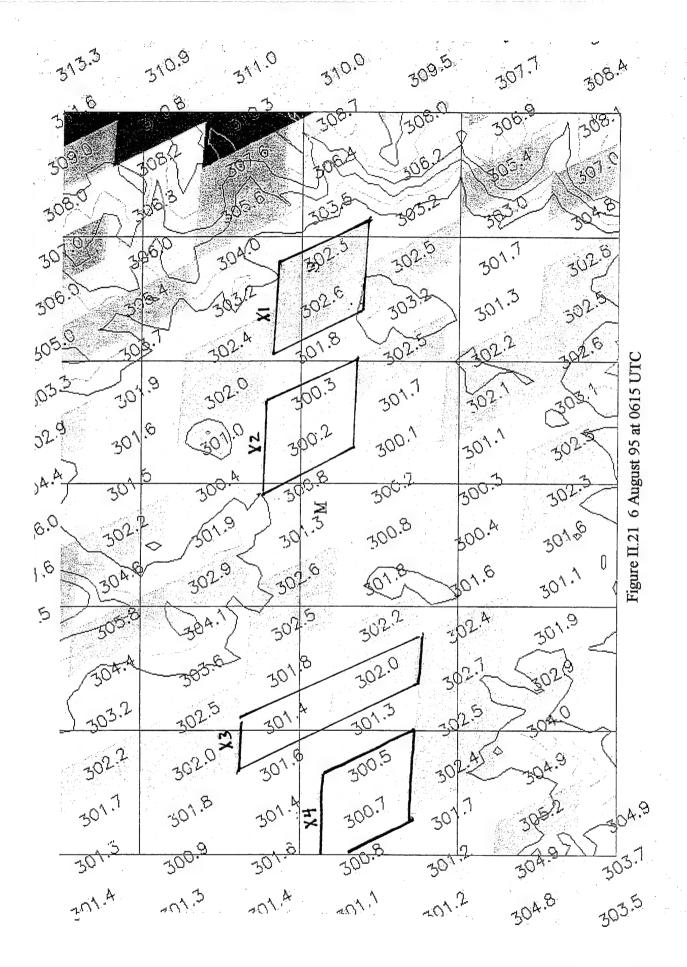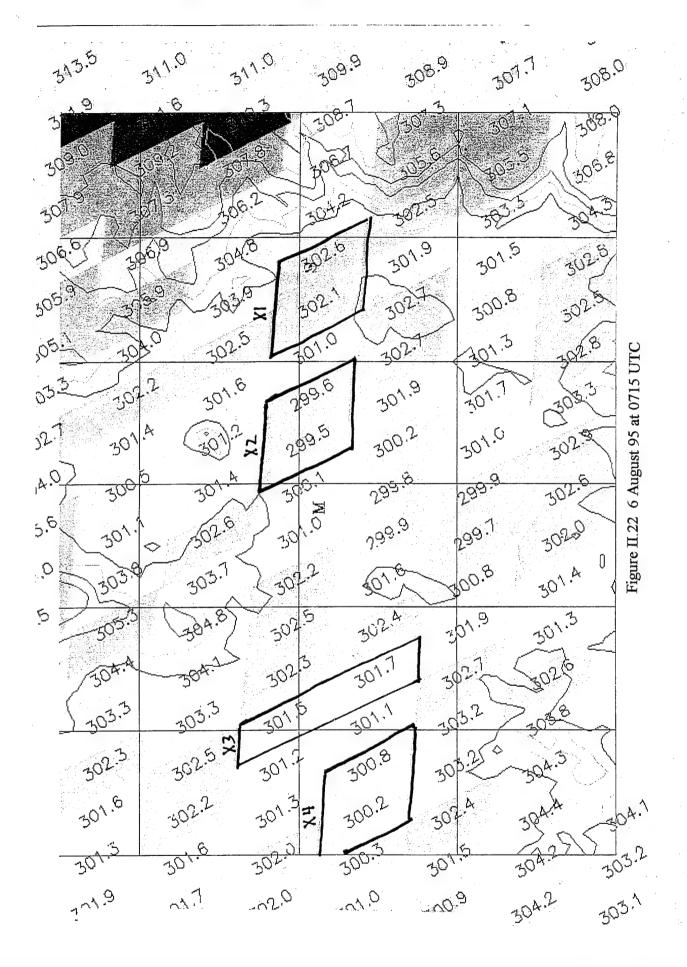
D. Yampa Valley

Figures II.19 through II.23 depict the potential temperatures of the Montrose to Delta region. The letters S and M represent the approximate locations of the towns of Steamboat and Milner, respectively. Elevation contours are from 1829 meters (6000 feet) to 3048 meters (10000 feet) in 152.4 meter (500 feet) intervals. Four areas were selected along the valley floor to represent the along valley gradient. These regions are outlined in bold and labeled X(1) through X(4).
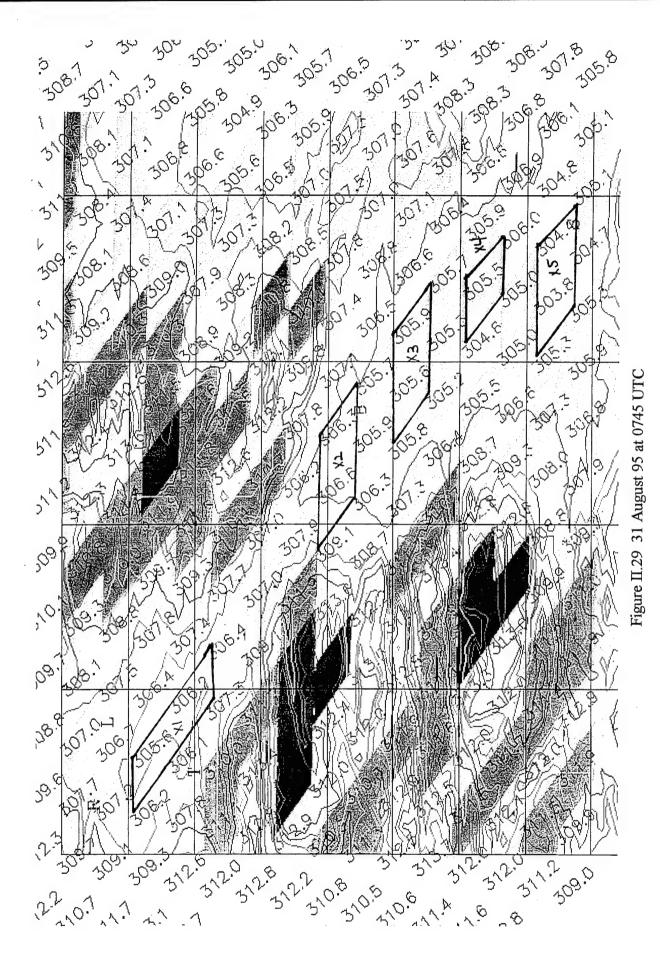
Figure II.19 6 August 95 at 0315 UTC

Figure II.20 6 August 95 at 0515 UTC

Figure II.21 6 August 95 at 0615 UTC

Figure II.22 6 August 95 at 0715 UTC

Figure II.23 6 August 95 at 0745 UTC

E. Leadville to Salida

Figures II.24 through II.29 depict the potential temperatures of the Leadville to Salida region. The letters R, L, T, B, and S represent the approximate locations of Sugar Loaf Reservoir, Leadville, Twin Lakes, Buena Vista, and Salida, respectively. Elevation contours are from 2438 meters (8000 feet) to 3810 meters (12500 feet) in 152.4 meter (500 feet) intervals. Five areas were selected along the valley floor to represent the along valley gradient. These regions are outlined in bold and labeled X(1) through X(5).

Figure II.24 31 August 95 at 0315 UTC

Figure II.25 31 August 95 at 0345 UTC

Figure II.26 31 August 95 at 0615 UTC

Figure II.27 31 August 95 at 0645 UTC

Figure II.28 31 August 95 at 0715 UTC

Figure II.29 31 August 95 at 0745 UTC

Appendix III

GIF IMAGES FOR 26 JULY 95 DEPICTING THE MEAN ELEVATIONS OF EACH PIXEL AND TOPOGRAPHY OF SELECTED VALLEY REGIONS

Figures III.1 through III.6 depict the mean elevations derived for each pixel on 26 July 95 for each of the valley regions evaluated.

In figure III.1, the letters P, H, C, O and D depict the approximate locations of the towns of Paonia, Hotchkiss, Cedaredge, Orchard City and Delta, respectively. Elevation contours are from 1524 meters (5000 feet) to 3353 meters (11000 feet) in 152.4 meter (500 feet) intervals.

In figure III.2, the letters D and P represent the approximate locations of the towns of Delta and Palisade, respectively. G represents the approximate location of the Grand Junction (GJT) weather service office (WSO). Elevation contours are from 1524 meters (5000 feet) to 2591 meters (8500 feet) in 152.4 meter (500 feet) intervals.

In figure III.3, the letters M, D, O and H represent the approximate locations of the towns of Montrose, Delta, Orchard City, and Hotchkiss, respectively. Elevation contours are from 1524 meters (5000 feet) to 3048 meters (10000 feet) in 152.4 meter (500 feet) intervals.

In figure III.4, the letters P and G represent the approximate locations of the town of Parachute and the GJT WSO, respectively. Elevation contours are from 1524 meters (5000 feet) to 2743 meters (9000 feet) in 152.4 meter (500 feet) intervals.

In figure III.5, the letters S and M represent the approximate locations of the towns of Steamboat and Milner, respectively. Elevation contours are from 1829 meters (6000 feet) to 3048 meters (10000 feet) in 152.4 meter (500 feet) intervals.

In figure III.6, the letters R, L, T, B, and S represent the approximate locations of Sugar Loaf Reservoir, Leadville, Twin Lakes, Buena Vista, and Salida, respectively. Elevation contours are from 2438 meters (8000 feet) to 3810 meters (12500 feet) in 152.4 meter (500 feet) intervals.
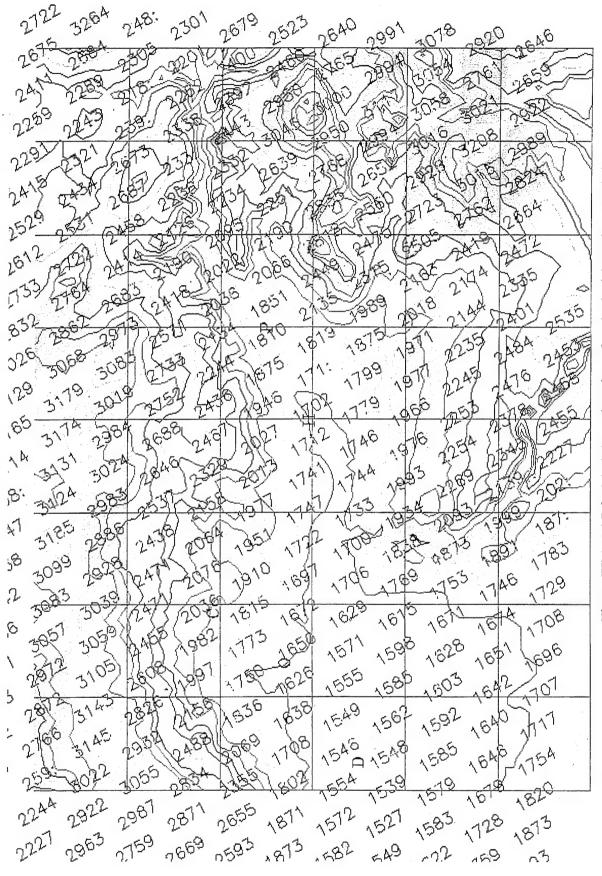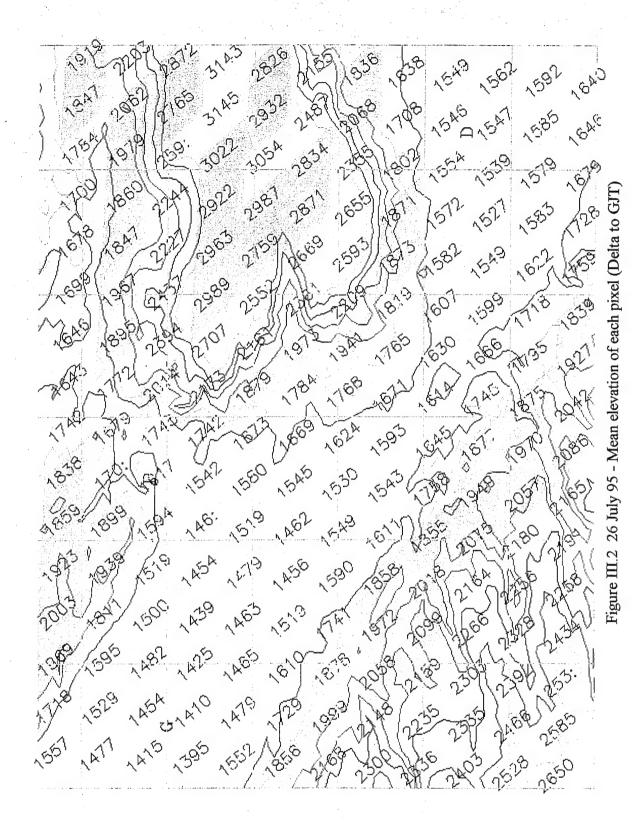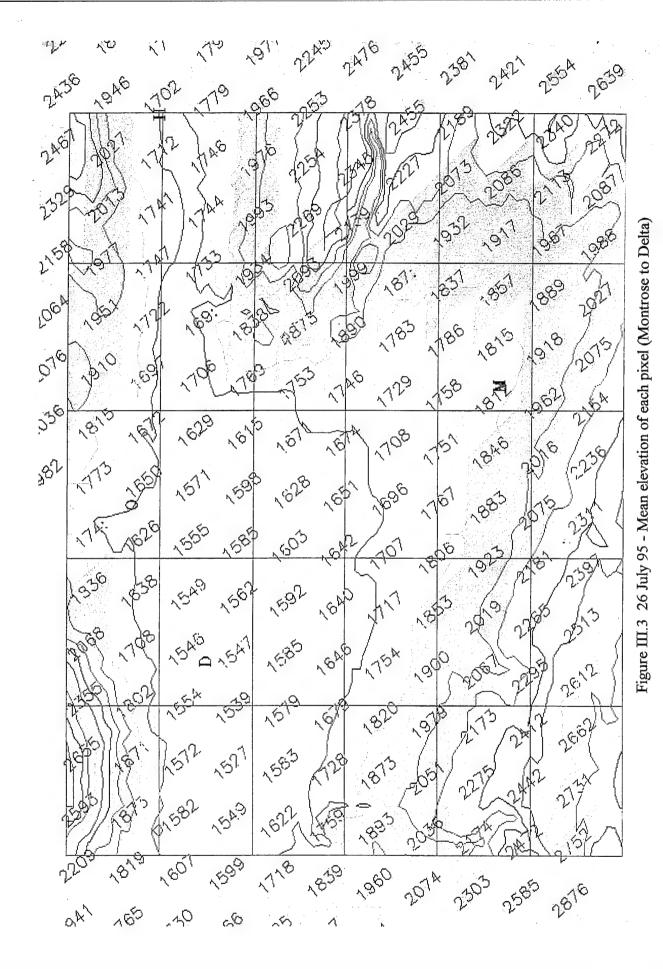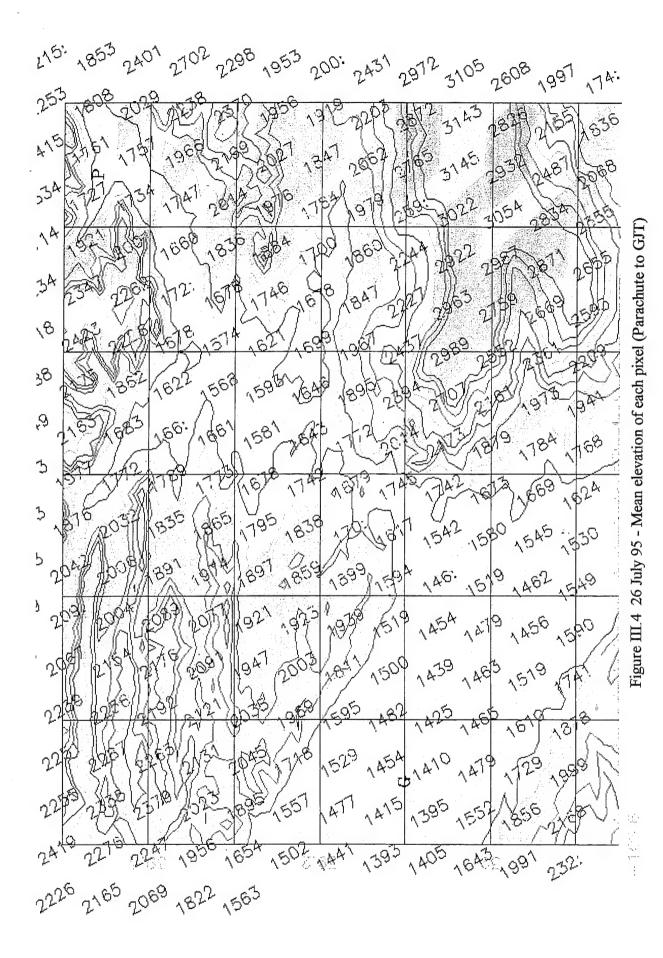
Figure III.1 26 July 95 - Mean elevation of each pixel (Paonia to Delta)

Figure III.2 26 July 95 - Mean elevation of each pixel (Delta to GJT)

Figure III.3 26 July 95 - Mean elevation of each pixel (Montrose to Delta)

Figure III.4 26 July 95 - Mean elevation of each pixel (Parachute to GJT)

Figure III.5 26 July 95 - Mean elevation of each pixel (Yampa Valley)

Figure III.6 26 July 95 - Mean elevation of each pixel (Leadville to Salida)

Appendix IV

GIF IMAGES FOR 31 AUG 95 DEPICTING THE MEAN ELEVATIONS OF EACH PIXEL AND TOPOGRAPHY OF SELECTED VALLEY REGIONS

Figures IV.1 through IV.4 depict the mean elevations derived for each pixel on 31 Aug 95. Note the orientation of the pixels on 6 Aug 95 were the same as those of 26 Jul 95; hence, the mean elevations of the pixels on 6 Aug 95 are the same as those of 26 Jul 95.

In figure IV.1, the letters P, H, C, O and D depict the approximate locations of the towns of Paonia, Hotchkiss, Cedaredge, Orchard City and Delta, respectively. Elevation contours are from 1524 meters (5000 feet) to 3353 meters (11000 feet) in 152.4 meter (500 feet) intervals.

In figure IV.2, the letters D and P represent the approximate locations of the towns of Delta and Palisade, respectively. G represents the approximate location of the Grand Junction (GJT) weather service office (WSO). Elevation contours are from 1524 meters (5000 feet) to 2591 meters (8500 feet) in 152.4 meter (500 feet) intervals.

In figure IV.3, the letters M, D, O and H represent the approximate locations of the towns of Montrose, Delta, Orchard City, and Hotchkiss, respectively. Elevation contours are from 1524 meters (5000 feet) to 3048 meters (10000 feet) in 152.4 meter (500 feet) intervals.

In figure IV.4, the letters R, L, T, B, and S represent the approximate locations of Sugar Loaf Reservoir, Leadville, Twin Lakes, Buena Vista, and Salida, respectively. Elevation contours are from 2438 meters (8000 feet) to 3810 meters (12500 feet) in 152.4 meter (500 feet) intervals.
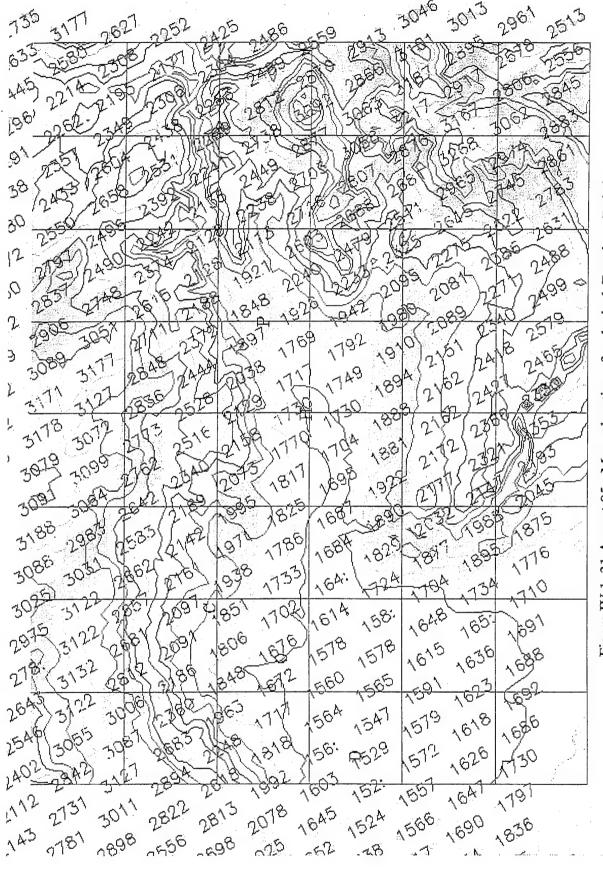
Figure IV.1 31 August 95 - Mean elevation of each pixel (Paonia to Delta)
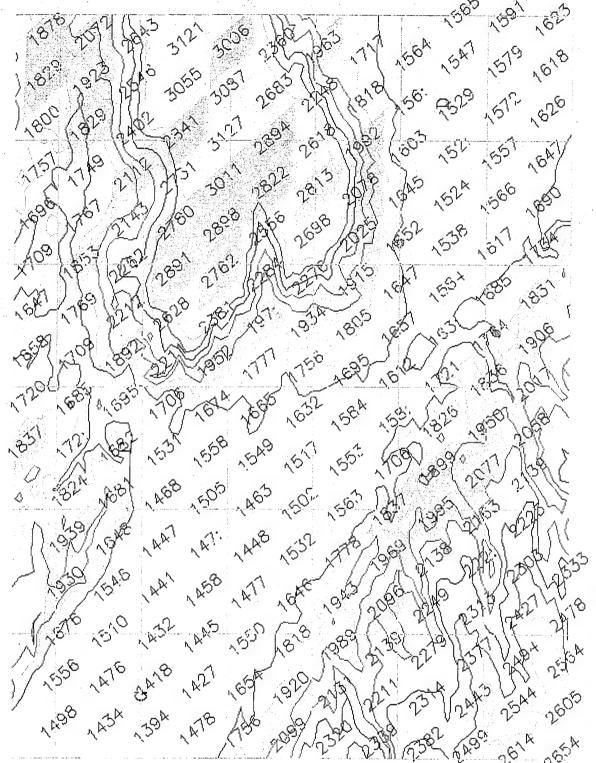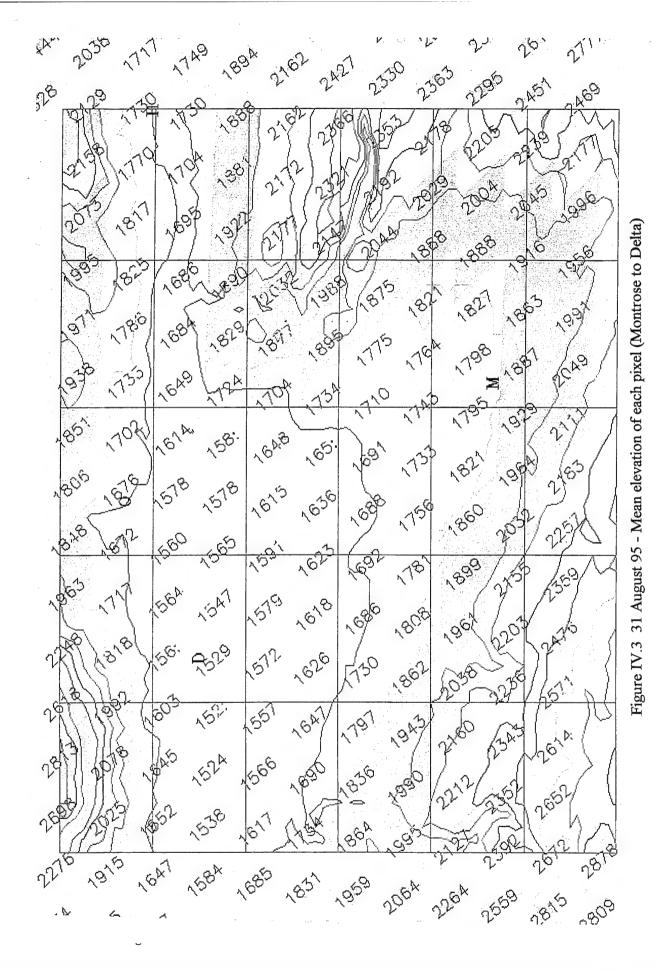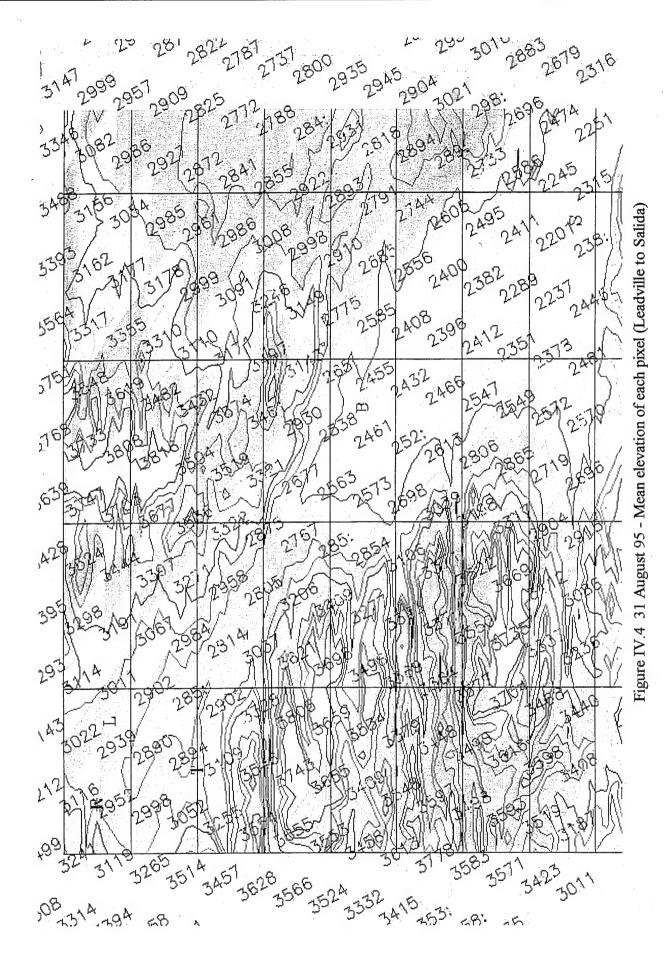
Figure IV.2 31 August 95 - Mean elevation of each pixel (Delta to GJT)

Figure IV.3 31 August 95 - Mean elevation of each pixel (Montrose to Delta)

IV-4

Figure IV.4 31 August 95 - Mean elevation of each pixel (Leadville to Salida)

Appendix V

GIF IMAGES FOR 26 JULY 95 DEPICTING THE TEMPERATURE ADJUSTMENT MADE TO EACH PIXEL AND TOPOGRAPHY OF SELECTED VALLEY REGIONS

Figures V.1 through V.6 depict the temperature adjustment made to each pixel on 26 July 95 for each of the valley regions evaluated.

In figure V.1, the letters P, H, C, O and D depict the approximate locations of the towns of Paonia, Hotchkiss, Cedaredge, Orchard City and Delta, respectively. Elevation contours are from 1524 meters (5000 feet) to 3353 meters (11000 feet) in 152.4 meter (500 feet) intervals.
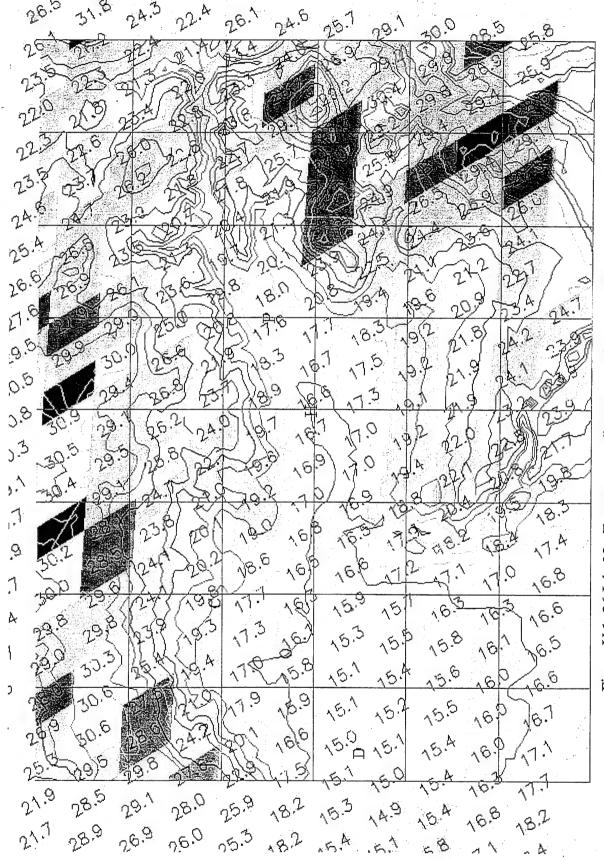
In figure V.2, the letters D and P represent the approximate locations of the towns of Delta and Palisade, respectively. G represents the approximate location of the Grand Junction (GJT) weather service office (WSO). Elevation contours are from 1524 meters (5000 feet) to 2591 meters (8500 feet) in 152.4 meter (500 feet) intervals.

In figure V.3, the letters M, D, O and H represent the approximate locations of the towns of Montrose, Delta, Orchard City, and Hotchkiss, respectively. Elevation contours are from 1524 meters (5000 feet) to 3048 meters (10000 feet) in 152.4 meter (500 feet) intervals.

In figure V.4, the letters P and G represent the approximate locations of the town of Parachute and the GJT WSO, respectively. Elevation contours are from 1524 meters (5000 feet) to 2743 meters (9000 feet) in 152.4 meter (500 feet) intervals.

In figure V.5, the letters S and M represent the approximate locations of the towns of Steamboat and Milner, respectively. Elevation contours are from 1829 meters (6000 feet) to 3048 meters (10000 feet) in 152.4 meter (500 feet) intervals.

In figure V.6, the letters R, L, T, B, and S represent the approximate locations of Sugar Loaf Reservoir, Leadville, Twin Lakes, Buena Vista, and Salida, respectively. Elevation contours are from 2438 meters (8000 feet) to 3810 meters (12500 feet) in 152.4 meter (500 feet) intervals.

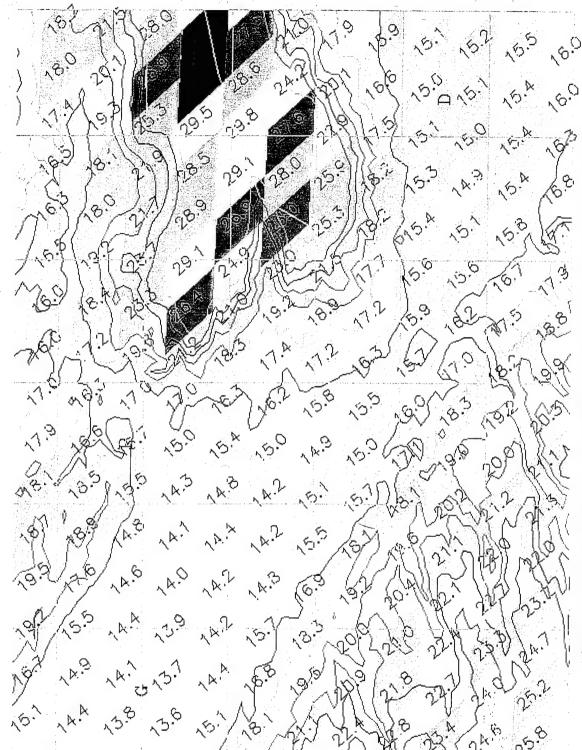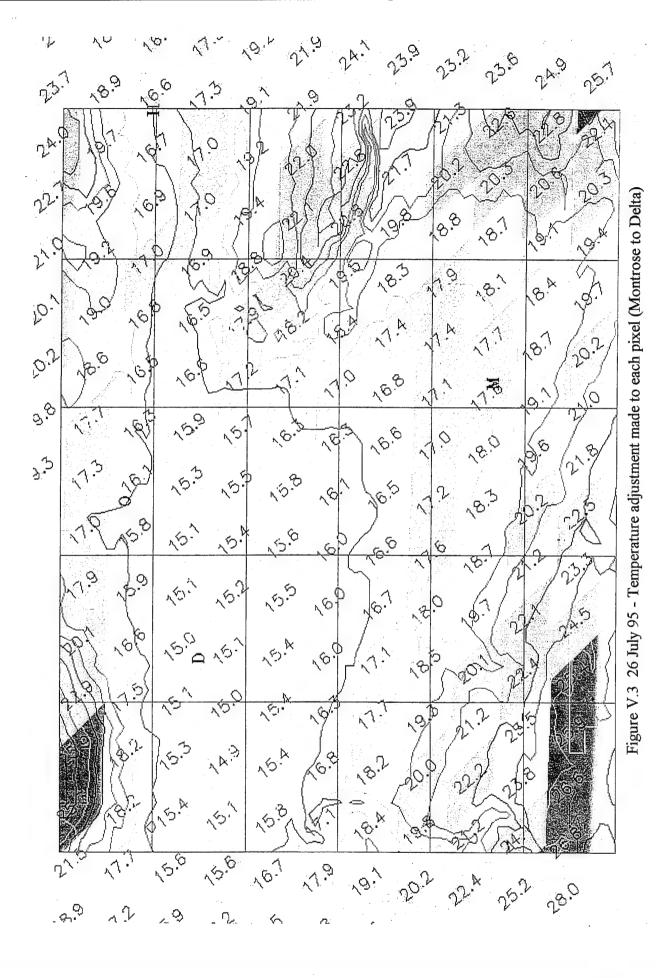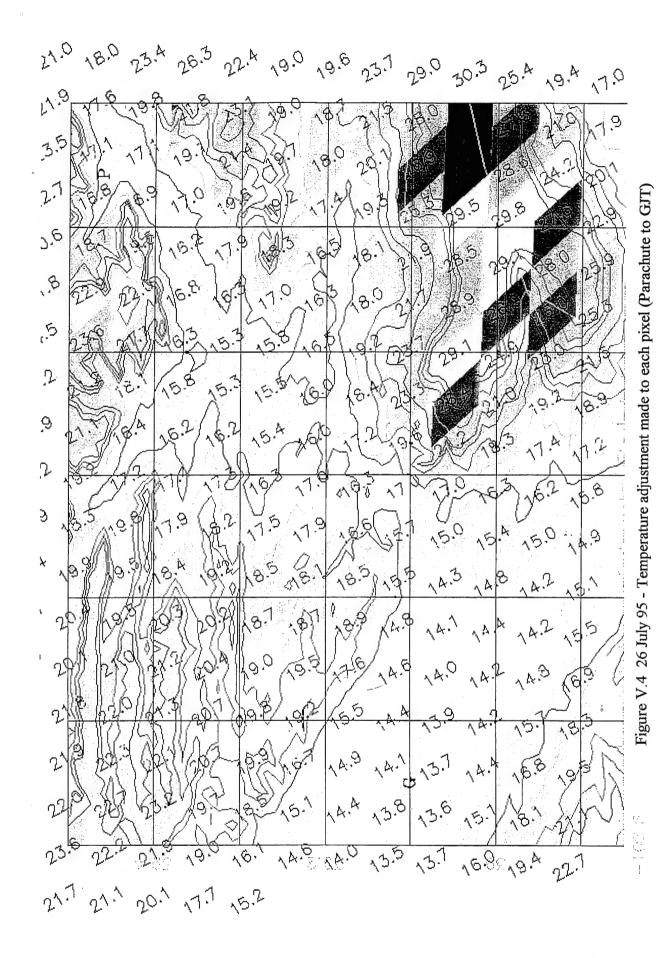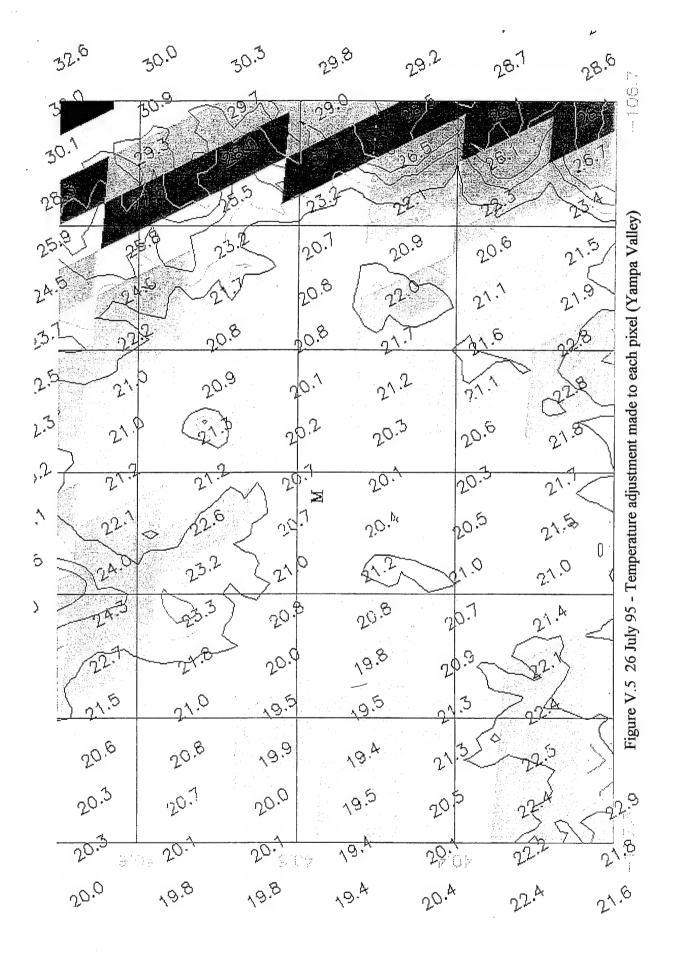Figure V.1 26 July 95 - Temperature adjustment made to each pixel (Paonia to Delta)

Figure V.2 26 July 95 - Temperature adjustment made to each pixel (Delta to GJT)

Figure V.3 26 July 95 - Temperature adjustment made to each pixel (Montrose to Delta)

Figure V.4 26 July 95 - Temperature adjustment made to each pixel (Parachute to GJT)

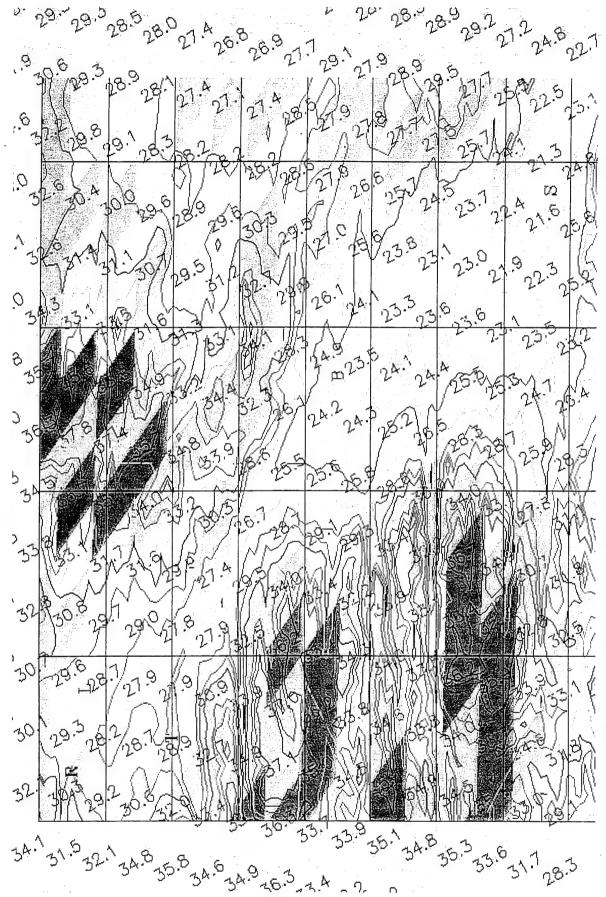Figure V.5 26 July 95 - Temperature adjustment made to each pixel (Yampa Valley)

Figure V.6 26 July 95 - Temperature adjustment made to each pixel (Leadville to Salida)

Appendix VI

GIF IMAGES FOR 31 AUG 95 DEPICTING THE TEMPERATURE ADJUSTMENT MADE TO EACH PIXEL AND TOPOGRAPHY OF SELECTED VALLEY REGIONS
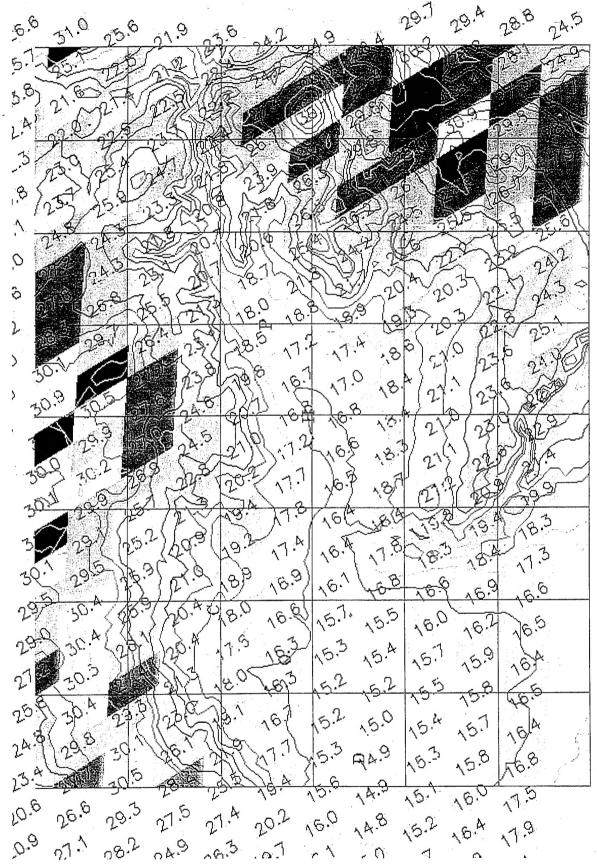
Figures VI.1 through VI.4 depict the mean elevations derived for each pixel on 31 Aug 95. Note the orientation of the pixels on 6 Aug 95 were the same as those of 26 Jul 95, resulting, in the same temperature adjustments for both dates..

In figure VI.1, the letters P, H, C, O and D depict the approximate locations of the towns of Paonia, Hotchkiss, Cedaredge, Orchard City and Delta, respectively. Elevation contours are from 1524 meters (5000 feet) to 3353 meters (11000 feet) in 152.4 meter (500 feet) intervals.

In figure VI.2, the letters D and P represent the approximate locations of the towns of Delta and Palisade, respectively. G represents the approximate location of the Grand Junction (GJT) weather service office (WSO). Elevation contours are from 1524 meters (5000 feet) to 2591 meters (8500 feet) in 152.4 meter (500 feet) intervals.

In figure VI.3, the letters M, D, O and H represent the approximate locations of the towns of Montrose, Delta, Orchard City, and Hotchkiss, respectively. Elevation contours are from 1524 meters (5000 feet) to 3048 meters (10000 feet) in 152.4 meter (500 feet) intervals.

In figure VI.4, the letters R, L, T, B, and S represent the approximate locations of Sugar Loaf Reservoir, Leadville, Twin Lakes, Buena Vista, and Salida, respectively. Elevation contours are from 2438 meters (8000 feet) to 3810 meters (12500 feet) in 152.4 meter (500 feet) intervals.

Figure VI.1 31 Aug 95 - Temperature adjustment made to each pixel (Paonia to Delta)
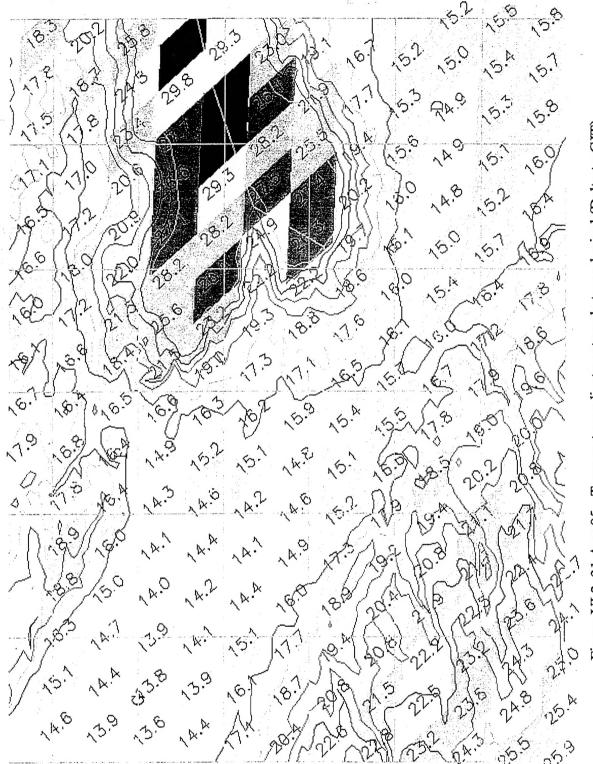
Figure VI.2 31 Aug 95 - Temperature adjustment made to each pixel (Delta to GJT)

Figure VI.3 31 Aug 95 - Temperature adjustment made to each pixel (Montrose to Delta)

Figure VI.4 31 Aug 95 - Temperature adjustment made to each pixel (Leadville to Salida)